

Robot arm control system design
based on human multi-joint arm
viscoelastic properties

Aihui Wang

Graduate School of Engineering
TOKYO UNIVERSITY
OF AGRICULTURE AND TECHNOLOGY

September, 2012

ACKNOWLEDGEMENTS

The guidance and support of the following people is invaluable. Without their advice and encouragement, a successful outcome would be unimaginable. I want to take the opportunity to sincerely appreciate their priceless help, support and dedication.

First and foremost, I would like to express my hearty thanks to my supervisor, Professor Mingcong Deng, for his insightful guidance, valuable advice and constant encouragement. His important guidance has kept me moving in the right direction, which highly improved my research ability. Without his support and encouragement, it would be impossible to complete this dissertation.

I would like to express my appreciation to my supervisor Professor Shinji Wakui, whose valuable suggestions and encouragement helped me finish my research.

Besides my supervisors, I would like to express my gratitude to the rest of my dissertation committee: Professor Hitoshi Kitazawa, Professor Akira Yamada and Associate Professor Ken Nagasaka, for their encouragement, insightful comments and hard questions.

Special gratitude goes to Professor Dongyun Wang (Zhongyuan University of Technology, China) and Tiejun Chen (Zhengzhou University, China). Thanks for their continuous support and encouragement.

Special gratitude goes to my colleagues and friends at Japan or outside who have supported me and offered help in various ways. Especially thanks

go to Dr. Shengjun Wen, Dr. Changan Jiang (RIKEN-RTI Collaboration Center for Human-Interactive Robot Research, Japan), Dr. Shuhui Bi (Institute of Automation, Shandong Academy of Sciences, China), Dr. Ni Bu (Qingdao University of Science & Technology, China), and Professor Wudai Liao (Zhongyuan University of Technology, China).

I am deeply indebted to my parents, my old brothers and my sisters-in-law, who have provided much moral and material support during the long years of my education, as well as kept me away from family responsibilities and encouraged me to concentrate on my research.

Last, but certainly not the least, my deep appreciation goes to my devoted wife Chunli Zhao and my beloved son Mingqing Wang. My gratefully appreciation for my loving, encouraging and patient Chunli Zhao who brings up our son by herself and support faithfully during my Ph.D. I also thank my beloved son, Mingqing Wang, for his encouragement and understanding throughout this work.

SUMMARY

In this dissertation, the robot arm control systems design based on human multi-joint arm viscoelastic properties is studied. That is, to imitate the motion mechanism of human multi-joint arm viscoelasticity, three kinds of control schemes are proposed. First, a robot arm control scheme is discussed based on the human multi-joint arm viscoelastic properties and a modified forward gaze model. Second, an operator-based robust nonlinear tracking control for the robot arm is investigated based on the human multi-joint arm viscoelastic properties and a forward operator. Third, an operator-based robust nonlinear tracking control for the robot arm with unknown time-vary delay is presented based on the human multi-joint arm viscoelastic properties and a compensation operator. In the present control schemes, the real measured human multi-joint viscoelasticity is used to obtain the desired motion mechanism, and the terms related to the effect of CNS is compensated to make the designed robot arm move smoothly as a human multi-joint arm as possible.

Robot arms with human-simulated motion mechanism are created to imitate some of the same physical and mental tasks that the human multi-joint arms undergo daily. Scientists and specialists from many different fields including cognitive science, linguistics, and engineering combine their efforts to create some robot arms with human-simulated motion mechanism as the human multi-joint arms as possible. As we know, compared to the robot arm, a human multi-joint arm can exhibit outstanding manipulability by

adjusting the dynamic characteristics of musculoskeletal system in executing various tasks. Therefore, the development of the dexterous robot arms which are as dexterous as possible like the human multi-joint arms based on the dynamic characteristics of human multi-joint arms has aroused people's growing interests. However, till now, how to obtain and use the online dynamic characteristics of human multi-joint arms is still a challenge issue in building the robot arm which is as skillful as a human multi-joint arm.

During human multi-joint arm movements, it is widely believed that the central nervous system (CNS) first plans for a desired response trajectory, which is converted into appropriate commands to be generated by the mechanical properties of musculoskeletal system which can be mainly described as human multi-joint arm viscoelasticity. The human multi-joint arm viscoelasticity consists of multi-joint stiffness and multi-joint viscosity, which are adjusted by CNS to make the human multi-joint arm adapt to the external environment or moving objects. If the viscoelastic properties during human multi-joint arm movements can be used effectively in building the robot arm control system, there is a possibility that the skillful strategies of human multi-joint arm can be integrated into the robot arm motion control. Therefore, as an alternative to imitating the motion mechanism of human multi-joint arm viscoelasticity can be considered. Moreover, the term of multi-joint muscle generated torque related to the effect of CNS is usually removed in measuring the human multi-joint arm viscoelasticity, how to compensate the terms related to the effect of CNS needs also to be considered to make the designed robot arm move more smoothly and skillfully as a human

multi-joint arm as possible. As a result, in this dissertation, how to use the online measured real human multi-joint viscoelasticity to obtain the desired motion mechanism of human multi-joint arm viscoelasticity and how to compensate the terms related to the effect of CNS are investigated in designing a robot arm with human-simulated motion mechanism.

Firstly, a robot arm control scheme is proposed based on time-varying estimated viscoelastic properties and a forward gaze model. In general, during the human multi-joint arm movements, the multi-joint torque can be assumed to be a function of multi-joint stiffness matrix, multi-joint viscosity matrix, and motor command descending from CNS. In order to make the present robot arm move like a human multi-joint arm, a feedback controller and a forward gaze model are presented in the robot arm control system. That is, the feedback controller is designed to obtain the desired motion mechanism of human multi-joint arm viscoelasticity based on real measured data from human multi-joint arm viscoelasticity, and the forward gaze model in which steering gains are modified using a cost function by simulating driver's optimal fashion in driving a car is used to compensate the terms related to the effect of CNS during human multi-joint arm movements. The effectiveness of the proposed method is also confirmed by the simulation results based on experimental data.

Secondly, considering the highly nonlinear robot arm with uncertainties consisting of measurement error and disturbance, an operator-based robust nonlinear tracking control for the robot arm with human multi-joint arm-like viscoelastic properties is considered by using the robust right coprime fac-

torization approach and a forward operator. In detail, an operator controller based on the real measured data from human multi-joint arm viscoelasticity is designed to obtain desired motion mechanism of human multi-joint arm viscoelasticity, the forward operator is presented to compensate the term related to the effect of CNS during human multi-joint arm movements. Moreover, addressing the fact that the uncertain plant is unknown generates difficulties in designing the operator controllers to obtain the desired performance, and an operator-based nonlinear feedback control scheme is proposed to eliminate the effect of uncertainties. The robust stability of present control system is discussed, and the performance of tracking is realized. The effectiveness of the proposed method is also confirmed by the simulation results based on experimental data.

Thirdly, further, it produces unknown time-varying delays while the real measured data of human multi-joint arm viscoelasticity is fed to the designed controller based on human multi-joint arm viscoelastic properties. Considering this problem, a new operator-based robust nonlinear tracking control for the robot arm with unknown time-varying delays is proposed by using robust right coprime factorization approach, a delay operator and a compensation operator. That is, the unknown time-varying delay is described by a delay operator, and the compensation operator is designed to compensate the terms related to the effect of CNS during human multi-joint arm movements and to remove the effect of unknown time-varying delays. The effectiveness of the proposed design scheme is also confirmed by the simulation results based on experimental data.

In summary, this dissertation proposes three kinds of control schemes for the robot arm by using the human multi-joint arm viscoelastic properties. In designed control schemes, the motion mechanism of human multi-joint arm viscoelasticity is imitated, and the terms related to the effect of CNS during human multi-joint arm movements are compensated. That makes it is possibility that the designed robot arm move smoothly and skillfully like the human multi-joint arm.

Contents

1	Introduction	1
1.1	Background	1
1.2	Current development of robot arm with human-simulated motion mechanism	4
1.3	Motivations of the dissertation	8
1.4	Contributions of the dissertation	10
1.5	Organization of the dissertation	13
2	Preliminaries and problem statement	17
2.1	Introduction	17
2.2	Robot arm dynamics	18
2.2.1	Robot arm dynamic model	18
2.2.2	Cartesian trajectories and joint space	20
2.3	Human multi-joint arm viscoelasticity	21
2.3.1	Human multi-joint arm dynamic model	21
2.3.2	Human multi-joint arm viscoelasticity	22
2.4	Human multi-joint arm viscoelasticity estimation	23
2.4.1	Estimating algorithm	23

2.4.2	Experimental system	30
2.5	Problem statement	31
2.6	Conclusion	33
3	Robot arm control system design based on human multi-joint arm viscoelastic properties and a forward gaze model	35
3.1	Introduction	35
3.2	Forward gaze model	38
3.3	Robot arm control system design	40
3.3.1	Robot arm control system scheme	40
3.3.2	Controller design based on based on human multi-joint arm viscoelastic properties	41
3.3.3	Controller design based on a forward gaze model	41
3.3.4	Control algorithm based an optimal fashion principle	45
3.4	Simulation results based on experimental data	49
3.5	Conclusion	53
4	Robot arm control system design based on human multi-joint arm viscoelastic properties and operator theory	57
4.1	Introduction	57
4.2	Fundamental theories on operator	60
4.2.1	Definitions of spaces	60
4.2.2	Definitions of operators	62
4.2.3	Right coprime factorization	67

4.3	Robot arm control system design based on human multi-joint arm viscoelastic properties and a forward operator	73
4.3.1	Robust nonlinear tracking control scheme	73
4.3.2	Eliminating effect of model uncertainties	75
4.3.3	Main results on conditions of robust stability and tracking	78
4.3.4	Simulation results based on experimental data	82
4.4	Robot arm control system design based on human multi-joint arm viscoelastic properties and a compensation operator	85
4.4.1	Property of time-varying delay	85
4.4.2	Robust nonlinear tracking control scheme	87
4.4.3	Main results on conditions of robust stability and tracking	89
4.4.4	Simulation results based on experimental data	91
4.5	Conclusion	93
5	Conclusions	97
	Bibliography	101
A	Definition of parameters	119
A.1	Human multi-joint arm	119
A.2	Robot arm	120
B	Proof	121
B.1	Proof of Lemma 4.1	121

B.2 Proof of Lemma 4.2	123
B.3 Proof of Lemma 4.3	124
B.4 Proof of Lemma 4.4	124
B.5 Proof of Lemma 4.5	124
C Publications	129

List of Figures

2.1	Structure of two-link robot arm	19
2.2	Multi-joint human arm dynamic model	22
2.3	The <i>pdf</i> of generalized Gaussian distribution	26
2.4	Experimental system schematic illustration	30
2.5	Experimental system	31
3.1	The schematic of forward gaze model	39
3.2	The proposed robot arm control system scheme	40
3.3	The target trajectory and endpoint position	43
3.4	Estimated human multi-joint arm stiffness by experiment	51
3.5	Estimated human multi-joint arm viscosity by experiment	51
3.6	Estimated shape parameters γ_i in the experiment	52
3.7	The obtained optimal $K_A^*(t)$ by simulation	53
3.8	The obtained optimal $R_A^*(t)$ by simulation	54
3.9	The joint angles tracking results by simulation	54
3.10	The endpoint position tracking result by simulation	55
4.1	Diagram of operator	62

4.2	Right factorization of an operator process	68
4.3	Operator based nonlinear feedback control system	69
4.4	Operator based nonlinear feedback control system with uncertainty	70
4.5	Operator based MIMO nonlinear feedback system with uncertainties	72
4.6	The proposed operator-based robust nonlinear tracking control for the robot arm	74
4.7	An operator-based nonlinear feedback control scheme	76
4.8	Equivalent system of Figure 4.7	76
4.9	Equivalent block diagram Figure 4.8	78
4.10	Equivalent block diagram Figure 4.6	78
4.11	Equivalent block diagram Figure 4.5	81
4.12	Estimated human multi-joint arm stiffness by experiment . . .	82
4.13	Estimated human multi-joint arm viscosity by experiment . .	83
4.14	The joint angles tracking results by simulation	84
4.15	The endpoint position tracking result by simulation	84
4.16	The proposed operator-based robust nonlinear tracking control system	87
4.17	Equivalent block diagram of Figure 4.16	89
4.18	Equivalent block diagram of Figure 4.17	91
4.19	Estimated human multi-joint arm stiffness by experiment . . .	92
4.20	Estimated human multi-joint arm viscosity by experiment . .	93
4.21	The joint angles tracking results by simulation	94

4.22 The endpoint position tracking result by simulation 94

List of Tables

A.1	Parameters of human multi-joint arm	119
A.2	Parameters of robot arm	120

Chapter 1

Introduction

1.1 Background

Robots have always been inspired by the human body. From the first robotic systems appearing in movie theatres to modern motion pictures, the robotic system has always played the role of “replacing” and “confronting” the human being, often with a remarkable resemblance. At a macroscopic level, the same holds true for robot arms [1, 2, 3, 4]. The robot arms are a standard component in various fields, such as, industries, rehabilitation, welfare and sports, etc., and their kinematics of which are often clearly inspired by the human multi-joint arm [5, 6, 7, 8]. Due to these potential applications, some robot arms with human-simulated motion mechanism which move smoothly and skillfully like the human multi-joint arms have attracted a lot of attention from the academic and industrial communities. Over the past decades, the robot arms are becoming more and more compact, light and stable, and are often designed to operate in human environments. Such anthropomorphic robot arms must be capable of performing independent tasks in a human arm-

like way, which means that its movements must be versatile, fast, accurate, smooth and skillful. Scientists and specialists from many different fields including cognitive science, linguistics, and engineering combine their efforts to create the robot arms as the human multi-joint arms as possible [9, 10]. Till now, building the robot arm which is as skillful as a human multi-joint arm is still a challenge issue in the field of robotics.

As we all known, many of the methods have been used to control the robot arms. The simplest controller for the robot arms is designed by using the Proportional Integral Derivative (PID) control method or Linear Quadratic (LQ) method [11, 12, 13, 14]. In general, this type of controller is designed on the basis that the robot arm model is composed of independent coupled dynamic (differential) equations. While this controller is widely used in the industrial robot arms, depending on the task to be carried out, they do not always result in the best performance. Moreover, the robust stability also is not well guaranteed by these controllers in the presence of uncertainties of system [15, 16]. To improve performance and achieve robust tracking, some approaches such as optimal control [17, 18, 19, 20, 21], adaptive learning control [22, 23, 24, 25, 26], neural network control [27, 28], variable structure system theory [26], model predictive control [29], and sliding model control [15] have been used to design appropriate control rules. However, optimal control theory requires a precise model, but system identification against a “complex” robotic system having nonlinear dynamics and high-dimensional state space is difficult. Although adaptive control and neural network control approaches can obtain the uncertain parameters of system by repetitive

learning, but, the unknown load condition and dynamic parameters need to be identified on-line, they require heavy computation, therefore, control rules based on a reinforcement learning algorithms is also difficult due to the combinatorial explosion of the states and control action spaces. The variable structure system theory or sliding model control usually is limited to problem of the uncertain physical or structural parameters. Therefore, for mentioned approaches, designing *model – based* controllers require a precise the knowledge of dynamic model including the values of the physical parameters involved, other, *non – model – based* controllers is used mainly in academic applications and research prototypes. Moreover, in certain complex industrial tasks, stable, fast and accurate robot arm positioning is required, while in a number of nonindustrial tasks (e.g. domestic robotics, robotic-assisted surgery etc) dexterity and intelligent positioning is required.

Although a human can control his multi-joint arm flexibly and robustly, controlling such robot arm with human-simulated motion mechanism by the existing control methods would be difficult because of its complexity. As an alternative to such theoretical methods, studies on control methods imitating the motion mechanism of human multi-joint arm can be considered [30, 31, 32, 33, 34]. During the last decade, the robot arms are getting more and more closer to the human multi-joint arms by measuring or capturing the human multi-joint arm motion and converting to motion of the robot arm [35, 36]. Towards this goal, the multi-joint coordination of the human arm should be analyzed and modeled. If joint angles dependencies are modeled, then incorporating those synergies in the inverse kinematics algorithms results to

a biomimetic approach of the kinematic control of robot arms. However, the motion mechanism of the human multi-joint arm is not only related to the mechanical properties of human multi-joint musculoskeletal system, but also related to the central nervous system (CNS) [37, 38, 39, 40, 41], complex control signals are required for human multi-joint arm movement [42, 43, 44, 45]. As a result, how to use the mechanical properties of the human multi-joint musculoskeletal system and how to mimic or compensate the terms related to effect of CNS are key points in building robot arm which is as skillful as the human multi-joint arm.

1.2 Current development of robot arm with human-simulated motion mechanism

Robot arms with human-simulated motion mechanism are created to imitate some of the same physical and mental tasks that the human multi-joint arms undergo daily. Therefore, imitating the human multi-joint arm motion (e.g. drawing, handwriting) can be considered in order to generate human-simulated motion as closely as possible [3, 7]. These methods on biomimetic motion generation for robot arms are usually based on minimizing posture difference between the robot arm and the human multi-joint arm, using a specific recorded data set. Therefore, the robot arm configurations are exclusively based on the recorded data set. That is, the methods cannot generate new human multi-joint arm-simulated motion, which is quite important for the kinematic control of anthropomorphic robot arms, where the range of possible configurations should not be limited to the ones recorded from

humans. As a result, how to obtain the human multi-joint arm-like mathematical description of robot arm and how to use the motion mechanism of human multi-joint arm are key points in building the robot arms with human-simulated motion mechanism.

Many of the concepts that are used to describe the motion mechanism of human multi-joint arm have been borrowed from the robot arms [46, 47, 48, 49, 50, 51, 52, 53, 54, 55, 56, 57, 58, 59, 60, 61, 62, 63]. Among these concepts, equilibrium-point control hypothesis [46, 47], feedback and feedforward control [48], internal models [49, 50, 51, 52] are especially relevant for the present review. The equilibrium-point control hypothesis suggests that CNS utilizes the *spring – like* property of the human neuromuscular system to circumvent the computational complexities in coordinating multi-degree-of-freedom human arm movements. In equilibrium point control, force can be controlled separately by a series of equilibrium points and actively-controlled stiffness (or impedance) at the joints. In the feedback and feedforward control, the reference state the target position and the current state the location of the human multi-joint arm, the set of muscle activations that drives a reach towards a target is defined prior to arm displacement. As long as the human multi-joint arm has not reached the target, the motor command unfolds unaltered until the movement is completed. Internal models can be segregated into two categories, namely forward models and inverse models. The forward model is a way of using one’s knowledge about the plant model, and predicting the behavior of the motor system in response to a command and allowing CNS to estimate the current and future state. The inverse model

takes into account the inertial and viscous properties of the arm to estimate the motor command that will produce the desired displacement. This model is hypothesized to be learned over time, becoming more accurate by using the mismatch between the target response and the actual response. Based on above concepts, some existing methods such as learning control, optimal control and adaptive control have been used to design appropriate control rules. However, the learning control rules based on a reinforcement learning algorithms is difficult due to the combinatorial explosion of the states and control action spaces, the optimal control theory also requires a precise model, but system identification against the complex robot arm system having nonlinear dynamics and high-dimensional state space is difficult. To obtain a precise model and use optimal control theory, several trajectory formation models have been proposed for human arm movement control, such as minimum jerk model [61], minimum torque change model [62], and minimum muscle tension-change model [63]. A variety of given trajectories can be generated based on the optimal criterions of these models in the presence of learned information pairs. However, to generate different speed movement trajectories for the same motion task, information pairs for different speed movements would need to be learned and saved in advance. Therefore, it is difficult to achieve online control. Moreover, imitating the motion mechanism of the human multi-joint arm, some robot arms are built. A human-like robot arm control method based on the attractor selection model by imitating the anatomy of bones and muscles in human arm was proposed [64], owing to not depending on the control target model, this method can respond to

unpredictable disturbance or environmental change and control performance may not be optimal. Tsuji and Tanaka investigated human hand impedance in preparation for task operations, and discussed a bio-mimetic impedance control of robot arm for contact tasks [65]. Due to not considering the motion mechanism of CNS, the robot arm would not move skillfully and smoothly like the human multi-joint arm, and movements would tend to be jerky and inaccurate.

Several hypotheses suggest that it is possible to associate some cost functions to each human arm joint, and the human multi-joint arm performs movements that optimize these cost functions [1, 7, 20]. Examples of dynamic cost functions are the following: quadratic norm of joint control torques, jerks in joints, kinetic energy, input energy and input fatigue. Some proper combinations of these functions, rather than their individual application, are also suggested. The fact that a variety of cost functions has been used to explain the principles of human arm motor control indicates that the CNS does not obey any particular cost function, but also does not violate the general physical and technical principles of optimality from which particular cost functions come out. Whatever cost function is used, the key point is that this algorithm can simulate the comfortable level during human multi-joint arm movements like the driver's "feeling" [66]. Many methods are presented to make the drivers in an optimal and comfortable fashion in driving the cars [67, 68, 69]. Therefore, to reduce the jerkiness of the robot arm, the derived and modified methods by some operation models of the car can be used to mimic the cost functions of CNS by deriving and modifying.

Moreover, as we all known, the robot arm is a highly nonlinear system [70, 71, 72], which is subject to disturbances and model uncertainties [73, 74]. Many approaches have been proposed to develop controllers that are more robust so that their performance is not sensitive to modeling errors. Especially, the robust right coprime factorization approach has attracted much attention due to its convenient in researching input-output stability problems of nonlinear system with uncertainties [75, 76, 77, 78, 78, 80, 81, 82, 83, 84, 85, 86, 87, 88]. Therefore, how to extend the motion mechanism of human multi-joint arm to operator-based control design approach in designing the robot arm which is as skillful as the human multi-joint arm is also an effective path.

1.3 Motivations of the dissertation

During human multi-joint arm movements, it is widely believed that CNS first plans for the desired response trajectory, which is converted into appropriate commands to be generated by the human multi-joint arm musculoskeletal system, the mechanical properties of human multi-joint arm musculoskeletal system can be mainly described as the human multi-joint arm viscoelasticity. The human multi-joint arm viscoelasticity consists of multi-joint stiffness and multi-joint viscosity, which are adjusted by CNS to make the human multi-joint arm adapt to the external environment or moving objects [32, 33, 34, 37]. If the viscoelastic properties during human multi-joint arm movements can be used effectively in the robot arm with human-simulated motion mechanism control, there is a possibility that skillful strategies of the

human multi-joint arm can be integrated into the robot arm motion control. Therefore, to build the robot arm with human-simulated motion mechanism, the human multi-joint arm viscoelastic data during human multi-joint arm movements needs to be obtained online by measuring or estimation, and the obtained human multi-joint arm viscoelastic data is fed to the designed controller based on the motion mechanism of human multi-joint arm viscoelasticity in controlling robot arm. Moreover, to describe and compensate the terms related to the effect of CNS, an effective method is also essential.

To use online human multi-joint arm viscoelastic data during human multi-joint arm movements, an effective estimating method of human multi-joint arm viscoelasticity is indispensable. Several measuring methods of human multi-joint arm viscoelasticity have been reported, but none has finally been used in developing the robot arms with human-simulated motion mechanism [89, 90, 91, 92, 93, 94, 95]. During point-to-point movements on a horizontal plane, human multi-joint arm stiffness parameters were measured based on the equilibrium point hypothesis [89], but experimental apparatus are too complicated and expensive to be applied widely. Identification of human multi-joint limb viscoelasticity was presented based on robotics methods, the estimation viscoelasticity can be as important diagnosis variables [90], but cannot be adopted effectively in robot arm control because human multi-joint arm viscoelasticity was only estimated during passive movements. A method was presented for estimating human multi-joint arm stiffness using electromyogram (EMG) of muscle and an artificial neural network model [91], this method was merely able to provide trend analysis between stiffness

and EMG, the real viscoelasticity cannot be obtained. Moreover, for estimating the stiffness and viscosity properties during voluntary movements, in which restoring force and positional responses of many trials were required. An integrated study procedure on real-time estimation of time varying human multi-joint arm viscoelasticity has been proposed [96, 97, 98, 99], the proposed method can obtain online human multi-joint arm viscoelastic data during movements. Therefore, it is possible that the human multi-joint arm viscoelastic data can be fed to the designed controller based the motion mechanism of human multi-joint arm viscoelasticity.

Motivated by the above issues, this dissertation is focused on the control system design for the robot arm with human-simulated motion mechanism based on human multi-joint arm viscoelastic properties. That is, imitating the motion mechanism of human multi-joint arm, how to use the real human multi-joint arm viscoelastic data and how to describe and compensate the terms related to the effect of CNS during human multi-joint arm movements are investigated in building the robot arm.

1.4 Contributions of the dissertation

Addressing a challenge issue in the field of robotics, namely, how to build the robot arm with human-simulated motion mechanism by mimicking the functions of human multi-joint arm, in this dissertation, the robot arm control system design by using human multi-joint arm viscoelastic properties and simulating the terms related to effect of CNS during human multi-joint arm movements is investigated. The key contributions of the research can be

categorized into three groups:

(1) The motion mechanism of human multi-joint arm viscoelasticity is used in designing robot arm control systems, and the real measured experimental data of human multi-joint arm viscoelasticity is used in simulation results.

During human multi-joint arm movements, the control input torque vector can be assumed to be a function of multi-joint viscosity matrix, multi-joint stiffness matrix, and motor command descending from CNS. Based on the motion mechanism of human multi-joint arm, the controller based the human multi-joint arm viscoelasticity consisting multi-joint viscosity matrix, multi-joint stiffness matrix is designed to obtain desired human arm-like motion mechanism like a human multi-joint arm. Moreover, to confirm the effectiveness of the proposed methods, the real measured experimental data of human multi-joint arm viscoelasticity is also used in simulation results.

(2) The terms related to the effect of CNS during human multi-joint arm movements are simulated in designing robot arm control systems.

CNS is not necessary for movement, but without it movements of the human multi-joint arm tend to jerky, tremulous, and inaccurate. Therefore, how to model dynamic knowledge of CNS is also a key point in building the robot arm by mimicking the functions of human multi-joint arm. The terms related to the effect of CNS can also be described as a part of human multi-joint arm viscoelasticity. However, it is difficult to obtain this part related properties. Moreover, this part is usually not considered in estimating the

human multi-joint arm viscoelasticity. Therefore, how to mimic or compensate the terms related to the effect of CNS during human multi-joint arm movements is very important. As a result, in this dissertation, two methods are proposed to describe or compensate the terms related to the effect of CNS during human multi-joint arm movements in designing the robot arm control scheme. The first method is to use a modified forward gaze model to simulate the terms related to the effect of CNS, the main reason to use the forward gaze model is that the method has been used for preview driver control in driver's comfortable fashion, namely, the model can reduce the jerkiness. The second method is to use the operator to mimic the terms related to the effect of CNS during human multi-joint arm movements, where, two different operators, namely, a forward operator and a compensation operator are designed.

(3) Operator-based robust nonlinear tracking for robot arm is proposed.

A basic problem in controlling robot arms is to make the robot arm follow a preplanned desired trajectory, where, input-output stability and multivariable tracking problems are key points to obtain the desired running performance. However, the robot arm is a multi-input multi-output (MIMO) highly nonlinear system. There also exist unknown modeling errors in measuring structural parameters of the robot arm and external disturbances in real situations. Considering these problems, operator-based robust nonlinear tracking for the robot arm is proposed. In proposed control scheme, the following key contributions are obtained. That is, firstly, addressing the

fact that the uncertain plant is unknown generates limitations in designing controllers to obtain the desired performance based the former so-called universal condition, in this dissertation, in order to solve that, an operator-based nonlinear feedback control scheme is designed to eliminating effect of uncertainties. Secondly, an operator-based feedback control is summarized by using motion mechanism of human multi-joint arm viscoelasticity, two robust stability and tracking conditions without time-varying delays and with time-varying delays are obtained, respectively, operator-based control design approach are derived to robot arm control.

1.5 Organization of the dissertation

This dissertation is organized as follows.

In **Chapter 2**, the robot arm dynamic model is introduced, and the relationship between Cartesian trajectories and joint space is explained. Human multi-joint arm dynamic model and human multi-joint arm viscoelasticity are described, and estimation method of human multi-joint arm viscoelasticity consisting of estimating algorithm and experimental system is introduced. All these provide the theoretical basis for this dissertation. Moreover, the objective of this dissertation is presented in problem statement.

In **Chapter 3**, first, the forward gaze model is introduced. Then, a robot arm control system is proposed based on time-varying estimated human multi-joint arm viscoelasticity and a modified forward gaze model. In detail, based on the motion mechanism of human multi-joint arm, namely, the multi-joint torque is assumed to be a function of multi-joint stiffness ma-

trix, multi-joint viscosity matrix, and motor command descending from CNS in human multi-joint arm movements, a feedback controller and a forward gaze model are presented in the robot arm control system design to make the present robot arm move like a human multi-joint arm. The feedback controller is designed to obtain the desired motion mechanism of human multi-joint arm viscoelasticity based on real measured data from human multi-joint arm viscoelasticity, and the forward gaze model in which steering gains are modified using a cost function is used to compensate the terms related to the effect of CNS during human multi-joint arm movements. The effectiveness of the proposed method is also confirmed by the simulation results based on experimental data.

In **Chapter 4**, first, fundamental theories on operator are introduced. Then, an operator-based robust nonlinear tracking control for a robot arm with human multi-joint arm-like viscoelastic properties is considered by using robust right coprime factorization approach and a forward operator. That is, an operator controller based on real measured data from human multi-joint arm viscoelasticity is designed to obtain desired motion mechanism of human multi-joint arm viscoelasticity, the forward operator is presented to compensate the term related to the effect of CNS during human multi-joint arm movements. Considering the fact that the uncertain plant is unknown generates difficulties in designing controllers to obtain the desired performance, an operator-based nonlinear feedback control scheme is proposed to eliminate effect of the uncertainties of dynamic model consist of measurement error and disturbance. The robust stability and the performance of output

tracking of present control system are discussed. Moreover, considering it produces unknown time-varying delays while the real measured data of human multi-joint arm viscoelasticity is fed to the designed controller based on human multi-joint arm viscoelastic properties, a new operator-based robust nonlinear tracking control for a robot arm with unknown time-varying delays is proposed by using robust right coprime factorization approach, a delay operator and a compensation operator. The unknown time-varying delay is described by a delay operator, and the compensation operator is designed to compensate the effect of CNS during human multi-joint arm movements and to remove the effect of unknown time-varying delays. The effectiveness of the proposed method is also confirmed by the simulation results based on experimental data.

In **Chapter 5**, the proposed design schemes are summarized. It is concluded that by using the proposed design schemes, the human arm-simulated motion mechanism is obtained by using human multi-joint arm viscoelastic properties and simulating the terms related to the effect of CNS in designing the robot arm, the desired results are confirmed by simulation results based on experimental data.

Chapter 2

Preliminaries and problem statement

2.1 Introduction

This chapter provides the mathematical and theoretical background for remaining the following chapters in this dissertation. It also serves a foundation for other research topics in the robot arm control system design.

In **Section 2.2**, two-link rigid robot arm dynamics in the horizontal plane is introduced, and the relationship between Cartesian trajectories and joint space is described.

In **Section 2.3**, two-link rigid human arm dynamics in the horizontal plane is described by second-order nonlinear differential equation, and how to obtain the mathematical description of human multi-joint arm viscoelasticity based on the human multi-joint arm dynamics is introduced.

In **Section 2.4**, an estimation method of human multi-joint arm viscoelasticity is described, where, how to design estimating algorithm and how to build experimental system are introduced.

In **Section 2.5**, the problem discussed in this dissertation is introduced. That is, how to design the robot arm control system based on human multi-joint arm viscoelastic properties is described.

2.2 Robot arm dynamics

2.2.1 Robot arm dynamic model

Two-link rigid robot arm dynamics in the horizontal plane can be generally modeled by the following second-order nonlinear differential equation [11, 12]:

$$\mathbf{M}(\theta)\ddot{\theta} + \mathbf{H}(\dot{\theta}, \theta) = \tau_{in} \quad (2.1)$$

where, θ , $\dot{\theta}$, and $\ddot{\theta}$ denote angle position, velocity and acceleration vectors, respectively, and $\theta = (\theta_1, \theta_2)^T$, $\theta_i(t)$ is joint angle of link i (see Figure 2.1). $\tau_{in} = (\tau_1, \tau_2)^T$, $\tau_i(t)$ is control input torque of link i , it is assumed that the first joint driving torque, τ_1 , acts between the base and link 1, and that the second joint driving torque, τ_2 , acts between links 1 and 2. \mathbf{M} and \mathbf{H} denote the inertial matrix (2×2) and Coriolis-Centrifugal force vector, and

$$\mathbf{M} = \begin{pmatrix} Z_1 + 2Z_2 \cos \theta_2 & Z_3 + Z_2 \cos \theta_2 \\ Z_3 + Z_2 \cos \theta_2 & Z_3 \end{pmatrix} \quad (2.2)$$

$$\mathbf{H} = \begin{pmatrix} -Z_2 \sin \theta_2 (\dot{\theta}_2^2 + 2\dot{\theta}_1 \dot{\theta}_2) \\ Z_2 \dot{\theta}_1^2 \sin \theta_2 \end{pmatrix} \quad (2.3)$$

where

$$\begin{cases} Z_1 = m_1 l_{g1}^2 + m_2 (l_1^2 + l_{g2}^2) + I_1 + I_2 \\ Z_2 = m_2 l_1 l_{g2} \\ Z_3 = m_2 l_{g2}^2 + I_2 \end{cases} \quad (2.4)$$

m_i denotes the masses of link i , l_{gi} denotes the distance between the joint i and to the center of mass of link i , I_i denotes the moment of inertia of link i about the center of mass, and l_i denotes the length of link i . Z_1 , Z_2 and Z_3 are the structural parameters which denote physical feature of the robot arm.

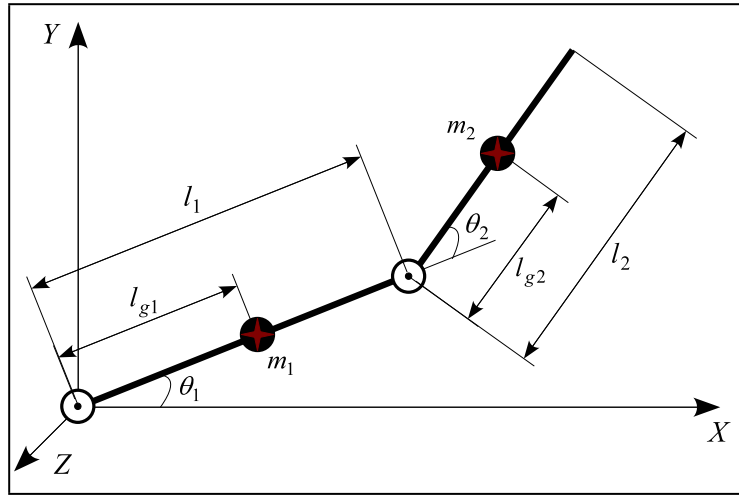


Figure 2.1: Structure of two-link robot arm

The robot arm dynamics given in (2.1) have a main property, that is, the inertia matrix is symmetric and positive definite, and satisfies the following inequalities:

$$\alpha_1 \|w\|^2 \leq w^T \mathbf{M}(\theta) w \leq \alpha_2 \|w\|^2 \quad \forall w \in R^n \quad (2.5)$$

where $\alpha_1, \alpha_2 \in R$ are positive constants and $\|\cdot\|$ denotes the standard Euclidean norm.

2.2.2 Cartesian trajectories and joint space

The basic problem in controlling the robot arm is to make the robot arm follow a preplanned desired trajectory. Before we can control the robot arm, it is necessary to know the desired path for performing a task. Throughout this dissertation it is assumed that there is given a prescribed path $(x_d(t), y_d(t))$ the robot arm should follow. We design control systems that make the robot arm follow this desired path or trajectory. In the robot arm applications, a desired task is usually specified in the workspace or Cartesian space, as this is where the motion of robot arm is easily described in relation to the external environment and workspace. However, trajectory-following control is easily performed in the joint space, as this is where the robot arm dynamics are more easily formulated. If we consider an articulated robot arm as a device for generating position and orientation, we need to know the relationships between these quantities and the joint variables, since it is the latter that we can easily measure and control. Position here refers to the position in space of the tip of robot arm, while the orientation refers to the direction of approach of the last link. Therefore, it is important to be able to find the desired joint space trajectory $\theta_d(t)$ given the desired Cartesian trajectory. This is accomplished using the inverse kinematics [70, 71, 72].

For the two-link rigid robot arm in the horizontal plane described in 2.1, the tip position can be found simply by the following relationship [71],

$$\mathbf{X} = \begin{bmatrix} x \\ y \end{bmatrix} = \begin{bmatrix} l_1 \cos \theta_1 + l_2 \cos(\theta_1 + \theta_2) \\ l_1 \sin \theta_1 + l_2 \sin(\theta_1 + \theta_2) \end{bmatrix} \quad (2.6)$$

$$\dot{\mathbf{X}} = \begin{bmatrix} \dot{x} \\ \dot{y} \end{bmatrix} = \mathbf{J} \begin{bmatrix} \dot{\theta}_1 \\ \dot{\theta}_2 \end{bmatrix} \quad (2.7)$$

where,

$$\mathbf{J} = \begin{bmatrix} -l_1 \sin \theta_1 - l_2 \sin(\theta_1 + \theta_2) & -l_2 \sin(\theta_1 + \theta_2) \\ l_1 \cos \theta_1 + l_2 \cos(\theta_1 + \theta_2) & l_2 \cos(\theta_1 + \theta_2) \end{bmatrix} \quad (2.8)$$

While the forward calculation of tip position from joint angles is always relatively straightforward, the inversion is intractable for robot arms with more than two links. For two-link rigid robot arm dynamics in the horizontal plane, we easily get the following inversion,

$$\cos(\theta_2) = \frac{(x^2 + y^2) - (l_1^2 + l_2^2)}{2l_1 l_2} \quad (2.9)$$

$$\cos(\theta_1) = \frac{x(l_1 + l_2 \cos(\theta_2)) + y l_2 \sin(\theta_2)}{\sqrt{(x^2 + y^2)(l_1^2 + l_2^2 + 2l_1 l_2 \cos(\theta_2))}} \quad (2.10)$$

2.3 Human multi-joint arm viscoelasticity

2.3.1 Human multi-joint arm dynamic model

Two-link rigid human arm dynamics in the horizontal plane can be generally modeled by the following second-order nonlinear differential equation [89, 96]:

$$\mathbf{M}_A(\mathbf{q})\ddot{\mathbf{q}} + \mathbf{H}_A(\dot{\mathbf{q}}, \mathbf{q}) = \tau_A(\dot{\mathbf{q}}, \mathbf{q}, \mathbf{u}) \quad (2.11)$$

where, \mathbf{q} , $\dot{\mathbf{q}}$, and $\ddot{\mathbf{q}}$ denote angular position, velocity and acceleration vectors, respectively, and, $\mathbf{q} = [\theta_s(t), \theta_e(t)]^T$, $\theta_s(t)$ is shoulder joint angular and $\theta_e(t)$ is elbow joint angular, the subscripts s and e denote shoulder joint and elbow

joint (see Figure 2.2), respectively. $\tau_A = [\tau_s, \tau_e]^T$ is the multi-joint muscle generated torque, which can be represented as a function of angular position, velocity, and motor command \mathbf{u} descending from CNS. \mathbf{M}_A and \mathbf{H}_A have the same structure as \mathbf{M} and \mathbf{H} in (2.1), respectively.

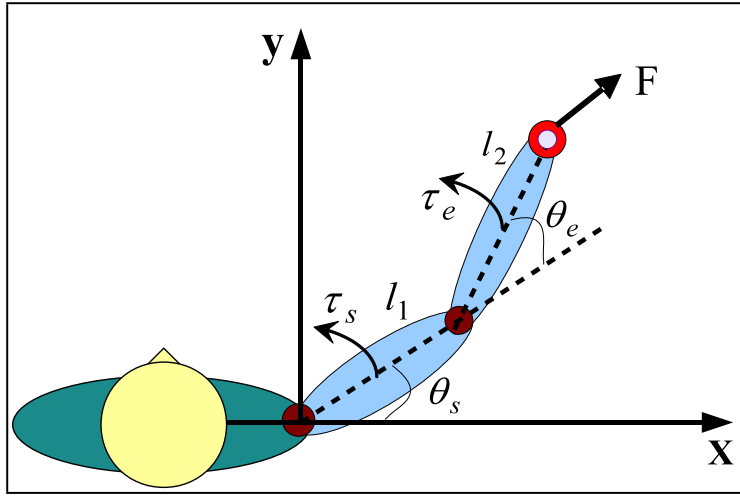


Figure 2.2: Multi-joint human arm dynamic model

2.3.2 Human multi-joint arm viscoelasticity

If the human multi-joint arm in (2.11) is assumed to be rigid body serial link system, such that:

$$\Psi(\ddot{\mathbf{q}}, \dot{\mathbf{q}}, \mathbf{q}) = \mathbf{M}_A(\mathbf{q})\ddot{\mathbf{q}} + \mathbf{H}_A(\dot{\mathbf{q}}, \mathbf{q}) = \tau_A(\dot{\mathbf{q}}, \mathbf{q}, \mathbf{u}) \quad (2.12)$$

Taking the derivative of (2.12):

$$\frac{\partial \Psi}{\partial \ddot{\mathbf{q}}} \frac{d\ddot{\mathbf{q}}}{dt} + \frac{\partial \Psi}{\partial \dot{\mathbf{q}}} \frac{d\dot{\mathbf{q}}}{dt} + \frac{\partial \Psi}{\partial \mathbf{q}} \frac{d\mathbf{q}}{dt} = \frac{\partial \tau_A}{\partial \dot{\mathbf{q}}} \frac{d\dot{\mathbf{q}}}{dt} + \frac{\partial \tau_A}{\partial \mathbf{q}} \frac{d\mathbf{q}}{dt} + \frac{\partial \tau_A}{\partial \mathbf{u}} \frac{d\mathbf{u}}{dt} \quad (2.13)$$

According to (2.11)-(2.13), then the following relationship can be obtained [89, 96]:,

$$\delta\tau_A = -\mathbf{R}_A(t)\delta\dot{\mathbf{q}} - \mathbf{K}_A(t)\delta\mathbf{q} + \frac{\partial\tau_A}{\partial\mathbf{u}}\delta\mathbf{u} \quad (2.14)$$

Where, $\mathbf{R}_A(t)$ and $\mathbf{K}_A(t)$ represent multi-joint viscosity and multi-joint stiffness matrix (2×2), respectively, and

$$-\frac{\partial\tau_A}{\partial\dot{\mathbf{q}}} \equiv \mathbf{R}_A(t) = \begin{pmatrix} R_{A-ss} & R_{A-se} \\ R_{A-es} & R_{A-ee} \end{pmatrix} \quad (2.15)$$

$$-\frac{\partial\tau_A}{\partial\mathbf{q}} \equiv \mathbf{K}_A(t) = \begin{pmatrix} K_{A-ss} & K_{A-se} \\ K_{A-es} & K_{A-ee} \end{pmatrix} \quad (2.16)$$

The subscript ss of $\mathbf{R}_A(t)$ and $\mathbf{K}_A(t)$ represent the shoulder single-joint effect on each coefficient, se and es denote cross-joint effects, ee denotes the elbow single-joint effect.

2.4 Human multi-joint arm viscoelasticity estimation

2.4.1 Estimating algorithm

To estimate online human multi-joint arm viscoelasticity, a band-pass recursive filter based on score function approach for the human multi-joint arm model with uncertain factors was designed, the filtered torque τ_A^f , the angular positions θ_s^f and θ_e^f , and the velocities $\dot{\theta}_s^f$ and $\dot{\theta}_e^f$ satisfy the following relationship [96, 97, 98, 99],

$$\tau_A^f = \mathbf{E}\mathbf{S} + \Delta + \zeta_1 \quad (2.17)$$

where \mathbf{E} is the regression vector, \mathbf{S} is the time-varying parameter to be estimated,

$$\mathbf{E} = \begin{pmatrix} \theta_s^f & \theta_e^f & \dot{\theta}_s^f & \dot{\theta}_e^f & 0 & 0 & 0 & 0 \\ 0 & 0 & 0 & 0 & \theta_s^f & \theta_e^f & \dot{\theta}_s^f & \dot{\theta}_e^f \end{pmatrix} \quad (2.18)$$

$$\mathbf{S} = (K_{A-ss} \ K_{A-se} \ R_{A-ss} \ R_{A-se} \ K_{A-es} \ K_{A-ee} \ R_{A-es} \ R_{A-ee})^T \quad (2.19)$$

$\Delta = [\Delta_1, \Delta_2]^T$ consists of the structural uncertainties which are assumed to be Gaussian. $\zeta_1 = [\bar{\zeta}_{11}, \bar{\zeta}_{22}]^T$ is the non-Gaussian measurement error of filtered measurement noise. When the sampling time is little enough, the term of $\frac{\partial \tau_A}{\partial \mathbf{u}} \delta \mathbf{u}$ related to the effect of CNS in (2.14) can be seen as a low frequency non-Gaussian noise. By using a band-pass filter for the model (2.14), the high frequency and low frequency measurement noise can be removed within sufficiently small sampling time period, namely, the human multi-joint arm viscoelasticity can be estimated based on the following dynamic model,

$$\delta \tau_A = -\mathbf{R}_A(t) \delta \dot{\mathbf{q}} - \mathbf{K}_A(t) \delta \mathbf{q} \quad (2.20)$$

In human multi-joint arm viscoelasticity estimation, the above uncertainties should be considered to reduce estimation errors. In order to reduce the effect of uncertainties, a filtering algorithm for estimating human multi-joint arm viscoelasticity is designed. To design the filtering algorithm, the model (2.17) needs to be converted into its discrete time state-space form as follows,

$$\begin{cases} \mathbf{S}(t + T_s) = \mathbf{S}(t) + \zeta_2, \\ \tau_A^f(t + T_s) = \mathbf{E}(t + T_s) \mathbf{S}(t + T_s) + \Delta(t + T_s) + \zeta_1(t + T_s) \end{cases} \quad (2.21)$$

where, T_s is sampling time, ζ_2 is white noise.

The fundamental problem associated with experimental system is to estimate viscoelasticity by using the generated torques τ_s and τ_e . In the following, the problem is to design the recursive filter based on score function approach for the human multi-joint arm model with uncertain factors. The score function approach along with generalized Gaussian approximation of the innovations process probability density function (*pdf*) can be used for state estimation of non-Gaussian system. The shape parameters of *pdf* can determine the shape of the distribution. For the generalized Gaussian uncertainty factor $\Delta_i(t) + \bar{\zeta}_{ii}(t)$ ($i = 1, 2$) with zero mean, variance σ_i^2 and shape parameter γ_i is given by the following relationship [100, 101],

$$p_i(x_i; \sigma_i, \gamma_i) = \frac{\alpha_i(\gamma_i)\gamma_i}{2\sigma_i\Gamma(1/\gamma_i)} e^{-[\alpha_i(\gamma_i)|\frac{x_i}{\sigma_i}]^{\gamma_i}}, \quad x_i \in R, \quad i = 1, 2 \quad (2.22)$$

$$\alpha_i(\gamma_i) = \sqrt{\frac{\Gamma(3/\gamma_i)}{\Gamma(1/\gamma_i)}} \quad (2.23)$$

where $\Gamma(\cdot)$ is the Gamma function. As we notice above, when $\gamma = 1$, the K distribution corresponds to a Laplacian or double exponential distribution, when $\gamma = 2$ corresponds to a Gaussian distribution, whereas in the limiting cases when $\gamma \rightarrow +\infty$ the *pdf* in (2.21) converges to a uniform distribution in $(-\sqrt{3}\sigma, \sqrt{3}\sigma)$, and when $\gamma \rightarrow 0+$ the distribution becomes a degenerate one in $\tilde{x}_i = 0$, shown in Figure 2.3.

So for the one-to-one correspondence between γ_i and the fourth-order even moment $\phi_i(\gamma_i)$ was used for estimating human multi-joint arm viscoelasticity. In this dissertation, the all-order case is considered as follows.

$$\phi_i(\gamma_i) = \frac{E(\tau_i^{2m})}{\sigma_i^{2m}} = \frac{\Gamma(\frac{2m+1}{\gamma_i})\Gamma^{m-1}(1/\gamma_i)}{\Gamma^m(3/\gamma_i)}, \quad m = 1, 2, \dots \quad (2.24)$$

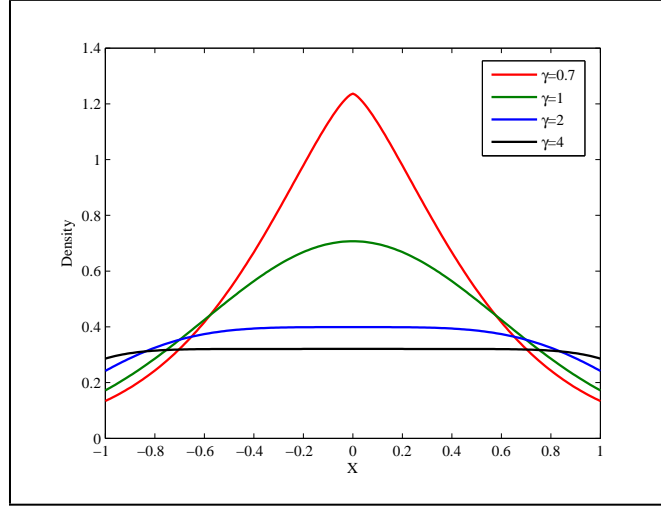


Figure 2.3: The *pdf* of generalized Gaussian distribution

where

$$\sigma_i^2 = \sigma_{\Delta_i}^2 + \sigma_{\bar{\zeta}_{ii}}^2 \quad (2.25)$$

$E(\tau_i^{2m})$ is a function of $\sigma_{\Delta_i}^2$, γ_{Δ_i} , $\sigma_{\bar{\zeta}_{ii}}^2$ and $\gamma_{\bar{\zeta}_{ii}}$. Variables $\sigma_{\Delta_i}^2$, γ_{Δ_i} , $\sigma_{\bar{\zeta}_{ii}}^2$ and $\gamma_{\bar{\zeta}_{ii}}$ are variance of Δ_i , shape parameter of Δ_i , variance of $\bar{\zeta}_{ii}$ and shape parameter of $\bar{\zeta}_{ii}$, respectively. The odd moments vanish, because the *pdf* is symmetrical. Since the generalized Gaussian *pdf* decay rate increases with the increase of the shape parameter, consider a relationship of *pdf* and moment, we assume that

$$\phi_i(\gamma_i) = \frac{l_{2i} e^{-l_{1i} \gamma_i}}{\sigma_i^{2m}}, \quad m = 1, 2, \dots; \quad i = 1, 2 \quad (2.26)$$

where the design parameters l_{2i} and l_{1i} can be obtained by matching (2.23) in advance, and $\phi_i(\gamma_i)$ is in the log domain. That is, using a fixed shape parameter, we can calculate the design parameters l_{1i} and l_{2i} by simulation,

where the fixed shape parameter is obtained as an average value from the experiment of shape parameter estimation. The unmatched part will be of uncertain factor.

From the equations (2.24) and (2.26), the shape parameter γ_i is given as follow,

$$\gamma_i = -\frac{1}{l_{1i}} \log\left(\frac{E(\tau_i^{2m})}{l_{2i}}\right), \quad i = 1, 2 \quad (2.27)$$

here, $E(\tau_i^{2m})$ is solved for each processing time step.

Considering the generalized Gaussian *pdf* of (2.21), the score function-based algorithm is obtained,

$$\hat{\mathbf{S}}(t+T) = \hat{\mathbf{S}}(t) + \mathbf{k}(t) \begin{pmatrix} g_1(\tau_{A1}) \\ g_2(\tau_{A2}) \end{pmatrix}, \quad \tau_{A1} = \tau_s, \tau_{A2} = \tau_e \quad (2.28)$$

$$\mathbf{k}(t) = (W(t)N(t)W(t)^T + L)X^T \quad (2.29)$$

where,

$$\begin{cases} g_i(\tau_{Ai}) = \gamma_i \left(\frac{\alpha_i(\gamma_i)}{\sigma_i}\right)^{\gamma_i} \tau_{Ai}^{\gamma_i-1}, & i = 1, 2 \\ \sigma_{\Delta_1}^2 = X(W(t)N(t)W(t)^T + L)X^T(1, 1) \\ \sigma_{\Delta_2}^2 = X(W(t)N(t)W(t)^T + L)X^T(2, 2) \end{cases} \quad (2.30)$$

$N(t)$ is a diagonal matrix and $W(t)$ is an upper-triangular matrix with unit entries along the diagonal. L is positive definite and is the covariance matrix of ζ_2 . $\hat{\mathbf{S}}$ is an estimate parameter vector of \mathbf{S} . In the above filter, equation (2.29) is for multiple innovations process, ill-conditioned matrix and the derivative of the score function can be avoided using $\bar{U}D\bar{U}^T$ factorization algorithm $W(t)N(t)W(t)^T$ in (2.30), the shape parameter can be obtained

on-line using (2.28), the real time viscoelasticity is estimated online. Meanwhile, the proposed algorithm guarantees that all the estimated elements of viscoelasticity are bounded.

During human multi-joint arm movements, the desired stiffness-torque relationship and viscosity-torque relationship are described as follows [89, 102],

$$\begin{bmatrix} K_{A-ss} & K_{A-se} \\ K_{A-es} & K_{A-ee} \end{bmatrix} = \begin{bmatrix} A_{11}|\tau_{s-m}| + B_{11} & A_{12}|\tau_{e-m}| + B_{12} \\ A_{21}|\tau_{e-m}| + B_{21} & A_{22}|\tau_{e-m}| + B_{22} \end{bmatrix} \quad (2.31)$$

$$\begin{bmatrix} R_{A-ss} & R_{A-se} \\ R_{A-es} & R_{A-ee} \end{bmatrix} = \begin{bmatrix} C_{11}|\tau_{s-m}| + D_{11} & C_{12}|\tau_{e-m}| + D_{12} \\ C_{21}|\tau_{e-m}| + D_{21} & C_{22}|\tau_{e-m}| + D_{22} \end{bmatrix} \quad (2.32)$$

where τ_{s-m} and τ_{e-m} are the desired joint torques, can be obtained through the following inverse dynamics,

$$\begin{bmatrix} \tau_{s-m} \\ \tau_{e-m} \end{bmatrix} = \mathbf{M}_A(\mathbf{q}_d)\ddot{\mathbf{q}}_d + \mathbf{H}_A(\dot{\mathbf{q}}_d, \mathbf{q}_d) \quad (2.33)$$

subscripts s and e denote the shoulder and elbow joints, respectively. A_{ij} , B_{ij} , C_{ij} and D_{ij} are the parameters of the linear model.

To calculate the multi-joint stiffness \mathbf{K}_A and the multi-joint viscosity \mathbf{R}_A from the torque desired τ_{s-m} and τ_{e-m} , the parameters A_{ij} , B_{ij} , C_{ij} and D_{ij} should be determined beforehand. To obtain the appropriate values of the parameters, the so-called equilibrium point control model is employed. The equilibrium control hypothesis is one of the theories used to explain the underlying principle of human motor control. In the hypothesis, the neuromuscular system is regarded to have a spring-like and damper-like property, and

the joint torque is determined by the difference between the actual and equilibrium postures of the arm. In the horizontal plane, the equilibrium point trajectory of the hand can be expressed fairly accurately as a minimum-jerk trajectory [102, 91],

$$x(t) = x_i + (x_f - x_i)\left(10\left(\frac{t}{t_f}\right)^3 - 15\left(\frac{t}{t_f}\right)^4 + 6\left(\frac{t}{t_f}\right)^5\right) \quad (2.34)$$

where x_i is the initial point, x_f is the final point, and t_f is the duration of the movement. The equilibrium point trajectory is a straight line from the initial point to the final point.

Once the equilibrium point trajectory in the Cartesian space can be determined using inverse kinematics, the joint angle in the equilibrium posture (q_{eq}) can be calculated. Then, the desired joint torque is described by

$$\tau_{Ad} = \mathbf{K}_A(\mathbf{q}_{eq} - \mathbf{q}) - \mathbf{R}_A\dot{\mathbf{q}} \quad (2.35)$$

where τ_{Ad} is the desired joint torque vector, \mathbf{q}_{eq} is the joint angle at an equilibrium position, \mathbf{q} and $\dot{\mathbf{q}}$ are the actual joint angle and velocity vectors.

The desired joint torque vector can also be obtained through inverse dynamics when external force and inertial parameters of the subject's arm are determined. The parameters A_{ij} , B_{ij} , C_{ij} and D_{ij} can be determined from several trials of point-to-point movements. In simulation, the determined parameters A_{ij} , B_{ij} , C_{ij} and D_{ij} are expressed as:

$$\begin{pmatrix} A_{11} \\ A_{12} \\ A_{21} \\ A_{22} \end{pmatrix} = \begin{pmatrix} 20 \\ 12 \\ 12 \\ 28 \end{pmatrix}, \quad \begin{pmatrix} B_{11} \\ B_{12} \\ B_{21} \\ B_{22} \end{pmatrix} = \begin{pmatrix} 20 \\ 6 \\ 6 \\ 15 \end{pmatrix}, \quad (2.36)$$

$$\begin{pmatrix} C_{11} \\ C_{12} \\ C_{21} \\ C_{22} \end{pmatrix} = \begin{pmatrix} 0.6 \\ 0.4 \\ 0.4 \\ 0.8 \end{pmatrix}, \quad \begin{pmatrix} D_{11} \\ D_{12} \\ D_{21} \\ D_{22} \end{pmatrix} = \begin{pmatrix} 0.6 \\ 0.3 \\ 0.3 \\ 0.7 \end{pmatrix}. \quad (2.37)$$

Moreover, the measured results by experiment can be evaluated based on the obtained desired stiffness and viscosity by simulation by using the following formulations,

$$E_{\mathbf{K}_A} = \frac{|\Delta \mathbf{K}_{A-ss}| + |\Delta \mathbf{K}_{A-se}| + |\Delta \mathbf{K}_{A-es}| + |\Delta \mathbf{K}_{A-ee}|}{4}, \quad (2.38)$$

$$E_{\mathbf{R}_A} = \frac{|\Delta \mathbf{R}_{A-ss}| + |\Delta \mathbf{R}_{A-se}| + |\Delta \mathbf{R}_{A-es}| + |\Delta \mathbf{R}_{A-ee}|}{4}. \quad (2.39)$$

2.4.2 Experimental system

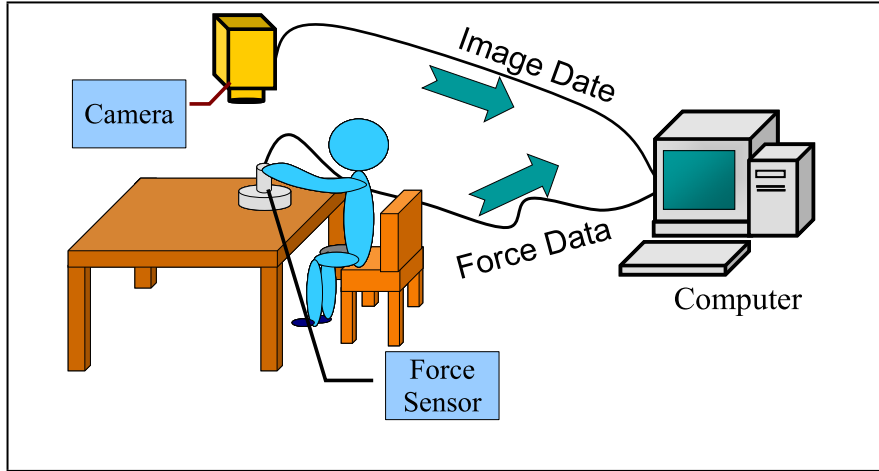


Figure 2.4: Experimental system schematic illustration

The experimental system of human multi-joint arm viscoelasticity estimation has two major parts (see Figures 2.4, 2.5): 1) Image measuring system; 2) Force measuring system. The image measuring system is comprised of a CCD camera (CIS corporation, VCC-8350CL, 648×492 , RGB24bit, 60fps)

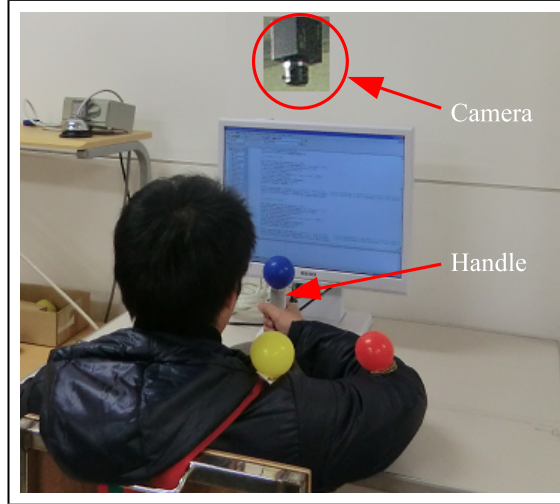


Figure 2.5: Experimental system

and an image input board (Linx, Ginga digital-CL2). The force measuring system is comprised of a force sensor and a handle, the handle is connected with the force sensor (NITTA IFS-67M25A15-I40, Ser. No. 3038), the hand holding the handle moves together, the force sensor can measure force exerted by the hand. Computer receives angular position information θ_s , θ_e from the image measuring system and generated torque information τ_s , τ_e from the force measuring system during human multi-joint arm movements. The measured experimental data of human multi-joint arm viscoelasticity is calculated online by a visual *C++* programmed real time package in the computer [96, 97, 98, 99].

2.5 Problem statement

Form (2.14), during human multi-joint arm movements, we can find that the control input torque vector can be assumed to be a function of multi-joint vis-

cosity matrix $\mathbf{R}_A(t)$, multi-joint stiffness matrix $\mathbf{K}_A(t)$, and motor command \mathbf{u} descending from CNS, and can be assumed to be divided into two parts $\tau_A(\dot{\mathbf{q}}, \mathbf{q})$ and $\tau_A(\mathbf{u})$. If we design the same structural parameters (Z_1, Z_2, Z_3) as the structural parameters (Z_{A1}, Z_{A2}, Z_{A3}) of a human multi-joint arm in building the robot arm with human-simulated motion mechanism, and the viscoelastic properties of human multi-joint arm are used in the robot arm control, there is a possibility that human skillful strategies can be integrated into the robot arm moving. Therefore, the motion mechanism of human multi-joint arm viscoelasticity and the dynamic knowledge of CNS can be considered in building the robot arm which moves like the human multi-joint arm. The real time-varying online measured human multi-joint arm viscoelasticity by proposed experimental method in [96] can be used to obtain desired the motion mechanism of human multi-joint arm-like viscoelasticity. However, the experimental method is proposed based on dynamic model (2.14), namely, the term of $\frac{\partial \tau_A}{\partial \mathbf{u}} \delta \mathbf{u}$ related to the effect of CNS of (2.14) has been removed in measuring the human multi-joint arm viscoelasticity. To make the designed robot arm move accurately and smoothly, the control input torque vector related to the effect of CNS need also to be compensated.

As a result, the objective of this dissertation is to design a robot arm which moves like a human multi-joint arm based on the motion mechanism of human multi-joint arm viscoelasticity and the dynamic knowledge of CNS. Addressing the mentioned key problems in building the robot arm by using the motion mechanism of human multi-joint arm viscoelasticity and the dynamic knowledge of CNS, in this dissertation, three different control schemes

are investigated. That is, in first scheme, the motion mechanism of human multi-joint arm viscoelasticity is used in designing robot arm control scheme, and a forward gaze model is used to compensate the terms related to the effect of CNS. In second scheme, an operator-based robust nonlinear tracking for the robot arm is proposed, an operator-based feedback control is summarized by using the motion mechanism of human multi-joint arm viscoelasticity, the motion mechanism of human multi-joint arm viscoelasticity is used in designing operator controller, an forward operator is used to compensate the terms related to the effect of CNS. In third scheme, considering it produces unknown time-varying delays while the real online measured data of human multi-joint arm viscoelasticity is fed to the designed operator controller, a new operator-based robust nonlinear tracking for the robot arm is proposed in the presence of unknown time-varying delay, the unknown time-varying delay is described by a delay operator, and the compensation operator is designed to compensate the effect of CNS and to remove the effect of unknown time-varying delay. The effectiveness of three methods is confirmed by simulation results based on experimental data.

2.6 Conclusion

In this chapter, the mathematical and theoretical background including two-link rigid robot arm dynamics, human multi-joint arm dynamics, human multi-joint arm viscoelasticity, and estimation method of human multi-joint arm viscoelasticity are introduced. Moreover, the problem discussed in this dissertation is described, which provides general outline of this dissertation.

Chapter 3

Robot arm control system design based on human multi-joint arm viscoelastic properties and a forward gaze model

3.1 Introduction

Compared with a robot arm, a human multi-joint arm exhibits outstanding manipulability in executing various tasks, especially involves contact force, such as opening a door, inserting a key and turning a knob. Some robot arms with human-simulated motion mechanism are created to imitate some of the same physical and mental tasks that the human multi-joint arm undergoes daily. Much research has been done on robot motion programming to perform tasks on the basis of human demonstrations, in which a mathematical model of skillful human movements for maneuvering a robot tool is expressed in terms of mechanical impedance. The properties of mechan-

ical impendence during human multi-joint arm movements can be mainly described as human multi-joint arm viscoelasticity. The human multi-joint arm viscoelasticity consists of multi-joint stiffness and multi-joint viscosity, which are adjusted by CNS to make the human multi-joint arm adapt to the external environment or moving objects. If the regulation mechanism of human multi-joint arm viscoelastic properties during human multi-joint movements can be clarified and modeled, we would be able to integrate these skillful human strategies into robot arm motion control.

To clarify and model the regulation mechanism of human multi-joint arm viscoelastic properties in building robot arm control system, how to obtain and use multi-joint stiffness and multi-joint viscosity and how to mimic or model the dynamic knowledge of CNS are key points. Fortunately, an integrated study procedure on real time estimation of time varying human multi-joint arm viscoelasticity has been proposed [96, 97, 98, 99], the proposed method can obtain online viscoelasticity data of human multi-joint arm during movements. Therefore, it is possible that the viscoelasticity data of human multi-joint arm is fed to the designed controller based on the motion mechanism of human multi-joint arm viscoelasticity. However, how to model or mimic the dynamic knowledge of CNS is still a challenge issue to develop robot arms with human-simulated motion mechanism. Several hypotheses suggest that it is possible to associate some cost functions to each human arm joint, and the human multi-joint arm performs movements that optimize these cost functions [1, 7, 20]. Examples of dynamic cost functions are the following: quadratic norm of joint control torques, jerks in joints,

kinetic energy, input energy and input fatigue. Some proper combinations of these functions, rather than their individual application, are also suggested. The fact that a variety of cost functions has been used to explain the principles of human arm motor control indicates that the CNS does not obey any particular cost function, but also does not violate the general physical and technical principles of optimality from which particular cost functions come out. Whatever cost function is used, the key point is that this algorithm can simulate the comfortable level during human multi-joint arm movements.

Addressing the above problems, in this chapter, a robot arm control system is designed based on time-varying viscoelastic properties which consist of multi-joint stiffness and multi-joint viscosity during human arm movements and a forward gaze model. Imitating human multi-joint arm movements, namely, in human multi-joint arm movements, the multi-joint torque is assumed to be a function of multi-joint stiffness matrix, multi-joint viscosity matrix, and motor command descending from central nervous system (CNS). In order to make the present robot arm move like a human multi-joint arm, a feedback controller and a modified forward gaze model are presented in the robot arm control system. That is, the feedback controller is designed to obtain desired motion mechanism based on real measured data from viscoelastic properties of human multi-joint arm, and the forward gaze model in which steering gains are modified using a cost function by simulating driver's optimal fashion in driving a car is used to compensate the terms related to the effect of CNS. The effectiveness of proposed method is confirmed by the simulation results based on experimental data.

In **Section 3.2**, the forward gaze model is introduced.

In **Section 3.3**, a robot arm control system design based on human multi-joint arm viscoelastic properties and a forward gaze model is investigated. To begin with, the robot arm control system scheme is proposed, where, the components of control scheme are introduced separately. Besides, how to mimic and compensate the dynamic knowledge of CNS during human multi-joint arm movements based on forward gaze model is discussed, where, by simulating the driver's optimal comfortable fashion in driving a car, and how to compensate the term related to the effect of CNS using the forward gaze model in which steering gains are modified using a cost function is explained.

In **Section 3.4**, simulation results based on experimental data is given to confirm the effectiveness of proposed control scheme.

In **Section 3.5**, the conclusion of this chapter is given.

3.2 Forward gaze model

The forward gaze model is used usually as an operation model of the car. In the forward gaze model, it is assumed that the driver watches a forward position A in Figure 3.1. At this time, the driver can predict the next position B based on the current motion state of the car. When the car go ahead through $L[m]$ to the X-axis direction, the coordinated value of Y in the gaze position A is

$$Y_L = y(t) + L\phi \quad (3.1)$$

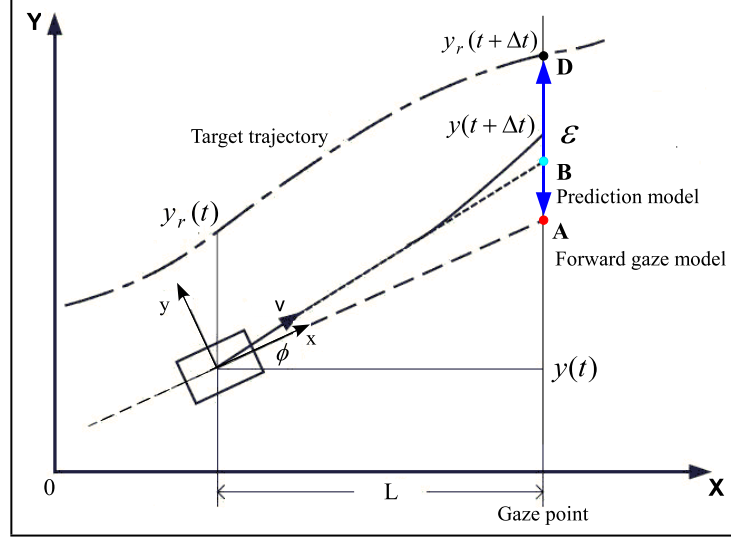


Figure 3.1: The schematic of forward gaze model

where the yaw ϕ is usual small enough. For the predictive displacement $y(t + \Delta t)$ to Y-axis direction, which can be also described by the following Taylor series,

$$y(t + \Delta t) = y(t) + \frac{dy}{dt} \Delta t + \frac{1}{2!} \frac{d^2y}{dt^2} \Delta t^2 + \frac{1}{3!} \frac{d^3y}{dt^3} \Delta t^3 + \dots \quad (3.2)$$

For this Taylor series,

$$\frac{dy}{dt} \Delta t = L\phi \quad (3.3)$$

From (3.1)-(3.3), we can find that the forward gaze model is a first-step prediction model. Based on (3.2), we can find that the predicted position B can be solved with infinite-steps prediction. In other words, the steering angle can be assumed to be fixed at a constant level throughout the preview horizon, or can be changed as frequently as every simulation step. It is obvious that larger predictive steps will result in better tracking performance.

However, it is unrealistic to expect that the drivers will change steering action more than 1-2 times over the preview horizon (0.5 to 2.0 seconds). Therefore, the modified steering is usually calculated based on the forward gaze model.

3.3 Robot arm control system design

In this section, a robot arm control system is designed based on human multi-joint arm viscoelastic properties and a forward gaze model. Where, the robot arm control system scheme, the designed controller based on the motion mechanism of human multi-joint arm viscoelastic properties, and the designed controller based on the forward gaze model by simulating driver's optimal fashion in driving a car are discussed, respectively. Firstly, the designed robot arm control system scheme is presented.

3.3.1 Robot arm control system scheme

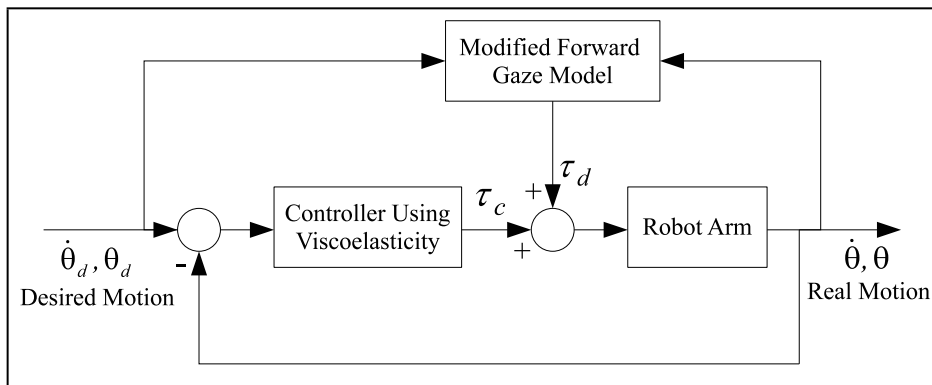


Figure 3.2: The proposed robot arm control system scheme

The designed robot arm control system is shown in Figure 3.2. In the present control system, the components, including the controller using human

multi-joint arm viscoelasticity to obtain desired motion mechanism of human multi-joint arm viscoelastic properties, the forward gaze model to compensate the terms related to effect of CNS, and a robot arm, are connected. The sum of the outputs of the controller using human multi-joint arm viscoelasticity and the modified forward gaze model is fed to the robot arm as the control input signal, namely, $\tau_{in} = \tau_c + \tau_d$.

3.3.2 Controller design based on based on human multi-joint arm viscoelastic properties

The controller using time-varying measured viscoelasticity of human multi-joint arm is designed as an ordinary feedback controller to obtain desired motion mechanism of human multi-joint arm viscoelasticity during movements, and is described by the following form,

$$\tau_c = \mathbf{R}(t)(\dot{\theta}_d - \dot{\theta}) + \mathbf{K}(t)(\theta_d - \theta) \quad (3.4)$$

where, the $\mathbf{R}(t)$ and $\mathbf{K}(t)$ are obtained by using the real measured multi-joint viscosity $\mathbf{R}_A(t)$ and stiffness $\mathbf{K}_A(t)$ data of human multi-joint arm by experiment, θ_d and θ are desired angle and real angle in robot arm control, respectively. In the following part of this section, how to design and obtain desired τ_d based the modified forward gaze model will be explained.

3.3.3 Controller design based on a forward gaze model

The modified forward gaze model is used to compensate the terms of $\frac{\partial \tau_A}{\partial \mathbf{u}} \delta \mathbf{u}$ related to the effect of CNS of (2.14) which is removed by a band-pass filter in measuring multi-joint viscosity and stiffness of human multi-joint arm. In

the following, how to compensate the terms of related to the effect of CNS using the modified forward gaze model is discussed.

Based on the forward gaze model, the lateral displacement ϵ between the gaze position A and the target position D is obtained by (see Figure 3.1):

$$\epsilon = y_r(t + \Delta t) - (y(t) + L\phi) \quad (3.5)$$

In this model, ϵ is used to calculate the modified steering. Where the dead time is little enough, the modified steering ϑ is proportional to ϵ as follows.

$$\vartheta = G\epsilon = G(y_r(t + \Delta t) - (y(t) + L\phi)) \quad (3.6)$$

G is the steering gain, which is defined as the amount of steering column shaft rotation in relation to the driver's steer angle. The steering column shaft rotation as proportional to the driver's steer angle. In driving process, steering torque, τ_p , is set proportional to driver's steer angle ϑ [rad] and steer angle rate $\dot{\vartheta}$ [rad/s], namely,

$$\tau_p = -G_1\vartheta - G_2\dot{\vartheta} = -G_1G\epsilon - G_2G\dot{\epsilon} \quad (3.7)$$

Defining $K_1 = GG_1$ and $R_1 = GG_2$, the following equation is obtained,

$$\tau_p = -K_1\epsilon - R_1\dot{\epsilon} \quad (3.8)$$

where K_1 and R_1 can be assumed to be scale factors. The effect of steering torque on the driver's feeling can be described by these objective parameters, these parameters indicate the driver's physical and mental workload, which is believed to closely relate to the driver's feeling.

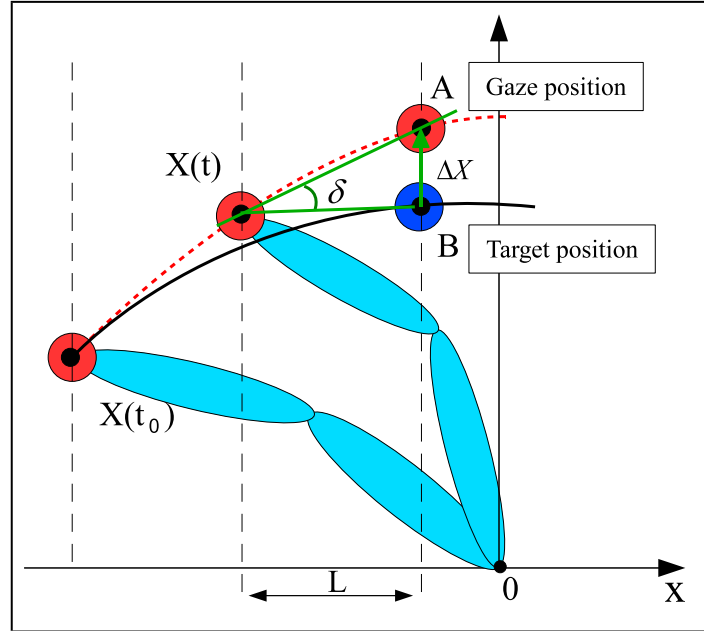


Figure 3.3: The target trajectory and endpoint position

From (2.12)-(2.14), we can find that the joint muscle generated torque is timely modified by adjusting multi-joint stiffness, multi-joint viscosity and CNS to make the human arm track the desired trajectory or moving objects in human multi-joint arm movement. Imitating human multi-joint arm, during the robot arm movement, when a new position X is given in the target trajectory (see Figure 3.3), the gaze position A can be predicted based on the forward gaze model. If there is a displacement between gaze position A and desired position B , the rotation angle and joint torques can be calculated in advance according to this displacement. So the modified forward gaze model to make a modification in endpoint position is proposed. In order to move directly from position X to target B in robot arm control system, the endpoint torque $\tau_e(t)$ in the proposed control system is calculated by

following equation,

$$\tau_e = -\mathbf{R}_c(t)\Delta\dot{\mathbf{X}} - \mathbf{K}_c(t)\Delta\mathbf{X} \quad (3.9)$$

where $\Delta\mathbf{X} = \overrightarrow{\mathbf{BA}}$ is the displacement vector from B to A . The relationship between the Cartesian variables and joint angles can be described,

$$\mathbf{X} = \begin{bmatrix} x \\ y \end{bmatrix} = \begin{bmatrix} l_1 \cos\theta_1 + l_2 \cos(\theta_1 + \theta_2) \\ l_1 \sin\theta_1 + l_2 \sin(\theta_1 + \theta_2) \end{bmatrix} \quad (3.10)$$

$$\dot{\mathbf{X}} = \begin{bmatrix} \dot{x} \\ \dot{y} \end{bmatrix} = \mathbf{J} \begin{bmatrix} \dot{\theta}_1 \\ \dot{\theta}_2 \end{bmatrix} \quad (3.11)$$

where, l_1 and l_2 denotes the length of upper and lower robot arm, respectively.

The Jacobian matrix J is given as,

$$\mathbf{J} = \begin{bmatrix} -l_1 \sin\theta_1 - l_2 \sin(\theta_1 + \theta_2) & -l_2 \sin(\theta_1 + \theta_2) \\ l_1 \cos\theta_1 + l_2 \cos(\theta_1 + \theta_2) & l_2 \cos(\theta_1 + \theta_2) \end{bmatrix} \quad (3.12)$$

\mathbf{R}_c and \mathbf{K}_c are the endpoint viscosity matrix and stiffness matrix in Cartesian space, respectively. Based on the endpoint viscosity matrix \mathbf{R}_c and stiffness matrix \mathbf{K}_c , the multi-joint viscosity matrix \mathbf{R} and multi-joint stiffness matrix \mathbf{K} in joint space can be obtained by the following relationship,

$$\mathbf{R} = \mathbf{J}^T \mathbf{R}_c \mathbf{J}, \quad \mathbf{K} = \mathbf{J}^T \mathbf{K}_c \mathbf{J} \quad (3.13)$$

from (3.9)-(3.13), we can get the following relationship,

$$\tau_d = -\mathbf{R}^*(t)(\dot{\theta}_d - \dot{\theta}) - \mathbf{K}^*(t)(\theta_d - \theta) \quad (3.14)$$

where, $\mathbf{R}^*(t)$ and $\mathbf{K}^*(t)$ are assumed to be multi-joint viscosity matrix and multi-joint stiffness matrix in joint space, respectively, which are assumed to be the term of generated torque $\frac{\partial \tau_A}{\partial \mathbf{u}} \delta \mathbf{u}$ related to the effect of CNS, namely,

the $\mathbf{R}_A^*(t)$ and $\mathbf{K}_A^*(t)$. The human multi-joint arm viscosity matrix $\mathbf{R}_A^*(t)$ can be assumed to have approximately nonlinear relationship with the human multi-joint arm stiffness matrix $\mathbf{K}_A^*(t)$, which can be described as follows [31, 32]:

$$\mathbf{R}_A^*(t) = \frac{0.42}{\sqrt{\dot{\mathbf{q}}^T(t)\dot{\mathbf{q}}(t) + 1}}\mathbf{K}_A^*(t) \quad (3.15)$$

According to (3.14) and (3.15), we can find that $\mathbf{K}_A^*(t)$ or $\mathbf{R}_A^*(t)$ can be obtained by the desired $\tau_d(t)$ in robot arm control. The following question is how to obtain $\tau_d(t)$ to control accurately and smoothly the robot arm in Figure 3.2.

3.3.4 Control algorithm based an optimal fashion principle

Imitating motion mechanism of the human multi-joint arm, the robot arm performance can be enhanced substantially. However, the benefits of human-simulated motion cannot be gained without knowledge of the principles that the CNS employs during the generation of human multi-joint arm movements. Several hypotheses suggest that it is possible to associate some cost functions to each human arm joint, and the human multi-joint arm performs movements that optimize these cost functions. Examples of dynamic cost functions are the following: quadratic norm of joint control torques, jerks in joints, kinetic energy, input energy and input fatigue. Some proper combinations of these functions, rather than their individual application, are also suggested. The fact that a variety of cost functions has been used to explain the principles of human arm motor control indicates that the CNS

does not obey any particular cost function, but also does not violate the general physical and technical principles of optimality from which particular cost functions come out. In this dissertation, special attention is paid to functions of joint “comfortable” like mentioned driver’s “feeling”. We assume the robot arm behaves in an optimal fashion, the optimal movement is determined by choosing the change in input torque ($\Delta\tau_{in}$, from current torque) such that the following cost function is minimized:

$$\Delta\tau_{inopt} = \min_{\Delta\tau_{in}} \left\{ J = \int_t^{t+T_p} [s(\eta)]^2 d\eta \right\} \quad (3.16)$$

where T_p is the preview time. The function $s(\eta)$ is defined as:

$$s(\eta) = \left(\lambda \dot{w}(\eta) \frac{d}{dt} + w(\eta) \right)^{n-1} \Theta_{err}(\eta) \quad (3.17)$$

where

$$\Theta_{err}(t) \equiv \Theta(t) - \Theta_d(t) \quad (3.18)$$

and $\Theta = [\theta^T, \dot{\theta}^T]^T$ is the real motion state of the robot arm, $\Theta_d = [\theta_d^T, \dot{\theta}_d^T]^T$ is the desired motion state of the robot arm. The constant n determines the number of derivative terms included in the function $s(\eta)$. For the case when $n=2$, (3.16) can be rewritten in the discrete-time format as,

$$\Delta\tau_{inopt} = \min_{\Delta\tau_{in}} \left\{ J = \sum_{i=1}^{N-1} \left[w(i)\Theta_{err}(t+iT) + \lambda \dot{w}(i)\dot{\Theta}_{err}(t+iT) \right]^2 \right\} \quad (3.19)$$

where the number of steps in the summation ($N-1$) is equal to preview time T_p over the step size ΔT . It can be seen that $s(\eta)$ depends on three weighting parameters: λ , $0 \leq w(i) \leq 1$, and $0 \leq \dot{w}(i) \leq 1$. The model parameters λ ,

$w(i)$, and $\dot{w}(i)$ can be adjusted repeatedly to fit different robot arms. In this paper, they are assumed to have the following form,

$$w(i) = \frac{\tanh[5/(T_p/2 - t(i)) + \beta] + 1}{2} \quad (3.20)$$

$$\dot{w}(i) = \frac{\tanh[5/(T_p/2 - t(i)) + \dot{\beta}] + 1}{2} \quad (3.21)$$

where, $t(i) \in [t_0, t_0 + \Delta T \dots T_p - \Delta T, T_p]$ is the preview time window. The $\tanh(\cdot)$ function was used to achieve a smooth transition and ensure monotonicity. By adjusting β and $\dot{\beta}$, the different preview windows can be obtained.

To find the optimal solution that minimizes the cost function given in (3.16), we use a predictive control framework. According to the robot arm dynamic model in (2.1), we can compute the forward dynamics,

$$\ddot{\theta} = \mathbf{M}(\theta)^{-1}(\tau_{in} - \mathbf{H}(\dot{\theta}, \theta)) \quad (3.22)$$

Using the standard equation of motion given in (3.22), we write $\Theta = [\theta^T, \dot{\theta}^T]^T$ in a mathematical formulation, namely, the dynamics of robot arm dynamic model can be rewritten in terms of state space as follows,

$$\dot{\Theta} = \mathbf{A}(\Theta) + \mathbf{B}(\Theta)\tau_{in} \quad (3.23)$$

where,

$$\mathbf{A}(\Theta) = \begin{bmatrix} \dot{\theta} \\ -\mathbf{M}(\theta)^{-1}\mathbf{H}(\dot{\theta}, \theta) \end{bmatrix} \quad (3.24)$$

$$\mathbf{B}(\Theta) = [\mathbf{0}, (\mathbf{M}(\theta)^{-1})^T]^T \quad (3.25)$$

Suppose (Θ_e, τ_{in}^e) is the equilibrium point and input of the system (3.23), applying the approximate linearization approach, the model (3.23) can be written as a linear state-space system using deviation variables,

$$\dot{\Omega} = \mathbf{F}\Omega + \mathbf{G}\tau_{in} \quad (3.26)$$

where, $\Omega = \Theta - \Theta_e$ is the deviation variable, and

$$\mathbf{F} = \left(\frac{\partial \mathbf{A}}{\partial \Theta} + \frac{\partial \mathbf{B}}{\partial \tau_{in}} \right) \Big|_{(\Theta^e, \tau_{in}^e)} \quad (3.27)$$

$$\mathbf{G} = \mathbf{B}(\Theta^e) \quad (3.28)$$

Based on (3.26), the output of the linear dynamics is decomposed into zero input response and zero state response,

$$\Omega(t + \zeta) = e^{\mathbf{F}\zeta}\Omega(t) + \int_0^\zeta e^{\mathbf{F}\varsigma} d\varsigma \mathbf{G}\tau_{in}(t) \equiv \mathbf{P}(\zeta)\Omega(t) + \mathbf{Q}(\zeta)\tau_{in}(t) \quad (3.29)$$

As long as the deviation variables remain small enough, the following relationship can be obtain,

$$\Theta(t) - \Theta_d(t) \equiv \Theta_{err}(t) = \Omega_{err}(t) \equiv \Omega(t) - \Omega_d(t) \quad (3.30)$$

According to (3.29) and (3.30), a simpler problem can be formulated by assuming $\tau_{in}(t + \zeta) = \tau_{inopt}$, $\forall \zeta \in [0, T_p]$, which can be solved much more easily, and the cost function given in (3.19) can be rewritten in a vector form,

$$\begin{aligned} J &= [\mathbf{W}\Theta_{err} + \lambda\dot{\mathbf{W}}\dot{\Theta}_{err}]^T [\mathbf{W}\Theta_{err} + \lambda\dot{\mathbf{W}}\dot{\Theta}_{err}] \\ &= [\mathbf{W}Q\Delta\tau_{in} + \mathbf{W}P + \lambda\dot{\mathbf{W}}\frac{d}{dt}(\mathbf{Q}\Delta\tau_{in} + \mathbf{P}) - \mathbf{W}\Theta_d - \lambda\dot{\mathbf{W}}\dot{\Theta}_d]^T \\ &\quad [\mathbf{W}Q\Delta\tau_{in} + \mathbf{W}P + \lambda\dot{\mathbf{W}}\frac{d}{dt}(\mathbf{Q}\Delta\tau_{in} + \mathbf{P}) - \mathbf{W}\Theta_d - \lambda\dot{\mathbf{W}}\dot{\Theta}_d] \quad (3.31) \end{aligned}$$

where $\mathbf{W} = \text{diag}(w)$ and $\dot{\mathbf{W}} = \text{diag}(\dot{w})$, weighting matrices with nonzero elements on the diagonals. The (3.31) can be rewritten in a more compact form as,

$$J = [\tilde{\mathbf{Q}}\Delta\tau_{in} + \tilde{\mathbf{P}} - \tilde{\Theta}_d]^T [\tilde{\mathbf{Q}}\Delta\tau_{in} + \tilde{\mathbf{P}} - \tilde{\Theta}_d] \quad (3.32)$$

where, $\tilde{\mathbf{Q}} = \mathbf{W}\mathbf{Q} + \lambda\dot{\mathbf{W}}\frac{d}{dt}\mathbf{Q}$, $\tilde{\mathbf{P}} = \mathbf{W}\mathbf{P} + \lambda\dot{\mathbf{W}}\frac{d}{dt}\mathbf{P}$, and $\tilde{\Theta}_d = \mathbf{W}\Theta_d + \lambda\dot{\mathbf{W}}\dot{\Theta}_d$. The optimal solution that minimizes the quadratic cost function (3.32) is

$$\Delta\tau_{in} = -\mathbf{U}^{-1}\mathbf{V} \quad (3.33)$$

where, $\mathbf{U} \equiv 2(\tilde{\mathbf{Q}}^T\tilde{\mathbf{Q}})$ and $\mathbf{V} \equiv 2(\tilde{\mathbf{P}} - \tilde{\Theta}_d)^T\tilde{\mathbf{Q}}$. In this research, the optimal fashion is considered that all elements of vector $\Delta\tau_{in}$ except the first are zero. As a result, using the on-line measured multi-joint viscosity $\mathbf{R}_A(t)$ and multi-joint stiffness $\mathbf{K}_A(t)$ data of human multi-joint arm obtained by experiment to get τ_c in the proposed control system, we can onlinely calculate the optimal τ_d which is assumed to be the term of generated torque $\frac{\partial\tau_A}{\partial u}\delta u$ related to the effect of CNS in (2.14), namely, the optimal $\mathbf{R}_A^*(t)$ and $\mathbf{K}_A^*(t)$ can be estimated by using (3.14) and (3.15). Then, the desired input torque $\tau_{in} = \tau_c + \tau_d$ is obtained by using human-simulated multi-joint arm viscoelastic properties to make the designed robot move skillfully and smoothly like the human multi-joint arm.

3.4 Simulation results based on experimental data

By using the designed experimental system and the proposed estimating method in [96], the multi-joint stiffness and multi-joint viscosity of a human

multi-joint arm are estimated online and shown in Figures 3.4 and 3.5, respectively, where, the human multi-joint arm (The structure parameters, $Z_1 = 0.4507$, $Z_2 = 0.1575$ and $Z_3 = 0.1530$, the physical parameters $l_1 = 0.27$ (m), $l_2 = 0.34$ (m)) moves from the start position $(x, y) = [14.32, 43.30]$ (cm) to the end position $(x, y) = [-46.68, 25.19]$ (cm). In recursive filter, the cut-off frequencies of the third-order band-pass filter to generate τ^f , θ_s^f , θ_e^f , $\dot{\theta}_s^f$ and $\dot{\theta}_e^f$ are 0.5[Hz] and 9.5[Hz]. For designing the filter, we use the case of $m = 3$, then $E(\tau_i^6)$ is obtained,

$$\begin{aligned} E(\tau_i^6) = & \sigma_{\Delta_i}^6 \phi_i^{(6)}(\gamma_{\Delta_i}) + 15\sigma_{\Delta_i}^4 \phi_i^{(4)}(\gamma_{\Delta_i})\sigma_{\zeta_{ii}}^2 \\ & + 15\sigma_{\Delta_i}^2 \phi_i(\gamma_{\zeta_{ii}})\sigma_{\zeta_{ii}}^4 + \sigma_{\zeta_{ii}}^6 \phi_i(\gamma_{\zeta_{ii}}) \end{aligned} \quad (3.34)$$

where, $\phi_i^{(6)}(\gamma_{\Delta_i}) = 15$ and $\phi_i^{(4)}(\gamma_{\Delta_i}) = 3$. The estimated shape parameters using the proposed method are shown in Figure 3.6. The experimental results have shown that the human multi-joint arm movement process is non-Gaussian, namely, the shape parameters are time varying.

In the robot arm control system simulation, the controlled robot arm is a human multi-joint arm model, the desired trajectory is the experimental trajectory of measuring human multi-joint arm stiffness and viscosity, and the estimated human multi-joint arm stiffness and viscosity are fed to the controller. Based the proposed modified forward gaze model, when a position $(x(t), y(t))$ is given during human arm-like robot movements, the estimated position $(x(t + \Delta t), y(t + \Delta t))$ after Δt seconds can be calculated based on the motion state of point $(x(t), y(t))$. If the difference is recognized between the estimated position $(x(t + \Delta t), y(t + \Delta t))$ and the desired position

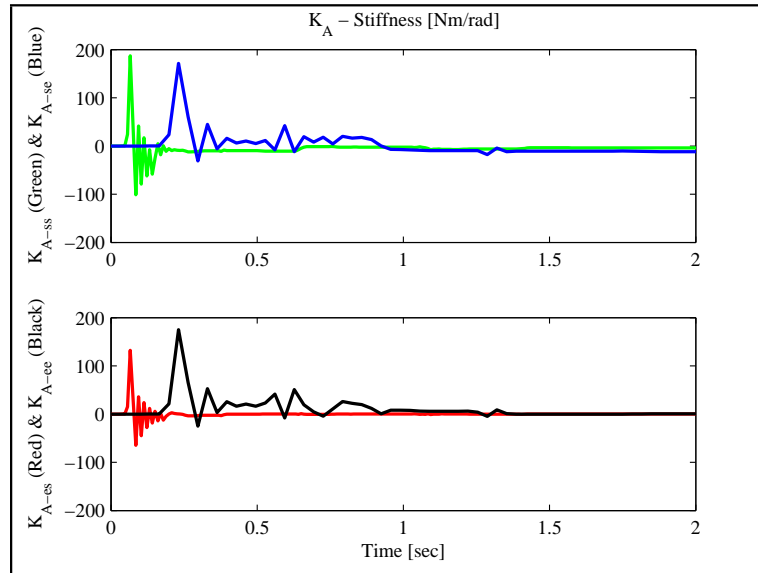


Figure 3.4: Estimated human multi-joint arm stiffness by experiment

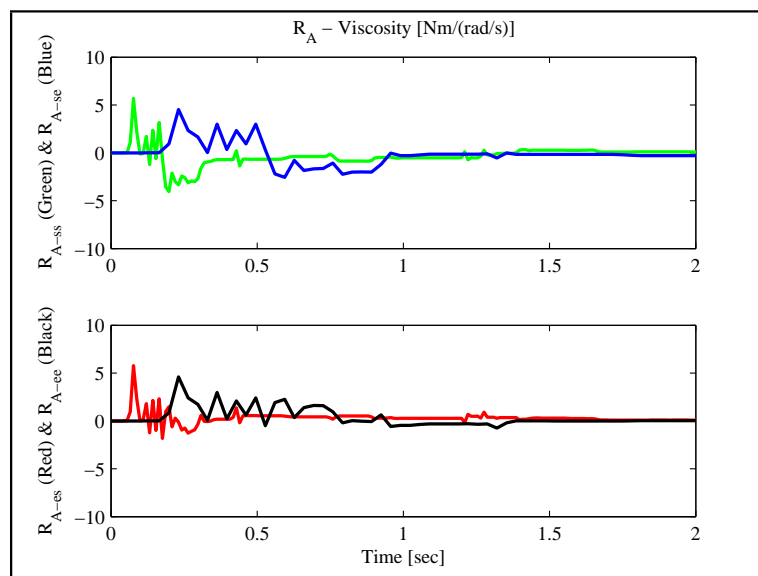


Figure 3.5: Estimated human multi-joint arm viscosity by experiment

$(x_d(t + \Delta t), y_d(t + \Delta t))$ of desired trajectory, to make the robot arm move directly to the new temporary goal point, a modification torque τ_d based the optimal $\mathbf{R}_A^*(t)$ or $\mathbf{K}_A^*(t)$ using the proposed algorithm can be obtained. To find the optimal solution that minimizes the cost function given in (3.16), firstly the parameters $\beta_y = \beta_{\dot{y}} = 0.7$ in (3.20) and (3.21), $\lambda=2$ in (3.17) are designed. Based the designed parameters and the proposed algorithm, the optimal $\mathbf{R}_A^*(t)$ and $\mathbf{K}_A^*(t)$ can be obtained and shown in Figures 3.7 and 3.8. The joint angles and endpoint position tracking simulation results using the proposed method are shown in Figures 3.9 and 3.10, respectively. From Figures 3.9 to 3.10, we can find that the simulation motion trajectory based the proposed method tracks the desired trajectory. The effectiveness of the proposed method is confirmed by simulation results based on experimental data.

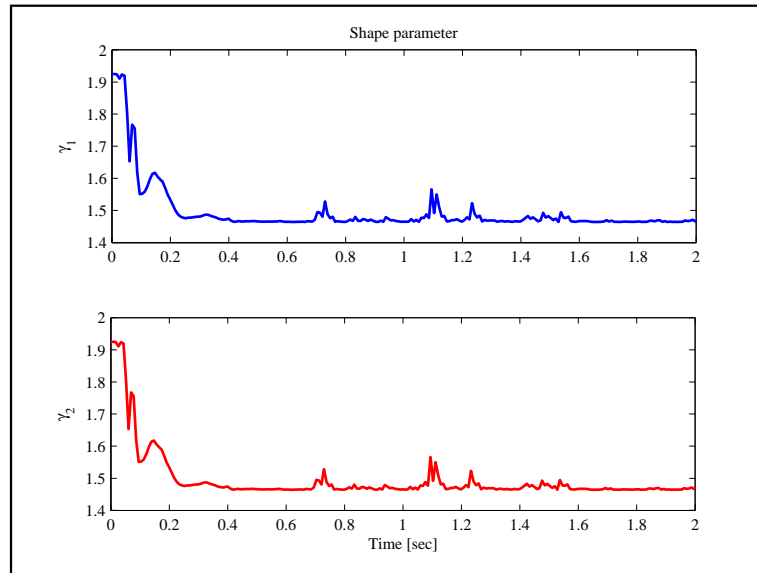


Figure 3.6: Estimated shape parameters γ_i in the experiment

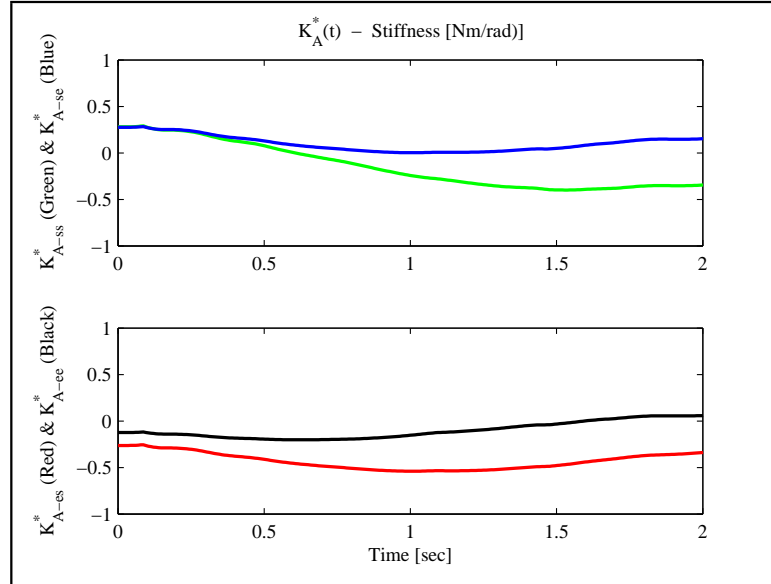


Figure 3.7: The obtained optimal $K_A^*(t)$ by simulation

3.5 Conclusion

In this chapter, the robot arm control system based on human multi-joint arm viscoelastic properties and the forward gaze model is given. The time-vary estimated viscoelastic properties of human multi-joint arm is used in designing controller of robot arm control system. The control input torque vector related to the effect of CNS is compensated by the modified forward gaze model. The feasibility of the proposed control scheme is confirmed by simulation results based on experimental data.

The merit of the proposed method is to design a controller to imitate the motion mechanism of human multi-joint arm viscoelasticity and use the forward gaze model to compensate the term related to the effect of CNS. That

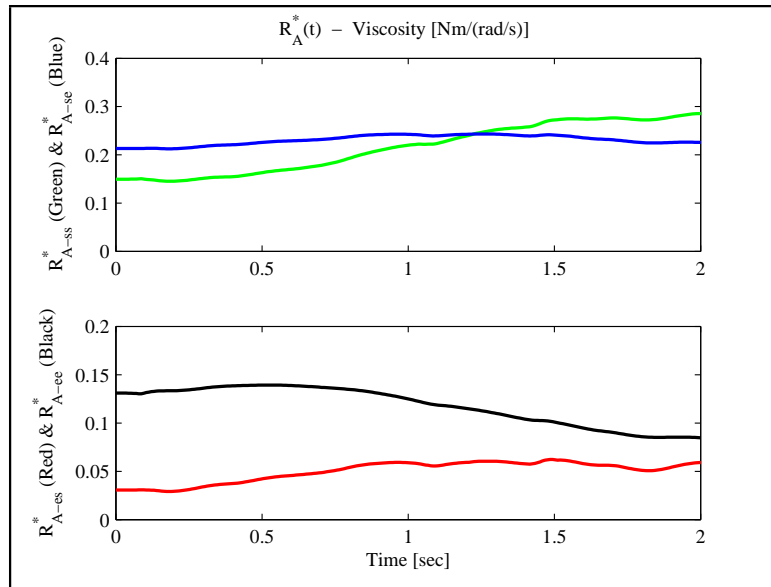


Figure 3.8: The obtained optimal $R_A^*(t)$ by simulation

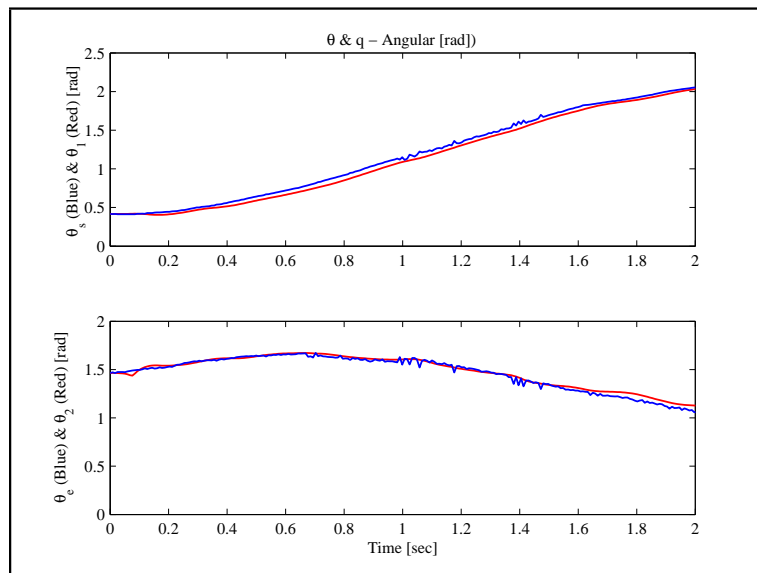


Figure 3.9: The joint angles tracking results by simulation

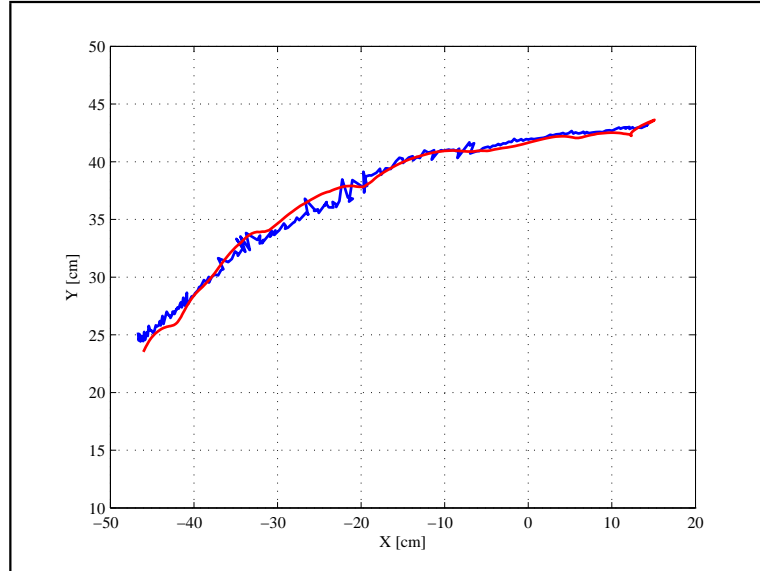


Figure 3.10: The endpoint position tracking result by simulation

is, in the proposed design scheme, the real measured data from human multi-joint arm viscoelastic properties is used to obtain desired motion mechanism, and the modified forward gaze model is proposed to compensate the term related to the effect of CNS. According to the present design scheme, the relationship between the desired response trajectory of robot arm and appropriate control input torques which are generated by the human arm-like multi-joint viscoelasticity is given, and the real trajectory can be adjusted promptly by the modified forward gaze model based on the error between desired response trajectory and predicted trajectory. The main reason to use the forward gaze model is that the method has been used for preview driver control. Namely, the model can reduce the jerkiness. As a result, the jerkiness of robot arm is reduced.

Chapter 4

Robot arm control system design based on human multi-joint arm viscoelastic properties and operator theory

4.1 Introduction

As far as we know, the robot arm is a highly nonlinear and dynamically coupled system, which is subject to disturbances and model uncertainties. Many approaches have been proposed to design controllers that are more robust so that their performance is not sensitive to modeling errors. For example, the disturbances were compensated by designing the disturbance observer based on the state space. In recent years, it is well known that the operator based approach has been a promising approach for analysis, design, stabilization and control of nonlinear system with disturbances and model uncertainties. Especially, the robust right coprime factorization approach has attracted much attention due to its convenient in researching input-output

stability problems of nonlinear system with uncertainties. Therefore, the motion mechanism of human multi-joint arm viscoelasticity and operator theory can be combined to make the designed robot arm with human-simulated motion mechanism to guarantee robust stability and realize the desired tracking performance in the presence of model uncertainties. As a result, in this Chapter, operator-based nonlinear robust stable tracking control system design for the robot arm based on human multi-joint arm viscoelastic properties and operator theory is considered.

In **Section 4.2**, the fundamental theories on operator are introduced. In detail, first, the definitions on spaces which are the basis of the research are given. Second, definitions on the characteristic of operators including linear and nonlinear, bounded input bounded output (BIBO) stable, invertible, causal, unimodular are defined, respectively. Also, the standard Lipschitz operator and generalized Lipschitz operator are described. Third, operator theory based right factorization, right coprime factorization and robust right coprime factorization of a nonlinear plant in a fairly general operator setting are introduced. Based on the conditions, BIBO stability of the nonlinear systems can be guaranteed, even for the system with unknown bounded uncertainty.

In **Section 4.3**, an operator-based robust nonlinear tracking control system design for a robot arm with human multi-joint arm-like viscoelastic properties is discussed by using robust right coprime factorization approach and a forward operator. Where, first, the robot arm control scheme is proposed, where, the components of control scheme, namely, an operator controller

based on real measured data from human multi-joint arm viscoelasticity to obtain desired motion mechanism, and the forward operator to compensate the term related to the effect of CNS are introduced separately. Secondly, an operator-based nonlinear feedback control scheme is proposed to eliminate the effect of uncertain plant. Finally, main results on conditions of robust stability and tracking are derived. Simulation results based on experimental data is given to confirm the effectiveness of proposed control scheme.

In **Section 4.4**, moreover, considering it produces unknown time-varying delays while the real measured data of human multi-joint arm viscoelasticity is fed to the designed controller based on human multi-joint arm viscoelastic properties, a new operator-based robust nonlinear tracking control system design for a robot arm with human multi-joint arm-like viscoelastic properties in the presence of unknown time-varying delays is proposed by using robust right coprime factorization approach, a delay operator and a compensation operator. To begin with, the robot arm control system scheme is proposed, where, the components of control scheme, namely, an operator controller based on real measured data from human multi-joint arm viscoelasticity to obtain desired motion mechanism, a delay operator to describe property of time-varying delay, and the compensation operator to compensate the term related to the effect of CNS and to remove the effect of unknown time-varying delay are introduced, respectively. Besides, main results on conditions of robust stability and tracking are derived. Simulation results based on experimental data is given to confirm the effectiveness of the proposed control scheme.

In **Section 4.5**, the conclusion of this Chapter is given.

4.2 Fundamental theories on operator

4.2.1 Definitions of spaces

In mathematics, a space is a set with some added structures. There are two basic spaces: linear spaces (called also vector spaces) and topological spaces, where, linear spaces are of algebraic nature, and topological spaces are of analytic nature. On linear spaces, there are real linear spaces (over the field of real numbers), complex linear spaces (over the field of complex numbers), and more generally, linear spaces over any field. In this dissertation, the used space is based on linear spaces.

Normed linear space:

Consider a space X of time functions, X is said to be a vector space if it is closed under addition and scalar multiplication. The space X is said to be *normed* if each element x in X is endowed with norm $\| \cdot \|_X$, which can be defined in any way so long as the following three properties are fulfilled:

- 1) $\|x\|$ is real, positive number and is different from zero unless x is identically zero.
- 2) $\|ax\| = |a|\|x\|$.
- 3) $\|x_1 + x_2\| \leq \|x_1\| + \|x_2\|$.

It should be mentioned that every normed space is a linear topological space.

Banach space:

Banach space is defined as a complete normed space. This means that a Banach space is a vector space X over the real or complex numbers with a norm $\|\cdot\|$ such that every Cauchy sequence (with respect to the metric $d(x, y) = \|x - y\|$) in X has a limit in X . Many spaces of sequences or functions are infinite dimensional Banach spaces.

Extended linear space:

Let Z be the family of real-valued measurable functions defined on $[0, \infty)$, which is a linear space. For each constant $T \in [0, \infty)$, let P_T be the Projection operator mapping from Z to another linear space, Z_T , of measurable functions such that

$$f_T(t) := P_T(f)(t) = \begin{cases} f(t), & t \leq T \\ 0, & t > T \end{cases} \quad (4.1)$$

where, $f_T(t) \in Z_T$ is called the truncation of $f(t)$ with respect to T . Then, for any given Banach space X of measurable functions, set

$$X^e = \{f \in Z : \|f_T\|_X < \infty, \text{ for all } T < \infty\}. \quad (4.2)$$

Obviously, X^e is a linear subspace of Z . The space so defined is called the extended linear space associated with the Banach space X .

It should be noted that the extended linear space is not complete in norm in general, and hence not a Banach space, but it is determined by a relative Banach space. The reason of using extended linear space is that all the control signals are finite time-duration in practice, and many useful techniques and results can be carried over from the standard Banach space X to the extended space X^e if the norm is suitably defined.

4.2.2 Definitions of operators

Let X and Y be linear spaces over the field of real numbers, and let X_s and Y_s be normed linear subspaces, called the stable subspaces of X and Y , respectively, defined suitably by two normed linear spaces under certain norm $X_s = \{x \in X : \|x\| < \infty\}$ and $Y_s = \{y \in Y : \|y\| < \infty\}$.

Operator:

An operator $Q : \mathbf{X} \rightarrow \mathbf{Y}$ is a mapping defined from input space \mathbf{X} to the

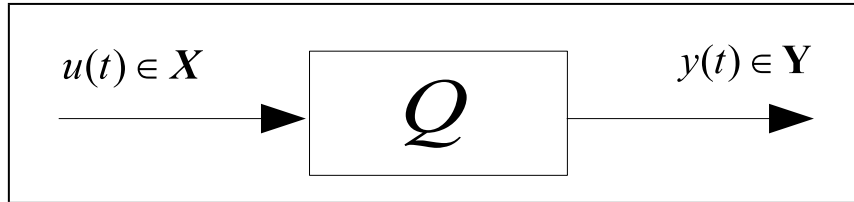


Figure 4.1: Diagram of operator

output space \mathbf{Y} . The operator Q can be described as shown in Figure 4.1 and it can also be expressed in the mathematical form as $y(t) = Q(u)(t)$ where $u(t)$ is the element of \mathbf{X} and $y(t)$ is the element of \mathbf{Y} .

Linear and nonlinear operator:

Let $Q : X \rightarrow Y$ be an operator mapping from X to Y , and denote by $\mathcal{D}(Q)$ and $\mathcal{R}(Q)$, respectively, the domain and range of Q . If the operator $Q : \mathcal{D}(Q) \rightarrow Y$ satisfies Addition Rule and Multiplication Rule

$$Q : ax_1 + bx_2 \rightarrow aQ(x_1) + bQ(x_2)$$

for all $x_1, x_2 \in \mathcal{D}(Q)$ and all $a, b \in \mathcal{C}$, then Q is said to be linear, otherwise, it is said to be nonlinear. Since linearity is a special case of nonlinearity,

in what follows ‘nonlinear’ will always mean ‘not necessarily linear’ unless otherwise indicated.

Bounded input bounded output (BIBO) stability:

Let Q be a nonlinear operator with its domain $\mathcal{D}(Q) \subseteq X^e$ and range $\mathcal{R}(Q) \subseteq Y^e$. If $Q(X) \subseteq Y$, Q is said to be input output stable. If Q maps all input functions from X_s into the output space Y_s , that is $Q(X_s) \subseteq Y_s$, then operator Q is said to be bounded input bounded output (BIBO) stable or simply, stable. Otherwise, namely, if Q maps some inputs from X_s to the set $Y^e \setminus Y_s$ (if not empty), then Q is said to be unstable. For any stable operators defined here and later in this dissertation, they always mean BIBO stable.

Invertible:

An operator Q is said to be invertible if there exists an operator P such that

$$Q \circ P = P \circ Q = I. \quad (4.3)$$

P is called the inverse of Q and is denoted by Q^{-1} , where, I is identity operator, and $Q \circ P$ (or simply $Q(P(\cdot))$ or QP) is an operation satisfying

$$\mathcal{D}(Q \circ P) = P^{-1}(\mathcal{R}(P) \cap \mathcal{D}(Q)). \quad (4.4)$$

Unimodular operator:

Let $\mathcal{S}(X, Y)$ be the set of stable operators mapping from X to Y . Then, $\mathcal{S}(X, Y)$ contains a subset defined by

$$\mathcal{U}(X, Y) = \{M : M \in \mathcal{S}(X, Y), M \text{ is invertible with } M^{-1} \in \mathcal{S}(Y, X)\}. \quad (4.5)$$

Elements of $\mathcal{U}(X, Y)$ are called unimodular operators.

Lipschitz operator:

For any subset $D \subseteq X$, let $\mathcal{F}(D, Y)$ be the family of nonlinear operators Q such that $\mathcal{D}(Q) = D$ and $\mathcal{R}(Q) \subseteq Y$. Introduce a (semi)-norm into (a subset of) $\mathcal{F}(D, Y)$ by

$$\|Q\| := \sup_{\substack{x, \tilde{x} \in D \\ x \neq \tilde{x}}} \frac{\|Q(x) - Q(\tilde{x})\|_Y}{\|x - \tilde{x}\|_X}$$

if it is finite. In general, it is a semi-norm in the sense that $\|Q\| = 0$ does not necessarily imply $Q = 0$. In fact, it can be easily seen that $\|Q\| = 0$ if Q is a constant operator (need not to be zero) that maps all elements from D to the same element in Y .

Let $Lip(D, Y)$ be the subset of $\mathcal{F}(D, Y)$ with its all elements Q satisfying $\|Q\| < \infty$. Each $Q \in Lip(D, Y)$ is called a Lipschitz operator mapping from D to Y , and the number $\|Q\|$ is called the Lipschitz semi-norm of the operator Q on D .

It is evident that a Lipschitz operator is both bounded and continuous on its domain. Next, generalized Lipschitz operator is introduced, which is defined on extended linear space.

Generalized Lipschitz operator:

Let X^e and Y^e be extended linear spaces associating respectively with two given Banach spaces X and Y of measurable functions defined on the time domain $[0, \infty)$, and let D be a subset of X^e . A nonlinear operator $Q : D \rightarrow Y^e$ is called a generalized Lipschitz operator on D if there exists a constant

L such that

$$\| [Q(x)]_T - [Q(\tilde{x})]_T \|_Y \leq L \|x_T - \tilde{x}_T\|_X \quad (4.6)$$

for all $x, \tilde{x} \in D$ and for all $T \in [0, \infty)$. Note that the least such constant L is given by the norm of Q with

$$\begin{aligned} \|Q\|_{Lip} &:= \|Q(x_0)\|_Y + \|Q\| \\ &= \|Q(x_0)\|_Y \\ &+ \sup_{T \in [0, \infty)} \sup_{\substack{x, \tilde{x} \in D \\ x_T \neq \tilde{x}_T}} \frac{\| [Q(x)]_T - [Q(\tilde{x})]_T \|_Y}{\|x_T - \tilde{x}_T\|_X} \end{aligned} \quad (4.7)$$

for any fixed $x_0 \in D$.

Based on (4.7), it follows immediately that for any $T \in [0, \infty)$

$$\begin{aligned} \| [Q(x)]_T - [Q(\tilde{x})]_T \|_Y &\leq \|Q\| \|x_T - \tilde{x}_T\|_X \\ &\leq \|Q\|_{Lip} \|x_T - \tilde{x}_T\|_X. \end{aligned} \quad (4.8)$$

Lemma 4.1 *Let X^e and Y^e be extended linear spaces associating respectively with two given Banach spaces X and Y , respectively, and let D be a subset of X^e . The following family of Lipschitz operators is a Banach space:*

$$Lip(D, Y^e) = \left\{ Q : D \rightarrow Y^e \mid \|Q\|_{Lip} < \infty \text{ on } D \right\}. \quad (4.9)$$

Proof. The proof is given in **Appendix B.1** [80].

It should be remarked that the family of standard Lipschitz operator and generalized Lipschitz operator are not comparable since they have different domains and ranges. The definition of generalized Lipschitz operator has

been proved more useful than standard Lipschitz operator for nonlinear system control and engineering in the considerations of stability, robustness, uniqueness of internal control signals. For any operators defined throughout the paper, they are always assumed to be generalized Lipschitz operators. For simplicity, Lipschitz operator is always mean the one defined in generalized case in this dissertation.

In this dissertation, $Lip(D) = Lip(D^e, D^e)$. In the following, the causality is introduced, which is a basic requirement for realizing a physical system.

Causal:

Let X^e be the extended linear space associated with a given Banach space X , and let $Q : X^e \rightarrow X^e$ be a nonlinear operator describing a nonlinear control system. Then, Q is said to be causal if and only if

$$P_T Q P_T = P_T Q \quad (4.10)$$

for all $T \in [0, \infty)$, where P_T is the projection operator.

The physical meaning behind the definition of causality may be understood as follows. If the system outputs depend only on the present and past values of the corresponding system inputs, then we have $Q P_T(u) = Q(u)$ for all input signals u in the domain of Q , so that $P_T Q P_T = P_T Q$. Conversely, if $P_T Q P_T = P_T Q$ for all $T \in [0, \infty)$, then we have $P_T Q (I - P_T)(u) = 0$ for all input u in the domain of Q , which implies that any future value of a system input, $(I - P_T)(u)$, does not affect the present and past values of the corresponding system output given by $P_T Q(\cdot)$, or in other words, system outputs depend only on the present and past values of the corresponding

system inputs.

Lemma 4.2 *A nonlinear operator $Q : X^e \rightarrow X^e$ is causal if and only if for any $x, y \in X^e$ and $T \in [0, \infty)$, $x_T = y_T$ implies $[Q(x)]_T = [Q(y)]_T$.*

Proof. The proof is given in **Appendix B.2** [80].

Lemma 4.3 *If $Q : X^e \rightarrow X^e$ is a generalized Lipschitz operator, then Q is causal.*

Proof. The proof is given in **Appendix B.3** [80].

Note that a nonlinear operator may produce non-unique outputs from an input, particularly for a set-valued mapping. However in real practice, the internal signals in the system are always required to be unique. It is clear from the definition of generalized Lipschitz operator that it guarantees the uniqueness requirement.

4.2.3 Right coprime factorization

Right factorization:

An operator based given process with right factorization P is shown in Figure 4.2, The operator process P is said to have a right factorization composed of two operators N and D , where operators N and D are stable and D is invertible. N and D^{-1} can be either linear or nonlinear. Suppose P is a nonlinear operator, for instance, both N and D are nonlinear operators in general. Such a factorization of P is denoted by (N, D) and space W is called a quasi-state space of P .

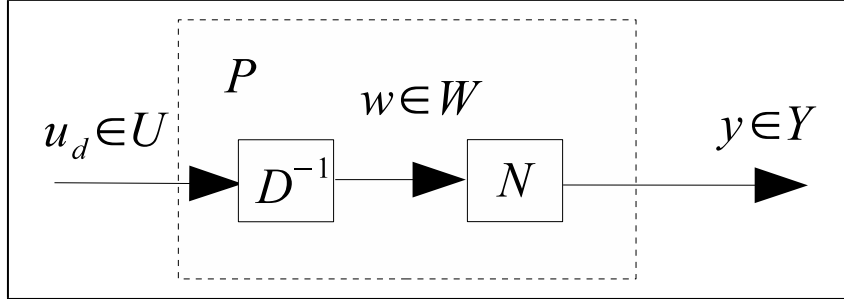


Figure 4.2: Right factorization of an operator process

Right coprime factorization:

Let (N, D) be a right factorization of P . If the two operators N and D together satisfy the following Bezout identity

$$SN + RD = M, \quad \text{for some } M \in \mathcal{U}(W, U) \quad (4.11)$$

for some operators A and B , where B is invertible and M is unimodular operator, then the right factorization is said to be coprime. An operator theory based right coprime factorization system is shown in Figure 4.3, U and Y are used to denote the input and output spaces of the given process operator P . Usually, P is unstable and (N, D, A, B) are to be determined.

It's worth to mention that the initial state should also be considered, that is, $AN(w_0, t_0) + BD(w_0, t_0) = M(w_0, t_0)$ should be satisfied. In this dissertation, $t_0 = 0$ and $w_0 = w_0(t_0)$ are selected.

In most of the research, the researchers choose $W = U$ briefly, meaning U and W are same linear space and $M = I$, I is the identity operator.

Well-posedness:

The feedback control system shown in Figure 4.3 is said to be well-posed, if

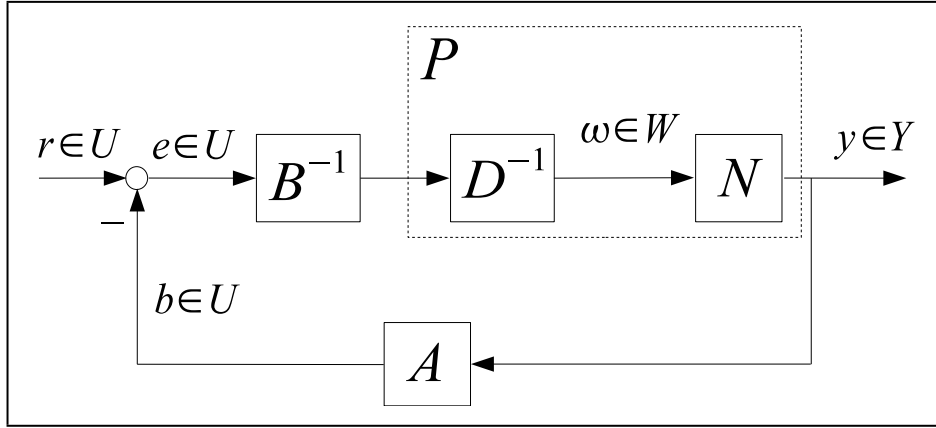


Figure 4.3: Operator based nonlinear feedback control system

for every input signal $r \in U$, all signals in the system (i.e., e , u , w , b and y) are uniquely determined.

Overall stable:

The feedback control system shown in Figure 4.3 is said to be overall stable, if $r \in U_s$, implies that $u \in U_s$, $y \in V_s$, $w \in W_s$, $e \in U_s$ and $b \in U_s$.

Lemma 4.4 *Assume that the system shown in Figure 4.3 is well-posed. If the system has a right factorization $P = ND^{-1}$, then the system is overall stable if and only if the operator L in (4.11) is a unimodular operator.*

Proof: The proof is given in **Appendix B.4** [80].

Robust right coprime factorization

Generally speaking, for nonlinear process, if the corresponding control system with uncertainty remains stable, the system is said to be robust stable. As for nonlinear feedback control systems with unknown bounded uncer-

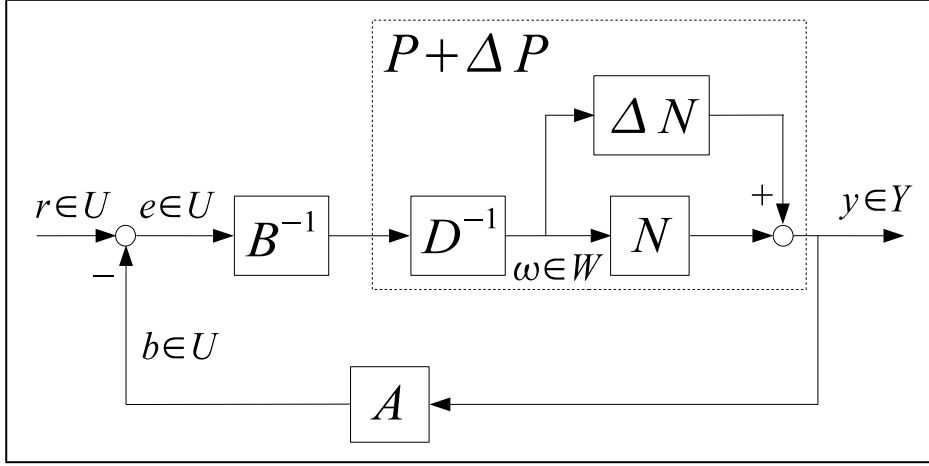


Figure 4.4: Operator based nonlinear feedback control system with uncertainty

tainty, a robust condition about right coprime factorization was derived in [81].

Operator theory based nonlinear feedback control system with uncertainty is given in Figure 4.4, where the nominal process and uncertainty are P and ΔP , respectively, and the overall process \tilde{P} is $\tilde{P} = P + \Delta P$. The right factorization of the nominal process P and the overall process \tilde{P} are

$$P = ND^{-1} \quad (4.12)$$

and

$$P + \Delta P = (N + \Delta N)D^{-1} \quad (4.13)$$

where N , ΔN , and D are stable operators, D is invertible, ΔN is unknown but the upper and lower bounds are known. According to (4.1) and **Lemma 4.4**, the BIBO stability of the nonlinear feedback control system with uncer-

tainty can be guaranteed provided that

$$A(N + \Delta N) + BD = \tilde{M} \quad (4.14)$$

where, \tilde{M} is unimodular operator. This Bezout identity is called perturbed Bezout identity in this dissertation. For obtaining this condition, [?] referred that if

$$A(N + \Delta N) = AN \quad (4.15)$$

then the system is stable because of the fact that

$$A(N + \Delta N) + BD = AN + BD = M. \quad (4.16)$$

As a matter of fact, the condition is restrictive and is difficult to design S satisfying (4.15) because that ΔN is unknown. For improving that, an extended condition, robust right coprime factorization condition was proposed in [81].

Lemma 4.5 *Let U_s^e be a linear subspace of the extended linear space U^e associated with a given Banach space U_B , and let $(A(N - \Delta N) + AN)M^{-1} \in Lip(U_s^e)$. Let the Bezout identity of the nominal process and the real process be $AN + BD = M \in \mathcal{U}(W, U)$, $A(N + \Delta N) + BD = \tilde{M}$, respectively. If*

$$\|(A(N + \Delta N) - AN)M^{-1}\| < 1 \quad (4.17)$$

then the system shown in Figure 4.4 is stable.

Proof: The proof is given in **Appendix B.5** [81] .

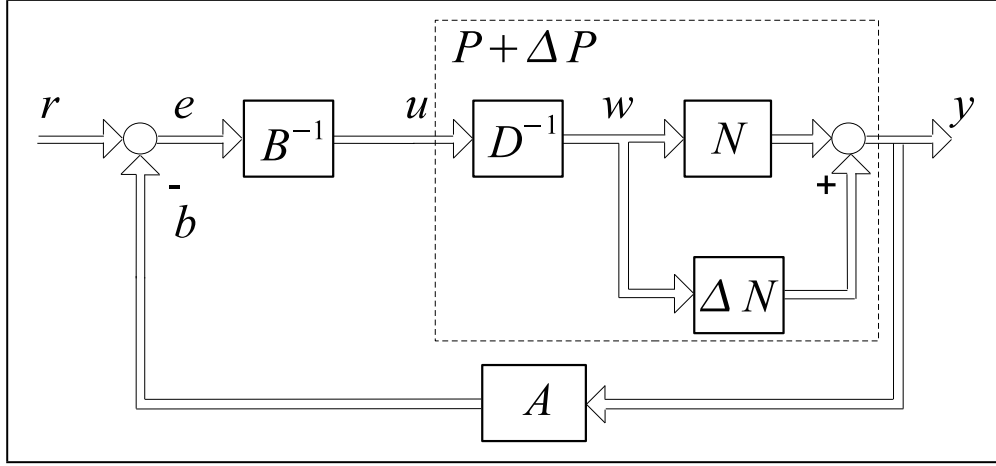


Figure 4.5: Operator based MIMO nonlinear feedback system with uncertainties

Similarly, operator theory based robust control for multi-input multi-output (MIMO) nonlinear systems with uncertainties shown in Figure 4.5 was considered in [88], where, $P = (P_1, \dots, P_n)$ is nominal plant and $\Delta P = (\Delta P_1, \dots, \Delta P_n)$ is uncertainty. Suppose that the nominal plant P and real plant $\tilde{P} = P + \Delta P$ have right factorization as $P = ND^{-1}$ and $\tilde{P} = \tilde{N}D^{-1} = (N + \Delta N)D^{-1}$, namely

$$\begin{cases} P_i = N_i D_i^{-1}, & i = 1, 2, \dots, n \\ P_i + \Delta P_i = (N_i + \Delta N_i) D_i^{-1}, & i = 1, 2, \dots, n \end{cases} \quad (4.18)$$

where N_i , ΔN_i and D_i are stable such that D_i^{-1} is invertible, ΔN_i is unknown but the upper and lower bounds are known. Consequently, for the MIMO nonlinear system with uncertainties and coupling effects, the Bezout identity of the nominal plant and the real plant are $A_i N_i + B_i D_i = M_i \in S(W, U)$, $A_i(N_i + \Delta N_i) + B_i D_i = \tilde{M}_i \in S(W, U)$, respectively, then the robust BIBO

stability can be guaranteed provided that

$$\left\| [A_i(N_i + \Delta N_i) - A_i N_i] M_i^{-1} \right\| < 1, \quad i = 1, 2, \dots, n \quad (4.19)$$

4.3 Robot arm control system design based on human multi-joint arm viscoelastic properties and a forward operator

In this section, an operator-based robust nonlinear tracking control for the robot arm based on human multi-joint arm-like viscoelastic properties and a forward operator is considered. Where, the robot arm control scheme is proposed, an operator-based nonlinear feedback control scheme is presented to eliminate effect of uncertain plant, and main results on conditions of robust stability and tracking are derived. Firstly, the robot arm control scheme is introduced.

4.3.1 Robust nonlinear tracking control scheme

According to the dynamic model of robot arm in (2.1), we can see that the two-input two-output process is nonlinear system with coupling effect. Generally, it is difficult to obtain the real values in modeling the structural parameters of robot arm. Therefore, there exists the measurement error between the actual value of structural parameters and the value obtained by measuring. Moreover, there exist unpredictable disturbances in the control system. In this dissertation, the measurement error and disturbances are considered to be uncertainties of model. For the robot arm

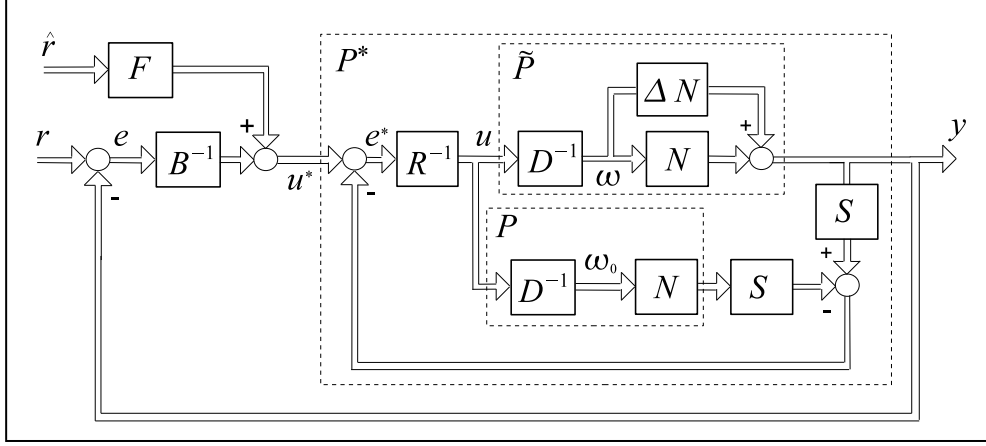


Figure 4.6: The proposed operator-based robust nonlinear tracking control for the robot arm

with uncertainties, an operator-based robust nonlinear output tracking control scheme is proposed by using robust right coprime factorization approach and the forward operator. The proposed robust nonlinear tracking structure is shown in Figure 4.6, where, the overall plant is $\tilde{P} = (\tilde{P}_1, \tilde{P}_2)$, which includes two parts, the nominal plant $P = (P_1, P_2)$ and the uncertain plant $\Delta P = (\Delta P_1, \Delta P_2)$, namely, $\tilde{P} = P + \Delta P$. The nominal plant P and overall plant \tilde{P} are assumed to have right factorization as $P_i = N_i D_i^{-1}$ ($i=1, 2$) and $\tilde{P}_i = P_i + \Delta P_i = (N_i + \Delta N_i) D_i^{-1}$ ($i=1, 2$), respectively, N_i , ΔN_i , and D_i ($i=1, 2$) are stable operators, D_i is invertible, ΔN_i is unknown but the upper and lower bounds are known. For the robot arm, right factorizations N and D of the robot arm dynamics in (2.1) are shown as the following forms,

$$\begin{cases} D_i(\omega_i)(t) = \mathbf{M}_i(\omega(t))\ddot{\omega}_i(t) + \mathbf{H}_i(\dot{\omega}(t), \omega(t)), & i = 1, 2 \\ N_i(\omega_i)(t) = \omega_i(t), & i = 1, 2 \end{cases} \quad (4.20)$$

$r = (\theta_{1d}, \theta_{2d})$ and $y = (\theta_1, \theta_2)$ are the reference input and plant output, respectively, $u = (u_1, u_2)$ is joint torque control input. $\hat{r} = (\hat{\theta}_1, \hat{\theta}_2)$ is an

estimated value of r , and is represented as the rapid prediction of movement. In this paper, for brevity, we limit the problem on the case of $\hat{r} = r$. The operator controllers S and R are designed to eliminate effect of model uncertainties, $u^* = (u_1^*, u_2^*)$ is the input of the equivalent plant P^* . The controller B is stable linear control operator and invertible, and is designed to obtain desired motion mechanism of human multi-joint arm using time-varying measured human multi-joint arm viscoelasticity. F is the forward operator, and is designed to compensate the effect of CNS during human multi-joint arm movements. In the following, how to design the operator controllers S and R to eliminate effect of model uncertainties, and how to design the operator controller B and the forward operator F to guarantee the robust stable tracking conditions will be explained.

4.3.2 Eliminating effect of model uncertainties

The fact that the uncertain plant ΔP is unknown generates difficulties in designing operator controllers to obtain the desired performance. In order to solve that, a nonlinear feedback control scheme based on operator approach as a part of the proposed robust nonlinear output tracking control system is designed, and is shown in Figure 4.7. Then, concerning the nonlinear control scheme with uncertainties shown in Figure 4.7, it follows that

$$\begin{aligned} e^*(t) &= u^*(t) - S(N + \Delta N)(\omega)(t) + SN(w_0)(t) \\ &= RD(w_0)(t) \end{aligned} \tag{4.21}$$

That is,

$$u^*(t) - S(N + \Delta N)(\omega)(t) = (RD - SN)(w_0)(t) \quad (4.22)$$

thus the equivalent block diagram of Figure 4.7 is given as Figure 4.8.

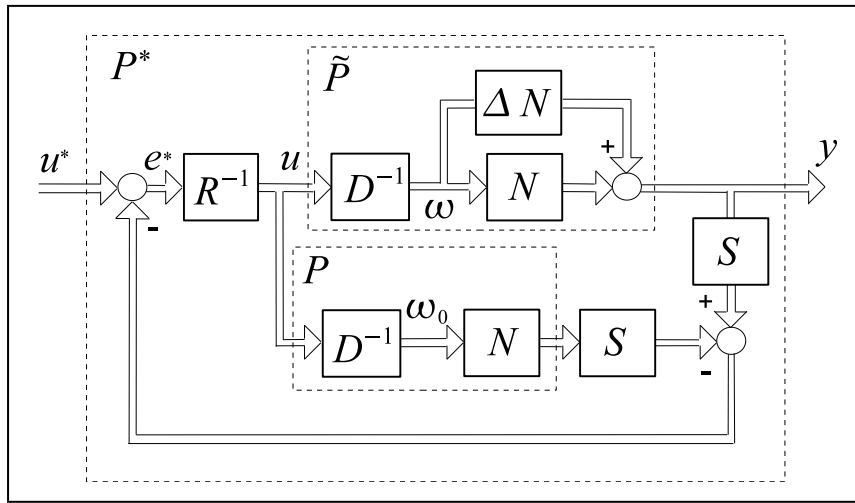


Figure 4.7: An operator-based nonlinear feedback control scheme

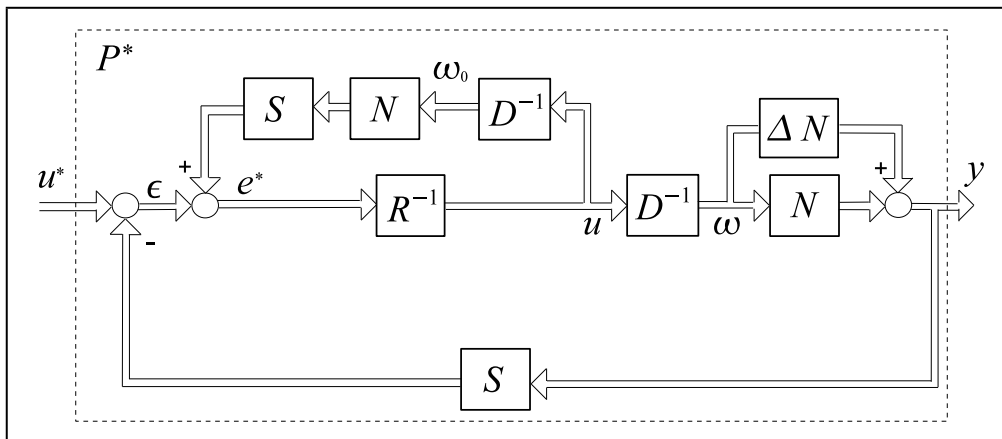


Figure 4.8: Equivalent system of Figure 4.7

Based on the concept of Lipschitz operator and Contraction Mapping

Theorem, the effect of uncertainties can be eliminated by designing the operator controllers S and R under the following conditions.

Theorem 1. The proposed nonlinear feedback control system with uncertainties shown in Figure 4.7, if

$$\begin{cases} SP = I \\ R = I \end{cases} \quad (4.23)$$

then the new equivalent plant $P^* = P$, and the effect of uncertainties can be eliminated, where, I is an identity operator.

Proof. For the nonlinear feedback system shown in Figure 4.8, if the conditions (4.23) are satisfied, it has that

$$u^*(t) - S(y)(t) + SND^{-1}(u)(t) = R(u)(t) \quad (4.24)$$

That is,

$$\begin{aligned} u^*(t) &= S(y)(t) - SP(u)(t) + R(u)(t) \\ &= P^{-1}(y)(t) - I(u)(t) + I(u)(t) \\ &= P^{-1}(y)(t) \end{aligned} \quad (4.25)$$

Then, $y(t) = P(u^*)(t)$, and the new equivalent plant $P^* = P$, the effect of uncertainties can be eliminated, this completes the proof. Then the equivalent block diagram of Figure 4.8 is given as Figure 4.9.

For the new equivalent plant P^* , right factorizations N^* and D^* of the plant P^* are shown as the following forms,

$$\begin{cases} D_i^*(\omega_i^*)(t) = \mathbf{M}_i(\omega_i^*(t))\dot{\omega}_i^*(t) + \mathbf{H}(\dot{\omega}_i^*(t), \omega_i^*(t)), & i = 1, 2 \\ N_i^*(\omega_i^*)(t) = \omega_i^*(t), & i = 1, 2 \end{cases} \quad (4.26)$$

where operators N_i^* and D_i^* are stable, and D_i^* are invertible.

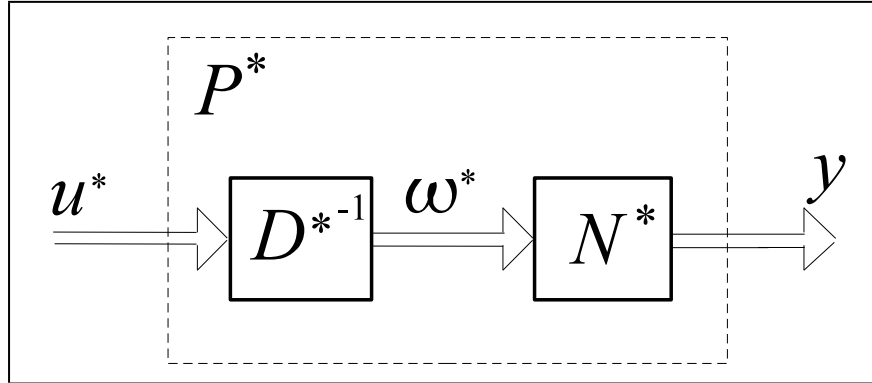


Figure 4.9: Equivalent block diagram Figure 4.8

4.3.3 Main results on conditions of robust stability and tracking

According to **Theorem 1**, the equivalent block diagram of Figure 4.6 can be obtained and shown in Figure 4.10.

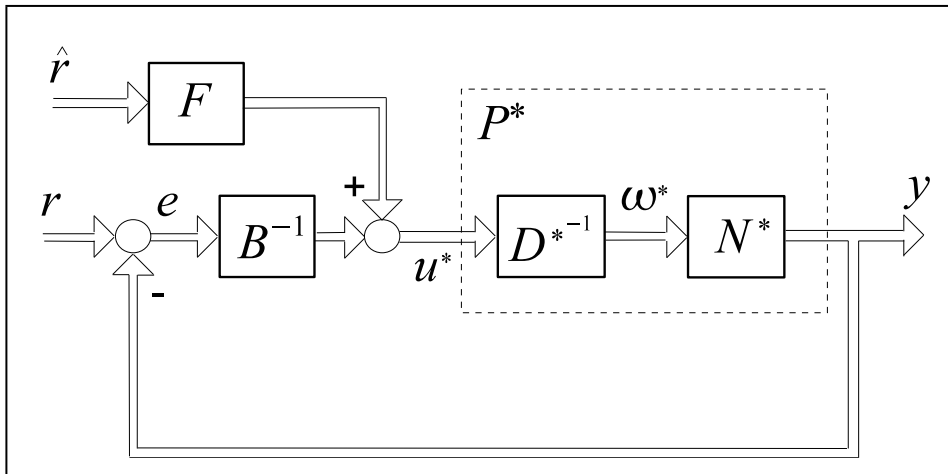


Figure 4.10: Equivalent block diagram Figure 4.6

Concerning the robust nonlinear tracking control system for the robot arm with uncertainties shown in Figure 4.6 or the equivalent system shown

in Figure 4.10, the operator controller B is designed to satisfy that $M_i = N_i^* + B_i D_i^*$ ($i=1, 2$) are unimodulars. The stable operator controller B is designed as following,

$$B^{-1}(e)(t) = -\mathbf{R}(t)\dot{e}(t) - \mathbf{K}(t)e(t) \quad (4.27)$$

where, $\mathbf{R}(t)$ and $\mathbf{K}(t)$ are assumed to be the desired time-varying two-joint viscosity and time-varying two-joint stiffness, respectively, and can be defined based on the dynamics of robot arm. According to robot arm dynamic model in (2.1), the following equation can be obtained,

$$\begin{aligned} \mathbf{M}(\theta)\frac{d\ddot{\theta}}{dt} + \frac{\partial \mathbf{H}(\dot{\theta}, \theta)}{\partial \dot{\theta}} \frac{d\dot{\theta}}{dt} + \left[\frac{\partial \mathbf{M}(\theta)\ddot{\theta}}{\partial \theta} + \frac{\partial \mathbf{H}(\dot{\theta}, \theta)}{\partial \theta} \right] \frac{d\theta}{dt} \\ = \frac{\partial \tau}{\partial \dot{\theta}} \ddot{\theta} + \frac{\partial \tau}{\partial \theta} \dot{\theta} \\ = -\mathbf{R}(t)\ddot{\theta} - \mathbf{K}(t)\dot{\theta} \end{aligned} \quad (4.28)$$

where, the viscosity matrix $\mathbf{R}(t)$ and the stiffness matrix $\mathbf{K}(t)$ are defined, respectively.

$$-\frac{\partial \tau}{\partial \dot{\theta}} \equiv \mathbf{R}(t) = \begin{pmatrix} R_{11} & R_{12} \\ R_{21} & R_{22} \end{pmatrix} \quad (4.29)$$

$$-\frac{\partial \tau}{\partial \theta} \equiv \mathbf{K}(t) = \begin{pmatrix} K_{11} & K_{12} \\ K_{21} & K_{22} \end{pmatrix} \quad (4.30)$$

In this research, the viscosity matrix $\mathbf{R}(t)$ and the stiffness matrix $\mathbf{K}(t)$ are obtained by using the online measured viscoelastic experimental data $\mathbf{R}_A(t)$ and $\mathbf{K}_A(t)$ of human multi-joint arm with the approximate same structural parameters as the robot arm.

Based on the equations (2.1) and (4.28), the following equation is obtained,

$$\mathbf{M}(\theta)\ddot{\theta} + \mathbf{H}(\dot{\theta}, \theta) = -\mathbf{R}(t)\dot{\theta} - \mathbf{K}(t)\theta + C \quad (4.31)$$

where C is an unknown constant. Based on the equations (4.27) and (4.31), and,

$$\begin{aligned} B^{-1}(e)(t) &= -\mathbf{R}(t)\dot{e}(t) - \mathbf{K}(t)e(t) \\ &= \mathbf{M}(e(t))\ddot{e}(t) + \mathbf{H}(\dot{e}(t), e(t)) \end{aligned} \quad (4.32)$$

According to the designed right factorizations $N_i^*(\omega_i^*)(t)$, $D_i^*(\omega_i^*)(t)$, and $B^{-1}(e)(t)$, the following relationship is obtained,

$$M_i = N_i^* + B_i D_i^* = 2\omega_i^*(t), \quad i = 1, 2 \quad (4.33)$$

are unimodulars.

Based on the designed operator controller B , then the output tracking performance can be realized by designing the forward operator F .

Theorem 2. The proposed nonlinear tracking control for the robot arm based on human multi-joint arm viscoelastic properties and the forward operator shown in Figure 4.6, if

$$FP = I \quad (4.34)$$

then the output $y(t)$ tracks to the reference input $r(t)$.

Proof. Based on the proposed design scheme, the system shown in Figure

4.11 is equivalent to Figure 4.10, where, $M = N^* + BD^*$, then,

$$\begin{aligned}
 y(t) &= NM^{-1}(r(t) + BF\hat{r}(t)) \\
 &= NM^{-1}(r(t) + BP^{-1}\hat{r}(t)) \\
 &= NM^{-1}(r(t) + BDN^{-1}\hat{r}(t)) \\
 &= NM^{-1}(r(t) + BD^*N^{-1}\hat{r}(t)) \\
 &= NM^{-1}(N^* + BD)N^{-1}r(t) \\
 &= NM^{-1}MN^{-1}r(t) \\
 &= r(t)
 \end{aligned} \tag{4.35}$$

This completes the proof.

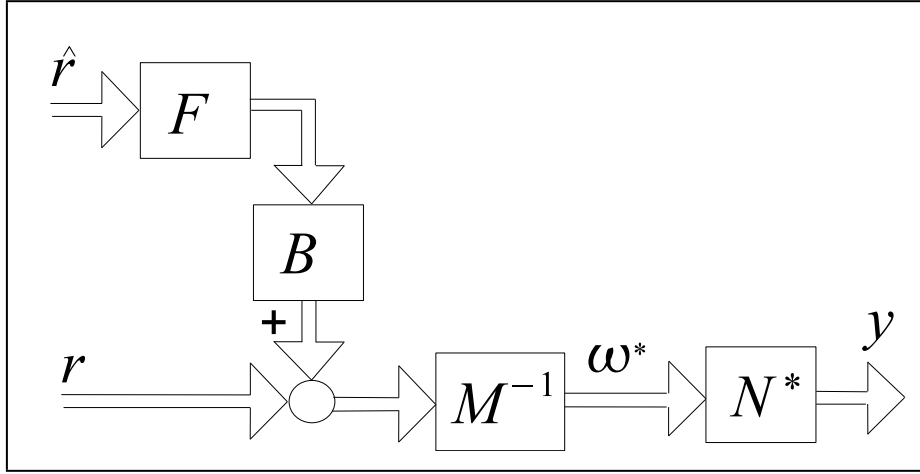


Figure 4.11: Equivalent block diagram Figure 4.5

From **Theorem 1** and **Theorem 2** we can find that based on the proposed robust nonlinear tracking scheme, the effect caused by the uncertain plant can be eliminated by designing the operator controllers S and R in the

designed operator-based nonlinear feedback control system, the BIBO stability can be guaranteed by the designed operator controller B . The output tracking performance can be realized by designed operator controller B and the forward operator F .

4.3.4 Simulation results based on experimental data

By using the designed experimental system and the proposed estimating method in [96], the multi-joint stiffness and multi-joint viscosity of a human multi-joint arm are estimated online and shown in Figures 4.12 and 4.13, respectively, where, the human multi-joint arm (The structure parameters, $Z_1 = 0.4507$, $Z_2 = 0.1575$ and $Z_3 = 0.1530$, the physical parameters $l_1=0.27(\text{m})$, $l_2=0.34(\text{m})$) moves from the start position $(x, y) = [-2.8728, 32.7503](\text{cm})$ to the end position $(x, y) = [21.9969, 36.1739](\text{m})$.

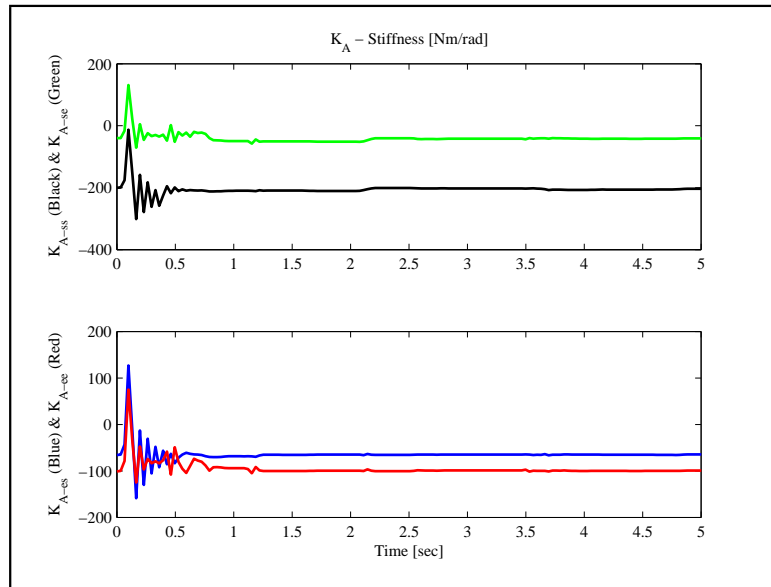


Figure 4.12: Estimated human multi-joint arm stiffness by experiment

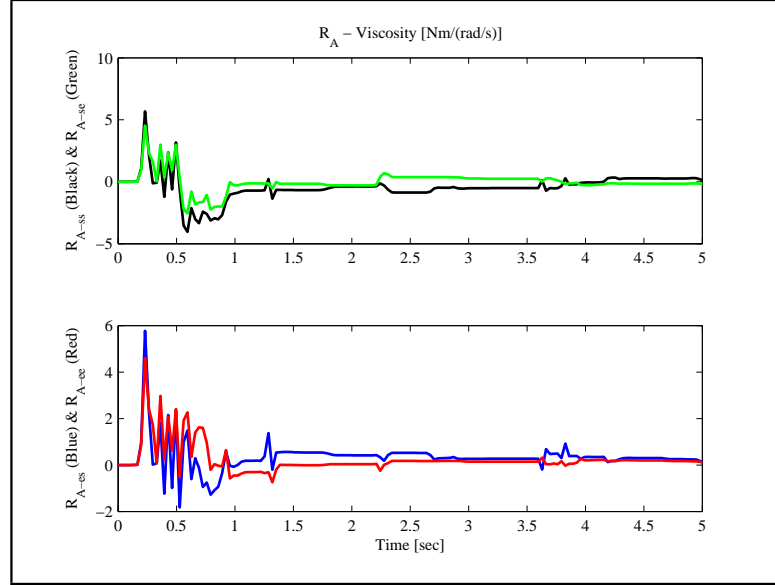


Figure 4.13: Estimated human multi-joint arm viscosity by experiment

In the proposed robot arm control system simulation, the controlled robot arm is a human multi-joint arm model, the desired trajectory is the experimental trajectory of measuring joint stiffness and joint viscosity of human multi-joint arm, and the estimated joint stiffness and joint viscosity are fed to the operator controller B . The controllers S and R are designed by conditions (4.23), namely, $SP = I$ and $R = I$. The forward operator F is designed based on conditions (4.34), namely, $FP = I$. The uncertainties of structural parameters of the robot arm is considered to be $Z_i = Z_i^* + \Delta Z_i$, $\Delta = 0.05$, where Z_i^* is assumed to be real value. Moreover, the disturbances is considered to be $\tau_d = 0.5 + 0.05 * \sin(2\pi t)$. The effect of structural uncertainties and disturbances is summarized into ΔN . Based on the proposed method, the joint angles and endpoint position tracking simulation results are shown

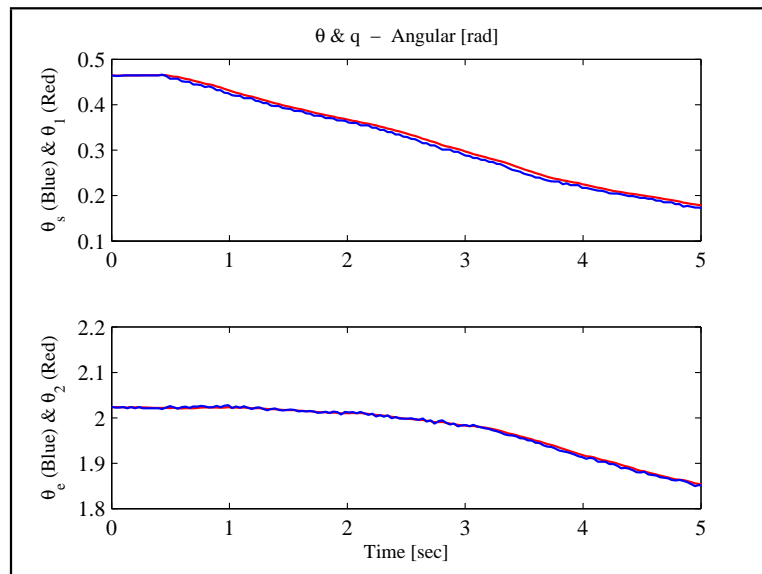


Figure 4.14: The joint angles tracking results by simulation

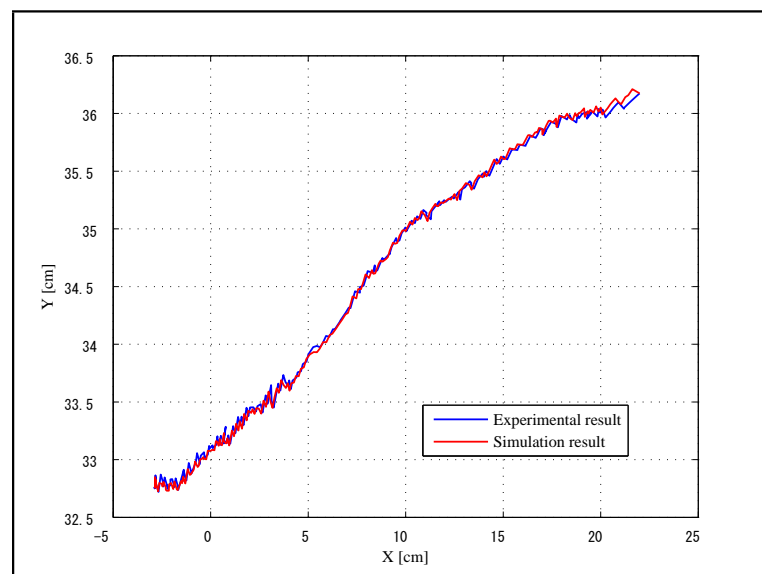


Figure 4.15: The endpoint position tracking result by simulation

in Figures 4.14 and 4.15, respectively. From Figures 4.14 and 4.15, we can find that the simulation motion trajectory based on the proposed method can track the desired trajectory, and the effectiveness of the proposed control system can be confirmed by simulation results based on experimental data.

4.4 Robot arm control system design based on human multi-joint arm viscoelastic properties and a compensation operator

In this section, moreover, considering it produces unknown time-varying delays while the real measured data of human multi-joint arm viscoelasticity is fed to the designed controller based on human multi-joint arm viscoelastic properties, a new operator-based robust nonlinear tracking control for a robot arm with unknown time-varying delays is proposed based on human multi-joint arm-like viscoelastic properties and a compensation operator. Where, the robot arm control system scheme is proposed, a delay operator is introduced to describe property of time-varying delay, and the compensation operator to compensate the term related to the effect of CNS and to remove the effect of unknown time-varying delay are introduced. First, how to describe the property of time-varying delay by operator will be discussed.

4.4.1 Property of time-varying delay

For the time-varying delay, many control methodologies have been proposed to deal with the control synthesis of delayed systems [103, 104, 105, 106],

such as Smith predictor method, observer-based control method, Lyapunov function based approach and so on. However, most of the existing control methods are based on constant time delay or a known upper bound on it, or the designed system is linear. As a result, these solutions do not allow for the direct use in controller design process of nonlinear systems with time-varying delays. In this section, an operator delay is defined, and the property of time-varying delay operator is discussed. Assume that in the operator-based nonlinear system, the output signal of controller is $\tilde{u}(t)$, and the unknown time-varying delay is $\tau(t)$, then the output signal after the delay is

$$u^*(t) = \tilde{u}(t - \tau)(t) \quad (4.36)$$

which can be denoted by a delay operator Γ , that is $u^*(t) = \Gamma(\tilde{u})(t) = \tilde{u}(t - \tau)(t)$.

The existence of time-varying delays makes the control problem more difficult because the time translation is not reversible. However, the property of the control process ensures that the time-varying delay is bounded and will not increase as fast as the time, that is, the time-varying delay $\tau(t)$ has the following performance

$$0 \leq \tau(t) \leq \tau_{max}, \quad \text{for all } t \geq 0 \quad (4.37)$$

where $\tau_{max} \geq 0$ is an upper bound on the delay. Thus, the delay operator Γ is stable.

On the other hand, for $u^*(t)$, because the time delay is irreversible, we assume that the signal is sent before $\delta(t)$, and the process is denoted by an

operator Φ , namely,

$$\tilde{u}(t) = u^*(t + \delta)(t) = \Phi(u^*)(t) \tag{4.38}$$

The operator Γ and Φ are indeed existing [84]. Also, based on the definition of BIBO stability, both of the operators Γ and Φ are stable. Based on the above discussion, it follows that the process from $\tilde{u}(t)$ to $u^*(t)$ and the process from $u^*(t)$ to $\tilde{u}(t)$ can be described by two stable operators, respectively.

4.4.2 Robust nonlinear tracking control scheme

Considering it produces unknown time-varying delays while the real measured data of human multi-joint arm viscoelasticity is fed to the designed controller based on human multi-joint arm viscoelastic properties, for the robot arm with uncertainties, a new operator-based robust nonlinear tracking control system design for a robot arm with unknown time-varying delays

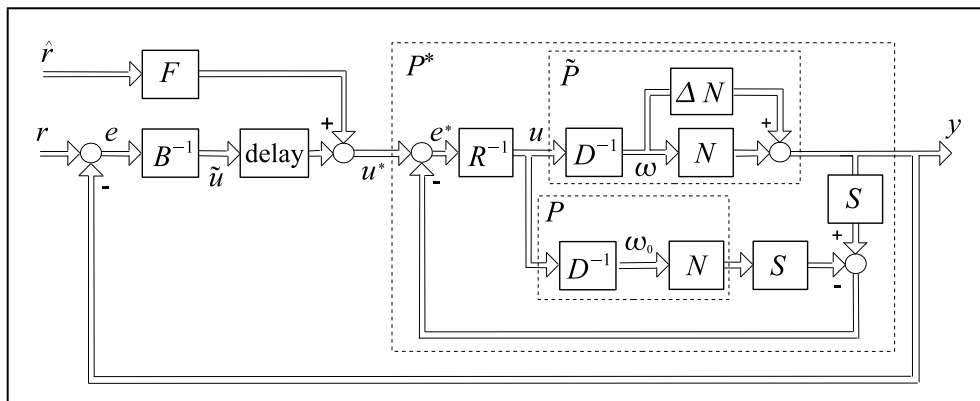


Figure 4.16: The proposed operator-based robust nonlinear tracking control system

is proposed based on human multi-joint arm-like viscoelastic properties and a compensation operator (see Figure 4.16), where, the overall plant is $\tilde{P} = (\tilde{P}_1, \tilde{P}_2)$, which includes two parts, the nominal plant $P = (P_1, P_2)$ and the uncertain plant $\Delta P = (\Delta P_1, \Delta P_2)$, namely, $\tilde{P} = P + \Delta P$. The nominal plant P and overall plant \tilde{P} are assumed to have right factorization as $P_i = N_i D_i^{-1}$ ($i=1, 2$) and $\tilde{P}_i = P_i + \Delta P_i = (N_i + \Delta N_i) D_i^{-1}$ ($i=1, 2$), respectively, N_i , ΔN_i , and D_i ($i=1, 2$) are stable operators, D_i is invertible, ΔN_i is unknown but the upper and lower bounds are known. For the robot arm, right factorizations N and D of robot arm dynamics are shown as the following forms,

$$\begin{cases} D_i(\omega_i)(t) = \mathbf{M}_i(\omega(t))\ddot{\omega}_i(t) + \mathbf{H}_i(\dot{\omega}(t), \omega(t)) \\ N_i(\omega_i)(t) = \omega_i(t), \quad i = 1, 2 \end{cases} \quad (4.39)$$

$r = (\theta_{1d}, \theta_{2d})$ and $y = (\theta_1, \theta_2)$ are the reference input and plant output, respectively, $u = (u_1, u_2)$ is joint torque control input. $\hat{r} = (\hat{\theta}_1, \hat{\theta}_2)$ is an estimated value of r , and is represented as the rapid prediction of movement. In this paper, for brevity, we limit the problem on the case of $\hat{r} = r$. The operator controllers S and R are designed to eliminate effect of uncertainties, $u^* = (u_1^*, u_2^*)$ is the input of the equivalent plant P^* . The controller B is stable operator and invertible, and is designed to obtain desired motion mechanism of human multi-joint arm viscoelasticity using online time-varying measured human multi-joint arm viscoelasticity. F is the compensation operator, and is designed to compensate the effect of CNS during human multi-joint arm movements and to remove the effect of unknown time-varying delays. In the following, and how to design the operator controller B and the compensation operator F to guarantee the robust stable tracking conditions will be

explained detailedly.

4.4.3 Main results on conditions of robust stability and tracking

According the results of **Sections 4.3.2** and **4.4.1**, the equivalent block diagram of the proposed control system shown in Figure 4.16 can be shown by Figure 4.17.

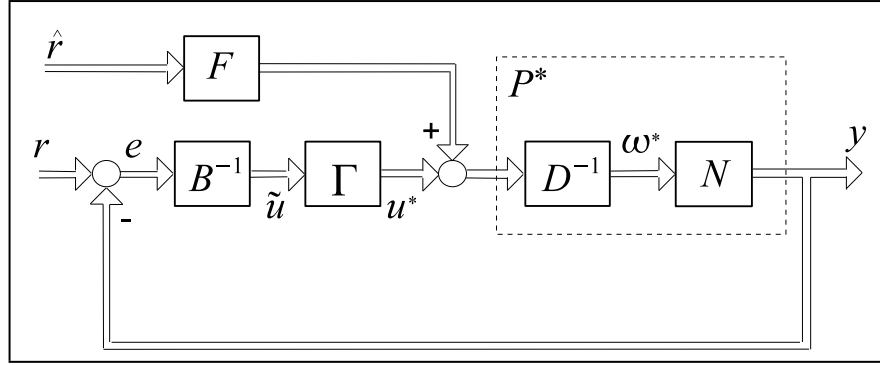


Figure 4.17: Equivalent block diagram of Figure 4.16

For the proposed control system shown in Figure 4.16 or the equivalent control system shown in 4.17, the operator controller B is designed to satisfy that $M_i = N_i + B_i D_i$ are unimodulars and described by following form,

$$B^{-1}(e)(t) = -\mathbf{R}(t)\dot{e}(t) - \mathbf{K}(t)e(t) \quad (4.40)$$

where, $\mathbf{R}(t)$ and $\mathbf{K}(t)$ are assumed to be the desired time-varying two-joint viscosity and time-varying two-joint stiffness, respectively, and can be defined based on the dynamics of robot arm. In this research, the assumed viscosity matrix $\mathbf{R}(t)$ and the stiffness matrix $\mathbf{K}(t)$ are obtained by using the online

measured viscoelastic experimental data $\mathbf{R}_A(t)$ and $\mathbf{K}_A(t)$ of human multi-joint arm with the approximate same structural parameters as the robot arm. According to the designed right factorizations $N_i(\omega_i)(t)$, $D_i(\omega_i)(t)$, and $B^{-1}(e)(t)$, we can find that,

$$M_i = N_i + B_i D_i = 2\omega_i(t), \quad i = 1, 2 \quad (4.41)$$

are also unimodulars.

Based on the designed operator controller B , then the tracking performance can be realized by designing the forward operator F .

Theorem 3. The proposed nonlinear tracking control for the robot arm with unknown time-varying delays shown in Figure 4.16, if

$$\|(B\Phi D - BD)M^{-1}\| < 1 \quad (4.42)$$

the BIBO stability can be guaranteed, and the output $y(t)$ tracks to the reference input $r(t)$ provided that $FP = I$.

Proof. Based on the proposed design scheme, the block diagram shown in Figure 4.18 is equivalent to Figure 4.16, where, $\tilde{M} = N + B\Phi D$, then,

$$\begin{aligned} y(t) &= N\tilde{M}^{-1}((r)(t) + B\Phi F(\hat{r})(t)) \\ &= N\tilde{M}^{-1}((r)(t) + B\Phi P^{-1}(\hat{r})(t)) \\ &= N\tilde{M}^{-1}((r)(t) + B\Phi DN^{-1}(\hat{r})(t)) \\ &= N\tilde{M}^{-1}(N + B\Phi D)N^{-1}(r)(t) \\ &= N\tilde{M}^{-1}\tilde{M}N^{-1}(r)(t) \\ &= r(t) \end{aligned} \quad (4.43)$$

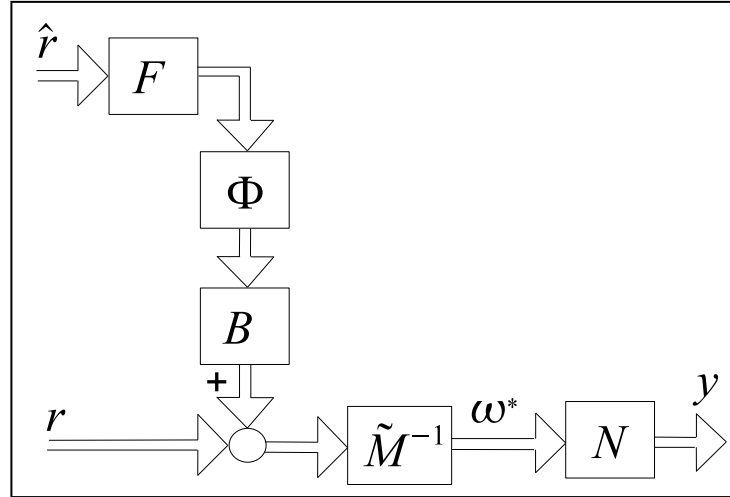


Figure 4.18: Equivalent block diagram of Figure 4.17

This completes the proof.

From **Theorem 1** and **Theorem 3** we can see that based on the proposed design scheme, the effect caused by the uncertain plant can be eliminated by designing the operator controllers S and R in the nonlinear feedback control system, the BIBO stability can be guaranteed by the designed operator controller B . The output tracking performance can be realized by designed operator controller B and the forward operator F .

4.4.4 Simulation results based on experimental data

By using the designed experimental system and the proposed estimating method in [96], the multi-joint stiffness and multi-joint viscosity of a human multi-joint arm are estimated online and shown in Figures 4.19 and 4.20, respectively, where, the human multi-joint arm (The structure parameters, $Z_1 = 0.4507$, $Z_2 = 0.1575$ and $Z_3 = 0.1530$, the physical parameters $l_1 = 0.29$ (m),

$l_2=0.32(\text{m})$) moves from the start position $(x, y) = [-41.8397, 33.8566](\text{cm})$ to the end position $(x, y) = [20.3261, 42.4389](\text{cm})$.

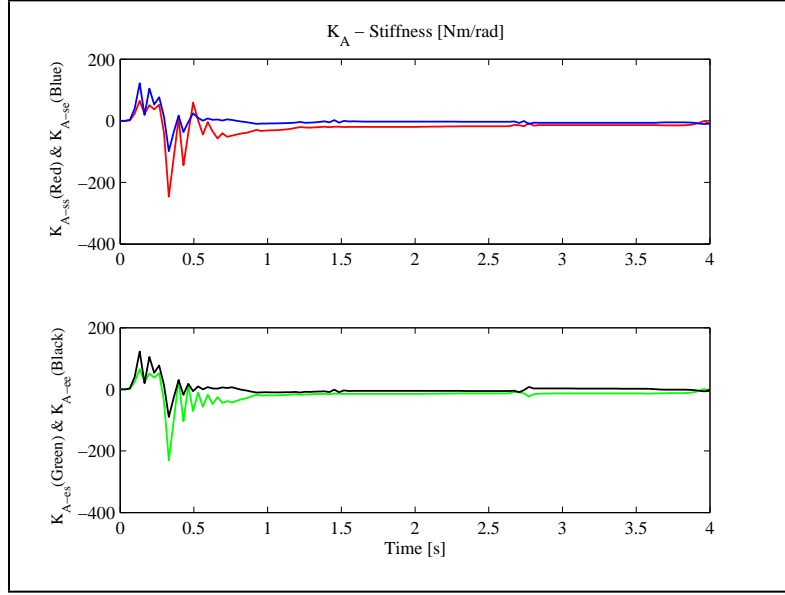


Figure 4.19: Estimated human multi-joint arm stiffness by experiment

In the proposed robot arm control system simulation, the controlled robot arm is a human multi-joint arm model, the desired trajectory is the experimental trajectory of measuring joint stiffness and joint viscosity of human multi-joint arm, and the estimated joint stiffness and joint viscosity are fed to the operator controller B . The controllers S and R are designed by conditions (4.23), namely, $SP = I$ and $R = I$. The forward operator F is designed based on conditions (4.42), namely, $FP = I$. The uncertainties of structural parameters of the robot arm is considered to be $Z_i = Z_i^* + \Delta Z_i$, $\Delta = 0.05$, where Z_i^* is assumed to be real value. Moreover, the disturbances is considered to be $\tau_d = 0.5 + 0.05 * \sin(2\pi t)$, and the time-varying delays are

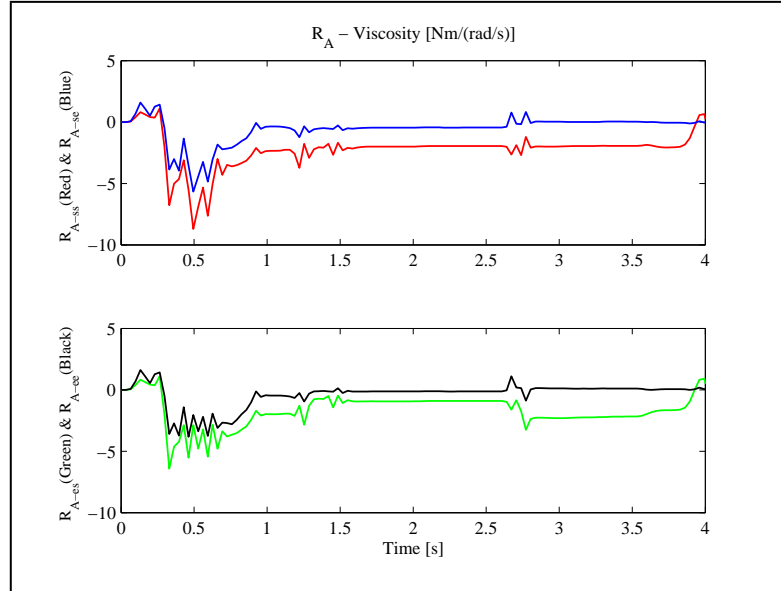


Figure 4.20: Estimated human multi-joint arm viscosity by experiment

considered to be $\tau(t) = 0.05 * \cos(2\pi t)$. The effect of structural uncertainties and disturbances is summarized into ΔN . Based on the proposed method, the joint angles and endpoint position tracking simulation results are shown in Figures 4.21 and 4.22, respectively. From Figures 4.21 and 4.22, we can find that the simulation motion trajectory can track the desired trajectory, and the effectiveness of the proposed control system can be confirmed by simulation results based on experimental data.

4.5 Conclusion

In this Chapter, two different operator-based robust nonlinear tracking control systems for the nonlinear robot arm with uncertainties are investigated by using robust right coprime factorization approach. The term of the ef-

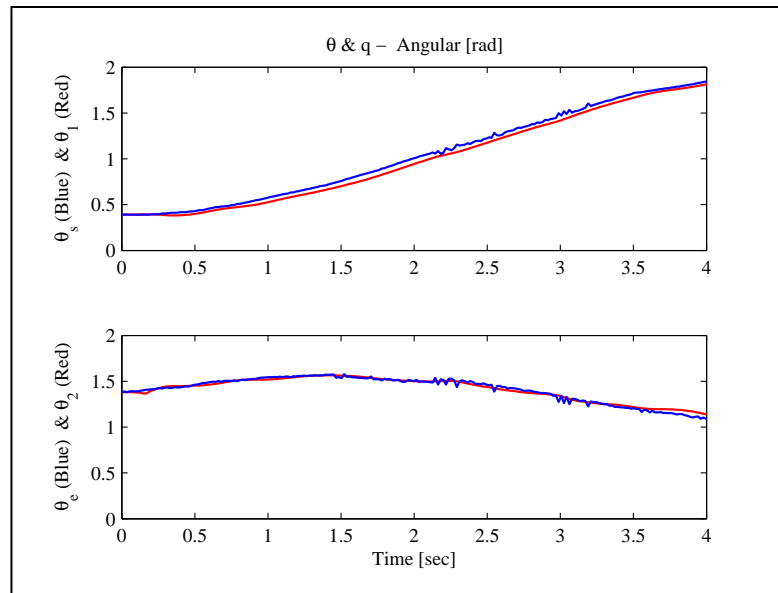


Figure 4.21: The joint angles tracking results by simulation

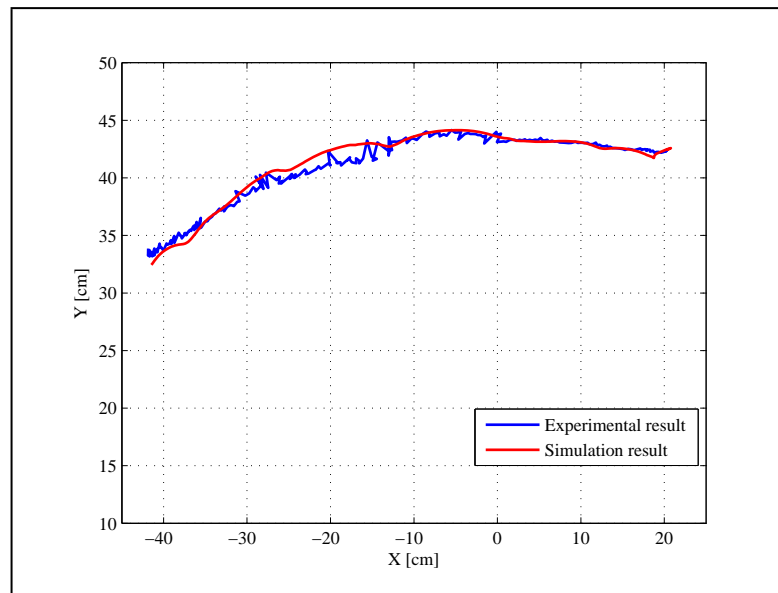


Figure 4.22: The endpoint position tracking result by simulation

fect of CNS during human multi-joint arm movements is compensated by the forward operator and compensation operator in two control schemes, respectively. The motion mechanism of human multi-joint arm viscoelasticity was considered in designing operator controller, and the time-vary estimated experimental data of human multi-joint arm viscoelasticity is used in simulation. The effect of uncertain plant was eliminated by designed the nonlinear feedback control system based on operator approach. Based on the proposed design scheme, the sufficient conditions for the robust stable were derived, and the output tracking performance was realized. The effectiveness of the proposed design scheme was confirmed by the simulation results based on experimental data.

The main merit of the proposed method is as follows. First, we extend a pioneering research of human multi-joint arm movement internal model to operator-based control design approach. That is, a design condition in (4.34) is proposed. Second, an operator-based feedback control in (4.27) or (4.40) is summarized by using motion mechanism of human multi-joint arm viscoelasticity obtained from experimental results. Third, considering the fact that the uncertain plant ΔP is unknown, generates limitations in obtaining the so-called universal condition that the output $y = (y_1, y_2)$ tracks to the reference input $r = (r_1, r_2)$ provided that $(N_i + \Delta N_i)\tilde{M}_i^{-1} = I$, in this research, the uncertain plant is eliminated by designed scheme and given conditions in (4.23), and the new tracking conditions in (4.34) without information of time-varying delays and (4.42) including information of time-varying delays were proposed, respectively.

Chapter 5

Conclusions

This dissertation has been devoted to the control system design for a robot arm with human-simulated motion mechanism based on human multi-joint arm viscoelastic properties. That is, imitating the motion mechanism of human multi-joint arm, how to use the real human multi-joint arm viscoelasticity data and how to describe and compensate the term related to the effect of CNS during human multi-joint arm movements are investigated in building robot arm control system.

In **Chapter 2**, the robot arm dynamic model and human multi-joint arm dynamic model are introduced, the relationship between Cartesian trajectories and joint space is explained detailed. Human multi-joint arm viscoelasticity is described, and estimation of human multi-joint arm viscoelasticity consisting of estimating algorithm and experimental system is introduced. All these provide the theoretical basis for this dissertation. Moreover, the objective of this dissertation is presented in problem statement.

In **Chapter 3**, a robot arm control system scheme is proposed based

on time-varying estimated viscoelastic properties and a modified forward gaze model. In detail, based on the motion mechanism of human multi-joint arm, namely, the multi-joint torque is assumed to be a function of multi-joint stiffness matrix, multi-joint viscosity matrix, and motor command descending from CNS in human multi-joint arm movements, a feedback controller and a modified forward gaze model are presented in the robot arm control system to make the present robot arm move like a human multi-joint arm. The feedback controller is designed to obtain desired motion mechanism of human multi-joint arm viscoelasticity based on real measured data from human multi-joint arm viscoelasticity, and the forward gaze model in which steering gains are modified using a cost function is used to compensate the terms related to the effect of CNS during human multi-joint arm movements. The effectiveness of the proposed method is also confirmed by the simulation results based on experimental data. Moreover, The main merit of the proposed method is also discussed.

In **Chapter 4**, two different operator-based robust nonlinear tracking control design schemes for the nonlinear robot arm with uncertainties are investigated by using robust right coprime factorization approach. The term of the effect of CNS during human multi-joint arm movements is compensated by the forward operator and the compensation operator in two control schemes, respectively. The motion mechanism of human multi-joint arm viscoelasticity is considered in designing operator controller, and the time-vary estimated experimental data of human multi-joint arm viscoelasticity is used in simulation. The effect of uncertain plant is eliminated by designed the

nonlinear feedback control system based on operator approach. Based on the proposed design scheme, the sufficient conditions of the robust stability are derived, and the output tracking performance is realized. The effectiveness of the proposed design schemes are confirmed by the simulation results based on experimental data. Moreover, the main merit of the proposed methods is also discussed.

In the future, the experiment on a robot arm as a remote which can be controlled online by measured human multi-joint arm viscoelastic properties will be considered to confirm further the effectiveness of the proposed method.

Bibliography

- [1] F. Campos and J. Calado, Approaches to human arm movement control- A review, *Annual Reviews in Control*, vol. 33, no. 1, pp. 69-77, 2009.
- [2] P. van der Smagt, M. Grebenstein, H. Urbanek, N. Fligge, M. Strohmayer, G. Stillfried, J. Parrish, and A. Gustus, Robotics of human movements, *Journal of Physiology-Paris*, vol. 103, no. 3-5, pp. 119-132, 2009.
- [3] K.T. Kalveram and A. Seyfarth, Inverse biomimetics: How robots can help to verify concepts concerning sensorimotor control of human arm and leg movements, *Journal of Physiology-Paris*, vol. 103, no. 3-5, pp. 232-243, 2009.
- [4] B. Berret, J.P. Gauthier, and C. Papaxanthis, How humans control arm movements, *Proceedings of the Steklov Institute of Mathematics*, vol. 261, no. 1, pp. 44-58, 2008.
- [5] A. Hemami and R. Labonville, Kinematic equations and solutions of a human-arm-like robot manipulator, *Robotics and Autonomous Systems*, vol. 4, no. 1, pp. 65-72, 1988.

- [6] A. Dutta and G. Obinata, Impedance control of a robotic gripper for cooperation with humans, *Control Engineering Practice*, vol. 10, no. 4, pp. 379-389, 2002.
- [7] V. Potkonjak, S. Tzafestas, D. Kostic, and G. Djordjevic, Human-like behavior of robot arms: general considerations and the handwriting task-Part I: mathematical description of human-like motion: distributed positioning and virtual fatigue, *Robotics and Computer-Integrated Manufacturing*, vol. 17, no. 4, pp. 305-15, 2001.
- [8] M.M. Rahman, R. Ikeura, and K. Mizutani, Investigation of the impedance characteristic of human arm for development of robots to cooperate with humans, *JSME international journal. Series C, Mechanical systems, machine elements and manufacturing*, vol. 45, no. 2, pp. 510-518, 2002.
- [9] C.A. Acosta-Calderon, H. Hu, Robot imitation: Body schema and body percept, *Applied Bionics and Biomechanics*, vol. 2, no. 3-4, pp. 131-148, 2005.
- [10] C. Breazeal and B. Scassellati, Robots that imitate humans, *Trends in Cognitive Sciences*, vol. 6, no. 11, pp. 481-487, 2002.
- [11] F.L. Lewis, D.M. Dawson, and C.T. Abdallah, *Robot Manipulator Control: Theory and Practice*, Marcel Dekker, Inc., 2004.
- [12] T. Yoshikawa, *Foundations of Robotics: Analysis and Control*, The MIT Press, 1990.

- [13] N. Hogan, Impedance control of industrial robots, *Robotics & Computer-Integrated Manufacturing*, vol. 1, no. 1, pp. 97-113, 1984.
- [14] R. Richardson, M. Brown, B. Bhakta, M. Levesley, Impedance control for a pneumatic robot-based around pole-placement, joint space controllers, *Control Engineering Practice*, vol. 13, no. 3, pp. 291-303, 2005.
- [15] S. Islam and X. Liu, Robust sliding mode control for robot manipulators, *IEEE Transactions on Industrial Electronics*, vol. 58, no. 6, pp. 2444-2453, 2011.
- [16] C.S. Kim, E.J. Mo, S.M. Han, M.S. Jie, and K.W. Lee, Robust visual servo control of robot manipulators with uncertain dynamics and camera parameters, *International Journal of Control, Automation, and Systems*, vol. 8, no. 2, pp. 308-313, 2010.
- [17] A.A. Ata, Optimal trajectory planning of manipulators: a review, *Journal of Engineering Science and Technology*, vol. 2, no. 1, pp. 32-54, 2007.
- [18] G. Simmons and Y. Demiris, Optimal robot arm control using the minimum variance model, *Journal of Robotic Systems*, vol. 22, no. 11, pp. 677-690, 2005.
- [19] Y. Zhu, J. Qiu, and J. Tani, Simultaneous optimization of a two-link flexible robot arm, *Journal of Robotic Systems*, vol. 18, no. 1, pp. 29-38, 2001.

- [20] V. Arakelian, J. L. Baron, P. Mottu, Torque minimisation of the 2-DOF serial manipulators based on minimum energy consideration and optimum mass redistribution, *Mechatronics*, vol. 22, no. 1, pp. 310-314, 2011.
- [21] S. Devasia, Nonlinear minimum-time control with pre- and post-actuation, *Automatica*, vol. 47, no. 7, pp. 1379-87, 2011.
- [22] P. Tomei, Adaptive PD controller for robot manipulators, *IEEE Transactions on Robotics and Automation*, vol. 7, no. 4, pp. 565-70, 1991.
- [23] J.H. Yang, F.L. Lian, and L.C. Fu, Nonlinear adaptive control for flexible-link manipulators, *IEEE Transactions on Robotics and Automation*, vol. 13, no. 1, pp. 140-148, 1997.
- [24] H. Le, S. Lee, and C. Lee, Integration model reference adaptive control and exact linearization with disturbance rejection for control of robot manipulators, *International Journal of Innovative Computing, Information and Control*, vol. 7, no. 6, pp. 3255-3268, 2011.
- [25] K. Althoefer, B. Krekelberg, D. Husmeier, and L. Seneviratne, Reinforcement learning in a rule-based navigator for robotic manipulators, *Neurocomputing*, vol. 37, no. 1-4, pp. 51-70, 2001.
- [26] C.C. Cheng, S.H. Chien, and F.C. Shih, Design of robust adaptive variable structure tracking controllers with application to rigid robot manipulators, *IET Control Theory & Applications*, vol. 4, no. 9, pp. 1655-1664, 2010.

- [27] T. Sun, H. Pei, Y. Pan, H. Zhou, and C. Zhang, Neural network-based sliding mode adaptive control for robot manipulators, *Neurocomputing*, vol. 74, no. 14-15, pp. 2377-2384, 2011.
- [28] N. Kumara, V. Panwarb, N. Sukavanamc, S.P. Sharmac, and J.H. Borma, Neural network-based nonlinear tracking control of kinematically redundant robot manipulators, *Mathematical and Computer Modelling*, vol. 53, no. 9-10, pp. 1889-901, 2011.
- [29] T. Henmi, T. Ohta, M. Deng, and A. Inoue, Tracking control of a two-link planar manipulator using nonlinear model predictive control, *International Journal of Innovative Computing, Information and Control*, vol. 6, no. 7, pp. 2977-2984, 2010.
- [30] P.K. Artemiadis, P.T. Katsiaris, and K.J. Kyriakopoulos, A biomimetic approach to inverse kinematics for a redundant robot arm, *Autonomous Robots*, vol. 29, no. 3-4, pp. 293-308, 2010.
- [31] K.P. Tee, E. Burdet, C.M. Chew, and T.E. Milner, A model of force and impedance in human arm movements, *Biological Cybernetics*, vol. 90, no. 5, pp. 368-375, 2004.
- [32] D.W. Franklin, E. Burdet, K.P. Tee, R. Osu, C.M. Chew, T.E. Milner, and M. Kawato, CNS learns stable, accurate, and efficient movements using a simple algorithm, *The Journal of Neuroscience*, vol. 28, no. 44, pp. 11165-11173, 2008.

- [33] M.A. Admiraal, M.J. Kusters, and S.C. Gielen, Modeling kinematics and dynamics of human arm movements, *Motor Control*, vol. 8, no. 3, pp. 312-338, 2004.
- [34] A.V. Gorkovenko, Methods of analysis of central motor commands related to realization of two-joint arm movements in humans, *Neurophysiology*, vol. 41, no. 1, pp. 51-53, 1993.
- [35] S. Jo, Adaptive biomimetic control of robot arm motions, *Neurocomputing*, vol. 71, no. 16-18, pp. 3625-3630, 2008.
- [36] J. Izawa, T. Kondo, and K. Ito, Biological arm motion through reinforcement learning, *Biological Cybernetics*, vol. 91, no. 1, pp. 10-22, 2004.
- [37] F. Mussa-Ivaldi, N. Hogan, and E. Bizzi, Neural, mechanical, and geometric factors subserving arm posture in humans, *The Journal of Neuroscience*, vol. 5, no. 10, pp. 2732-2743, 1985.
- [38] D.M. Wolpert, R.C. Miall, and M. Kawato, Internal models in the cerebellum, *Current Opinion in Neurology*, vol. 2, no. 9, pp. 338-347, 1998.
- [39] R.C. Miall, D.J. Weir, D.M. Wolpert, and J.F. Stein, Is the Cerebellum a Smith Predictor?, *Journal of Motor Behavior*, vol. 25, no. 3, pp. 203-216, 1993.
- [40] D.W. Franklin, E. Burdet, R. Osu, M. Kawato, and T.E. Milner, Functional significance of stiffness in adaptation of multijoint arm movements

- to stable and unstable dynamics, *Experimental Brain Research*, vol. 151, no. 2, pp. 145-157, 2003.
- [41] M. Darainy, N. Malfait, F. Towhidkhah, and D.J. Ostry, Transfer and durability of acquired patterns of human arm stiffness, *Experimental Brain Research*, vol. 170, no. 2, pp. 227-237, 2005.
- [42] P.L. Gribble, D.J. Ostry, V. Sanguineti, and R. Laboissiere, Are complex control signals required for human arm movement, *Journal of Neurophysiology*, vol. 79, no. 3, pp. 1409-1424, 1998.
- [43] E. Burdet, K.P. Tee, I. Mareels, T.E. Milner, C.M. Chew, D.W. Franklin, R. Osu, and M. Kawato, Stability and motor adaptation in human arm movements, *Biological Cybernetics*, vol. 94, no. 1, pp. 20-32, 2006.
- [44] D.R. Lametti, G. Houle, and D.J. Ostry, Control of movement variability and the regulation of limb impedance, *Journal of Neurophysiology*, vol. 98, no. 6, pp. 3516-3524, 2007.
- [45] J. Blouin, E. Guillaud, J.P. Bresciani, M. Guerraz, and M. Simoneau, Insights into the control of arm movement during body motion as revealed by EMG analyses, *Brain Research*, vol. 1309, pp. 40-52, 2010.
- [46] T. Flash, The control of hand equilibrium trajectories in multi-joint arm movements, *Biological Cybernetics*, vol. 57, no. 4-5, pp. 257-274, 1987.

- [47] H. Gomi and M. Kawato, Human arm stiffness and equilibrium-point trajectory during multi-joint movement, *Biological Cybernetics*, vol. 76, no. 3, pp. 163-171, 1997.

- [48] S. Stroeve, A learning feedback and feedforward neuromuscular control model for two degrees of freedom human arm movements, *Human Movement Science*, vol. 16, no. 5, pp. 621-651, 1997.

- [49] M. Kawato, Internal models for motor control and trajectory planning, *Current Opinion in Neurobiology*, vol. 9, no. 6, pp. 718-727, 1999.

- [50] K. Sarchilli, J.L. Vercher, G.M. Gauthier, and J. Cole, Does the oculo-manual co-ordination control system use an internal model of the arm dynamics?, *Neuroscience Letters*, vol. 265, no. 2, pp. 139-142, 1999.

- [51] R.C. Miall and D.M. Wolpert, Forward models for physiological motor control, *Neural Networks*, vol. 9, no. 8, pp. 1265-1279, 1996.

- [52] M. Desmurget and S. Grafton, Forward modeling allows feedback control for fast reaching movements, *Trends in Cognitive Sciences*, vol. 4, no. 11, pp. 423-431, 2000.

- [53] Y. Wada and M. Kawato, A neural network model for arm trajectory formation using forward and inverse dynamics models, *Neural Networks*, vol. 6, no. 7, pp. 919-932, 1993.

- [54] P.R. Davidson and D.M. Wolpert, Motor learning and prediction in a variable environment, *Current Opinion in Neurobiology*, vol. 13, no. 2, pp. 232-237, 2003.
- [55] M.J.E. Richardson and T. Flash, Comparing smooth arm movements with the two-thirds power law and the related segmented-control hypothesis, *The Journal of Neuroscience*, vol. 22, no. 18, pp. 8201-8211, 2002.
- [56] H. Gomi and M. Kawato, Neural network control for a closed-loop system using feedback-error-learning, *Neural Networks*, vol. 6, no. 7, pp. 933-946, 1993.
- [57] T. Tsuji and Y. Tanaka, Bio-mimetic impedance control of robotic manipulator for dynamic contact tasks, *Robotics and Autonomous Systems*, vol. 56, no. 4, pp. 306-316, 2008.
- [58] S.L. Hooper, Motor control: the importance of stiffness, *Current Biology*, vol. 16, no. 8, pp. R283-R285, 2006.
- [59] T. Bhattacharjee, Y. Oh, J.H. Bae, and S.R. Oh, Control design for human-like reaching movements using redundancy in robot arm-trunk systems, *International Journal of Control Automation and Systems*, vol. 9, no. 6, pp. 1173-1186, 2011.
- [60] A. Biess, M. Nagurka, and T. Flash, Simulating discrete and rhythmic multi-joint human arm movements by optimization of nonlinear performance indices, *Biological Cybernetics*, vol. 95, no. 1, pp. 31-53, 2006.

- [61] T. Flash and N. Hogan, The coordination of arm movements: an experimentally confirmed mathematical model, *The Journal of Neuroscience*, vol. 5, no. 7, pp. 1688-1703, 1985.
- [62] Y. Uno, M. Kawato, and R. Suzuki, Formation and control of optimal trajectory in human multijoint arm movement - minimum torque-change model, *Biological Cybernetics*, vol. 61, no. 2, pp. 89-101, 1989.
- [63] M. Dornay, Y. Uno, M. Kawato, and R. Suzuki, Minimum muscle tension change trajectories predicted by using a 17-muscle model of the monkey's arm, *Journal of Motor Behavior*, vol. 28, no. 2, pp. 83-100, 1996.
- [64] A. Sugahara, Y. Nakamura, I. Fukuyori, Y. Matsumoto, and H. Ishiguro, Generating circular motion of a human-like robotic arm using attractor selection model, *Journal of Robotics and Mechatronics*, vol. 22, no. 3, pp. 315-321, 2010.
- [65] T. Tsuji and Y. Tanaka, Tracking control properties of human-robotic systems based on impedance control, *IEEE Transactions on Systems, Man, and Cybernetics, Part A: Systems and Humans*, vol. 35, no. 4, pp. 523-535, 2005.
- [66] F. Yang, L. Ding, C. Yang, and X. Yuan, An algorithm for simulating human arm movement considering the comfort level, *Simulation Modelling Practice and Theory*, vol. 13, no. 5, pp. 437-449, 2005.
- [67] A. Ungoren and H. Peng, An adaptive lateral preview driver model, *Vehicle System Dynamics*, vol. 43, no. 4, pp. 245-59, 2005.

- [68] C. Brown, Gaze controls cooperating through prediction, *Image and Vision Computing*, vol. 8, no. 1, pp. 10-17, 1990.
- [69] S. Oh, N. Hata, and Y. Hori, Integrated motion control of a wheelchair in the longitudinal, lateral and pitch directions, *IEEE Transactions on Industrial Electronics*, vol. 55, no. 4, pp. 1855-1862, 2008.
- [70] B.J. Macukow, R. Gawronski, and I. Pardyka, Modelling the movement of a two-link manipulator, *Computers in Industry*, vol. 3, no. 3, pp. 187-198, 1982.
- [71] B.K.P. Horn, Kinematics, statics, and dynamics of two-dimensional manipulators, *Artificial Intelligence: An MIT Perspective*, vol. 2, pp. 273-310, 1979.
- [72] A. Hemami and R. Labonville, Kinematic equations and solutions of a human-arm-like robot manipulator, *Robotics and Autonomous Systems*, vol. 4, no. 1, pp. 65-72, 1988.
- [73] D. Braganzia, W.E. Dixon, D.M. Dawson, and B. Xian, Tracking control for robot manipulators with kinematic and dynamic uncertainty, *International Journal of Robotics and Automou*, vol. 23, no. 2, pp. 117-126, 2008.
- [74] Z.H. Man and M. Palaniswami, A robust tracking control scheme for rigid robotic manipulators with uncertain dynamics, *Computers & Electrical Engineering*, vol. 21, no. 3, pp. 211-220, 1995.

- [75] A. Banos, Stabilization of nonlinear systems based on a generalized bezout identity, *Automatica*, vol. 32, no. 4, pp. 591-95, 1996.
- [76] E. D. Sontag, Smooth stabilization implies coprime factorization, *IEEE Transactions on Automatic Control*, vol. 34, no. 4, pp. 435-443, 1989.
- [77] O. Staffans, Admissible factorizations of Hankel operators induce well-posed linear systems, *Systems & Control Letters*, vol. 37, no. 5, pp. 301-307, 1999.
- [78] M. S. Verma, Coprime fractional representations and stability of nonlinear feedback systems, *International Journal of Control*, vol. 48, no. 3, pp. 897-918, 1988.
- [79] M. S. Verma and L. R. Hunt, Right coprime factorizations and stabilization for nonlinear systems, *IEEE Transactions on Automatic Control*, vol. 38, no. 2, pp. 222-231, 1993.
- [80] G. Chen and Z. Han, Robust right coprime factorization and robust stabilization of nonlinear feedback control systems, *IEEE Transaction on Automatic Control*, vol. 43, no. 10, pp. 1505-1510, 1998.
- [81] M. Deng, A. Inoue, and K. Ishikawa, Operator-based nonlinear feedback control design using robust right coprime factorization, *IEEE Transactions on Automatic Control*, vol. 51, no. 4, pp. 645-648, 2006.

- [82] Bi, S. and M. Deng, Operator based robust control design for nonlinear plants with perturbation, *International Journal of Control*, vol. 84, no. 4, pp. 815-821, 2011.
- [83] N. Bu and M. Deng, System design for nonlinear plants using operator-based robust right coprime factorization and isomorphism, *IEEE Transactions on Automatic Control*, vol. 56, no. 4, pp. 952-57, 2011.
- [84] S. Bi, M. Deng, and S. Wen, Operator based output tracking control for nonlinear uncertain systems with unknown time-varying delays, *IET Control Theory & Applications*, vol. 5, no. 5, pp. 693-699, 2011.
- [85] S. Bi, M. Deng, and A. Inoue, Operator based internal model control of perturbed nonlinear systems, *Proc. of the 7th Asian Control Conference*, pp. 949-952, 2009.
- [86] V. F. Sokolov, Suboptimal robust synthesis for MIMO plant under coprime factor perturbations, *Systems & Control Letters*, vol. 57, no. 4, pp. 348-355, 2008.
- [87] Y. Zhou and Y. Wu, Output feedback control for MIMO nonlinear systems using factorization, *Nonlinear Analysis*, vol. 68, no. 5, pp. 1362-1374, 2008.
- [88] M. Deng, S. Bi, and A. Inoue, Robust nonlinear control and tracking design for multi-input multi-output nonlinear perturbed plants, *IET Control Theory & Applications*, vol. 3, no. 9, pp. 1237-1248, 2009.

- [89] H. Gomi and M. Kawato, Equilibrium-point control hypothesis examined by measured arm-stiffness during multi-joint movement, *Science*, vol. 272, no. 5258, pp. 117-120, 1996.
- [90] G. Venture, K. Yamane, and Y. Nakamura, Identification of human limb viscoelasticity using robotics methods to support the diagnosis of neuromuscular diseases, *The International Journal of Robotics Research*, vol. 28, no. 10, pp. 1322-1333, 2009.
- [91] H. Kim, B. Kang, B. Kim, and S. Park, Estimation of multi-joint stiffness using electromyogram and artificial neural network, *IEEE Transactions on Systems, Man, and Cybernetics, Part A: Systems and Humans*, vol. 39, no. 5, pp. 972-980, 2009.
- [92] Y. Xu and J. Hollerbach, Identification of human joint mechanical properties from single trial data, *IEEE Transactions on Biomedical Engineering*, vol. 45, no. 8, pp. 1051-1060, 1998.
- [93] E. Burdet, R. Osu, D.W. Franklin, T. Yoshioka, T.E. Milner, and M. Kawato, A method for measuring endpoint stiffness during multi-joint arm movements, *Journal of Biomechanics*, vol. 33, no. 12, pp. 1705-1709, 2001.
- [94] P.H. Chang and S.H. Kang, Stochastic estimation of human arm impedance under nonlinear friction in robot joints: A model study, *Journal of Neuroscience Methods*, vol. 189, no. 1, pp. 97-112, 2010.

- [95] R. Heliot, A.L. Orsborn, K. Ganguly, and J.M. Carmena, System architecture for stiffness control in brain-machine interfaces, *IEEE Transactions on Systems, Man, and Cybernetics, Part A: Systems and Humans*, vol. 40, no. 4, pp. 732-742, 2010.
- [96] M. Deng, A. Inoue, and Q. Zhu, An integrated study procedure on real time estimation of time varying multijoint human arm viscoelasticity, *Transactions of the Institute of Measurement and Control*, vol. 33, no. 8, pp. 919-941, 2011.
- [97] M. Deng, N. Saijo, H. Gomi, and A. Inoue, A robust real time method for estimating human multijoint arm viscoelasticity, *International Journal of Innovative Computing Information and Control*, vol. 2, no. 4, pp. 705-721, 2006.
- [98] M. Deng, A. Inoue, H. Gomi, and Y. Hirashima, Recursive filter design for estimating time varying multijoint human arm viscoelasticity, *The International Journal of Computers, Systems and Signal*, vol. 7, no. 1, pp. 2-18, 2006.
- [99] M. Deng, N. Bu, and A. Yanou, Framework of an estimation algorithm of time varying multijoint human arm viscoelasticity, *Proc. of the International Joint Conference on Biomedical Engineering Systems and Technologies*, 258-263, 2010.

- [100] H. Wang, Minimum entropy control for non-Gaussian dynamic stochastic systems, *IEEE Transactions on Automatic Control*, vol. 47, no. 2, pp. 398-03, 2002.

- [101] W. Niehsen, Robust kalman filtering with generalized gaussian measurement noise, *IEEE Transactions on Aerospace and Electronic Systems*, vol. 38, no. 4, pp. 1409-1412, 2002.

- [102] H. Gomi and R. Osu, Task-dependent viscoelasticity of human multijoint arm and its spatial characteristics for interaction with environments, *The Journal of Neuroscience*, vol. 18, no. 21, pp. 8965-8978, 1998.

- [103] W. Zhang, M.S. Branicky, and S.M. Phillips, Stability of networked control systems, *IEEE Control Systems Magazine*, vol. 21, no. 1, pp. 84-99, 2001.

- [104] W. Zhang, F. Allgower and T. Liub, Controller parameterization for SISO and MIMO plants with time delay, *Systems & Control Letters*, vol. 55, pp. 794-802, 2006.

- [105] M. Wang, S.S. Ge, and K.S. Hong, Approximation-based adaptive tracking control of pure-feedback nonlinear systems with multiple unknown time-varying delays, *IEEE Transactions on Neural Networks*, vol. 21, no. 11, pp. 1804-1816, 2010.

- [106] M. Deng and A. Inoue, Networked non-linear control for an aluminum plate thermal process with time delays, *International Journal of Systems Science*, vol. 39, no. 11, pp. 1075-1080, 2008.

Appendix A

Definition of parameters

A.1 Human multi-joint arm

Table A.1: Parameters of human multi-joint arm

\mathbf{q}	joint angular position
θ_s	shoulder joint angular position
θ_e	elbow joint angular position
\mathbf{u}	motor command descending from CNS
τ_A	multi-joint torque
$\mathbf{M}_A(\mathbf{q})$	inertial matrix
$\mathbf{H}_A(\dot{\mathbf{q}}, \mathbf{q})$	Coriolis-Centrifugal vector
\mathbf{R}_A	multi-joint viscosity matrix
\mathbf{K}_A	multi-joint stiffness matrix

A.2 Robot arm

Table A.2: Parameters of robot arm

θ	joint angular position
θ_1	joint angle of link 1
θ_2	joint angle of link 2
τ_{in}	control input torque
$\mathbf{M}(\theta)$	inertial matrix
$\mathbf{H}(\dot{\theta}, \theta)$	Coriolis-Centrifugal vector
\mathbf{R}	assumed multi-joint viscosity matrix
\mathbf{K}	assumed multi-joint stiffness matrix

Appendix B

Proof

B.1 Proof of Lemma 4.1

First, it is clear that $Lip(D, Y^e)$ is a normed linear space. Hence, it is sufficient to verify its completeness.

Let Q_n be a Cauchy sequence in $Lip(D, Y^e)$ such that $\|Q_m - Q_n\| \rightarrow 0$ as $m, n \rightarrow \infty$. We need to show that $\|Q_n - Q\| \rightarrow 0$ for some $Q \in Lip(D, Y^e)$ as $n \rightarrow \infty$.

Let $T \in [0, \infty)$ be fixed. For any $\tilde{x} \in D$, by definition of the Lipschitz norm with an $x_0 \in D$, we have

$$\begin{aligned} & \|[(Q_m - Q_n)(\tilde{x})]_T - [(Q_m - Q_n)(x_0)]_T\|_Y \\ & \leq \|Q_m - Q_n\|_{Lip} \|\tilde{x}_T - [x_0]_T\|_X \end{aligned} \tag{B.1}$$

so that

$$\begin{aligned} & \| [Q_m(\tilde{x})]_T - [Q_n(\tilde{x})]_T \|_Y = \| [(Q_m - Q_n)(\tilde{x})]_T \|_Y \\ & \leq \| [(Q_m - Q_n)(x_0)]_T \|_Y + \| Q_m - Q_n \|_{Lip} \|\tilde{x}_T - [x_0]_T\|_X. \end{aligned} \tag{B.2}$$

Since the right hand side of the above tends to zero as $m, n \rightarrow \infty$, it follows that the sequence $\{[Q_n(\tilde{x})]_T\}$ is Cauchy in the range Y^e (and in fact is uniformly Cauchy over each bounded subset of the domain D). Hence, for each fixed $T \in [0, \infty)$, $\tilde{v}_T := \lim[Q_n(\tilde{x})]_T$ exists in the range Y^e (and is uniform over bounded subsets of the domain D). Let v be a function such that $v_T = \tilde{v}_T$ for all $T \in [0, \infty)$, and define a nonlinear operator Q by $Q : \tilde{x} \rightarrow v$. Then, Q satisfies $[Q(\tilde{x})]_T = \tilde{v}_T$ for all $T \in [0, \infty)$. We will show that $Q \in Lip(D, Y^e)$. We first note that the operator Q so defined has domain D since in the above $\tilde{x} \in D$ is arbitrary. We then observe that Q is actually independent of T . Then, since $\|Q_m - Q_n\| \rightarrow 0$, we have $\lim \|Q_n\|_{Lip} = c$, a constant, so that for any $\tilde{x}_1, \tilde{x}_2 \in D$,

$$\begin{aligned} \|[Q(\tilde{x}_1)]_T - [Q(\tilde{x}_2)]_T\|_Y &= \lim_{n \rightarrow \infty} \|[Q_n(\tilde{x}_1)]_T - [Q_n(\tilde{x}_2)]_T\|_Y \\ &\leq \lim_{n \rightarrow \infty} \| [Q_n]_T \|_{Lip} \| [\tilde{x}_1]_T - [\tilde{x}_2]_T \|_X \\ &= c \| [\tilde{x}_1]_T - [\tilde{x}_2]_T \|_X. \end{aligned} \quad (\text{B.3})$$

Therefore, taking the supremum over D and then the supremum over $[0, \infty)$ yields

$$\sup_{T \in [0, \infty)} \sup_{\substack{\tilde{x}_1, \tilde{x}_2 \in D \\ [\tilde{x}_1]_T \neq [\tilde{x}_2]_T}} \frac{\|[Q(\tilde{x}_1)]_T - [Q(\tilde{x}_2)]_T\|_Y}{\|[\tilde{x}_1]_T - [\tilde{x}_2]_T\|_X} \leq c \quad (\text{B.4})$$

which implies that $\|Q\| \leq c < \infty$, so that $Q \in Lip(D, Y^e)$.

We finally verify that $\|Q_n - Q\|_{Lip} \rightarrow 0$ as $n \rightarrow \infty$. Since the above also proves (letting $\tilde{x} = x_0$ therein) that $\|[Q_n(x_0)]_T - [Q(x_0)]_T\|_Y \rightarrow 0$ as $n \rightarrow \infty$ for each $T \in [0, \infty)$, for $\epsilon > 0$ we can let N be such that $\|Q_m - Q_n\|_{Lip} \leq \epsilon/2$

and $\|[(Q_n - Q)(x_0)]_T\|_Y \leq \epsilon/2$ for $m, n \geq N$. Then for any given $\tilde{x}_1, \tilde{x}_2 \in D$, we have

$$\begin{aligned}
& \|[(Q - Q_n)(\tilde{x}_1)]_T - [(Q - Q_n)(\tilde{x}_2)]_T\|_Y \\
&= \lim_{k \rightarrow \infty} \|[(Q_k - Q_n)(\tilde{x}_1)]_T - [(Q_k - Q_n)(\tilde{x}_2)]_T\|_Y \\
&\leq \lim_{k \rightarrow \infty} \|Q_k - Q_n\|_{Lip} \|[\tilde{x}_1]_T - [\tilde{x}_2]_T\|_X \\
&= \epsilon/2 \|[\tilde{x}_1]_T - [\tilde{x}_2]_T\|_X
\end{aligned} \tag{B.5}$$

so that $\|Q_n - Q\|_{Lip} \leq \epsilon$ for $n \geq N$. This shows that $\|Q_n - Q\|_{Lip} \rightarrow 0$ as $n \rightarrow \infty$ and completes the proof of the lemma.

B.2 Proof of Lemma 4.2

Suppose that $Q : X^e \rightarrow X^e$ is causal. Then by definition we have that $P_T Q P_T = P_T Q$, so that if $x_T = y_T$, then

$$\begin{aligned}
[Q(x)]_T &= P_T Q(x) = P_T Q P_T(x) = P_T Q(x_T) = P_T Q(y_T) \\
&= P_T Q P_T(y) = P_T Q(y) = [Q(y)]_T.
\end{aligned} \tag{B.6}$$

Conversely, suppose that $x_T = y_T$ implies $[Q(x)]_T = [Q(y)]_T$ for all $x, y \in X^e$ and all $T \in [0, \infty)$. Fix a $T \in [0, \infty)$, for any $x \in X^e$, let $y = x_T$, then $x_T = y_T$, so that $[Q(x)]_T = [Q(y)]_T$. Consequently, we have that

$$\begin{aligned}
P_T Q P_T(x) &= P_T Q(x_T) = P_T Q(y) \\
&= [Q(y)]_T = [Q(x)]_T = P_T Q(x).
\end{aligned} \tag{B.7}$$

Since $x \in X^e$ and $T \in [0, \infty)$ are arbitrary, it follows that $P_T Q P_T = P_T Q$ for all $T \in [0, \infty)$, which implies that Q is causal.

B.3 Proof of Lemma 4.3

Since

$$\|[Q(x)]_T - [Q(y)]_T\|_X \leq \|Q\|_{Lip} \|x_T - y_T\|_X \quad (\text{B.8})$$

for all $x, y \in X^e$ and all $T \in [0, \infty)$. Hence, $x_T = y_T$ implies that $[Q(x)]_T = [Q(y)]_T$ for all $x, y \in X^e$ and all $T \in [0, \infty)$.

B.4 Proof of Lemma 4.4

Sufficiency: Since $M \in \mathcal{U}(W, U)$, for any $r \in U_s$, we have $r = (AN + BD)(w)$, that is $w = M^{-1}r \in W_s$. Moreover, since $y = Nw$, $e = BDw$, and $b = Ay = ANw$, the stability of A , B , N and D implies that $y \in V_s$, $e \in U_s$ and $b \in U_s$. Thus, the system is overall stable.

Necessity: First, it follows from the well-posedness and through the path of N and A that $M : W \rightarrow U$ is invertible. Then, it can be verified that both M and M^{-1} are stable. As a result, $M \in \mathcal{U}(W, U)$.

B.5 Proof of Lemma 4.5

To begin with, we recall a sufficient condition for judging operator's invertibility.

Lemma A. *Let X and Y be Banach space, $S \in Lip(X, Y)$ is an invertible operator, and R is an operator in $Lip(X, Y)$ such that $\|RS^{-1}\| < 1$ where, $Lip(X, Y) = \{S : X \rightarrow Y, \|S\|_{Lip} < \infty\}$. Then, the operator $R + S$ is*

invertible in $Lip(X, Y)$ and

$$\|(R + S)^{-1}\| \leq \|S^{-1}\|(1 - \|RS^{-1}\|)^{-1}. \quad (\text{B.9})$$

Proof of Lemma A. We first prove the following assertion: If one operator $J \in Lip(X)$ such that $\|J\| < 1$, then $I - J$ is invertible and

$$\|(I - J)^{-1}\| \leq (1 - \|J\|)^{-1}. \quad (\text{B.10})$$

In fact, for $x, y \in X$,

$$\begin{aligned} \|(I - J)x - (I - J)y\| &\geq \|x - y\| - \|Jx - Jy\| \\ &\geq (1 - \|J\|)\|x - y\|. \end{aligned} \quad (\text{B.11})$$

Thus, $I - J$ is injective. Next, we show that $I - J$ is surjective and $(I - J)^{-1} \in Lip(X)$.

Define that $Q_0 := I$ and $Q_n = I + JQ_{n-1} \forall n = 1, 2, \dots$, we can prove that for $x \in X$

$$\|Q_{n+1}(x) - Q_n(x)\| \leq \|J\|^n \|J(x)\|_X, \quad n = 1, 2, \dots. \quad (\text{B.12})$$

Then for any positive integer m , we have that

$$\begin{aligned} \|Q_{n+m}(x) - Q_n(x)\|_X &= \left\| \sum_{k=0}^{m-1} (Q_{n+k+1}(x) - Q_{n+k}(x)) \right\| \\ &\leq \sum_{k=0}^{m-1} \|J\|^{n+k} \|J(x)\|_X \leq \frac{\|J\|^n \|J(x)\|_X}{1 - \|J\|}. \end{aligned} \quad (\text{B.13})$$

Since $\|J\| < 1$ and X is Banach space, then $Q(x) = \lim_{n \rightarrow \infty} Q_n(x)$ exists and

$$\|Q(x) - Q_n(x)\|_X = \lim_{n \rightarrow \infty} \|Q_{n+m}(x) - Q_n(x)\| \leq \frac{\|J\|^n \|J(x)\|_X}{1 - \|J\|}. \quad (\text{B.14})$$

Since J is Lipschitz and hence is continuous, the

$$Q(x) = \lim_{n \rightarrow \infty} Q_n(x) = \lim_{n \rightarrow \infty} (I + JQ_{n-1})x = x + JQx \quad (\text{B.15})$$

that is, $Q = I + JQ$, namely, $(I - J)Q = I$, which implies that $I - J$ is surjective in $Lip(X)$. Then for $r, z \in \mathcal{R}(I - J)$,

$$\|(I - J)^{-1}r - (I - J)^{-1}z\| \leq (1 - \|J\|)^{-1}\|r - z\|. \quad (\text{B.16})$$

Thus, the assertion is proved. As a consequence, since $R + S = (I + RS^{-1})S$, then $\|RS^{-1}\| < 1$ follows that $(I + RS^{-1})^{-1}$ exists and $(R + S)^{-1} = S^{-1}(1 + RS^{-1})^{-1}$. This completes the proof of Lemma A.

Proof of Lemma 4.5 M is unimodular operator implies it is invertible.

From

$$AN + BD = M \quad (\text{B.17})$$

$$A(N + \Delta N) + BD = \tilde{M} \quad (\text{B.18})$$

we have

$$\begin{aligned} \tilde{M} &= M + [A(N + \Delta N) - AN] \\ &= [I + (A(N + \Delta N) - AN)M^{-1}]M \end{aligned} \quad (\text{B.19})$$

and $(A(N + \Delta N) - AN)M^{-1} \in Lip(D^e)$, then $I + (A(N + \Delta N) - AN)M^{-1}$ is invertible based on Lemma A, where I is the identity operator. Consequently

$$\tilde{M}^{-1} = M^{-1}[I + (A(N + \Delta N) - AN)M^{-1}]^{-1}. \quad (\text{B.20})$$

Meanwhile, since $(A(N + \Delta N) - AN)M^{-1} \in Lip(D^e)$ and $M \in \mathcal{U}(W, U)$, then $\tilde{M} \in \mathcal{U}(W, U)$ provided that the system shown in Figure ?? is well-posed. As

a result, for any $r \in U_s$, $w = \tilde{M}^{-1}r \in W_s$. Further, since $y = (N + \Delta N)w$, $e = BDw$ and $b = A(N + \Delta N)w$, the stability of A , B , N , D and ΔN implies that $y \in V_s$, $e \in U_s$ and $b \in U_s$. Then, the system is overall stable.

Appendix C

Publications

Journal papers

1. **A. Wang** and M. Deng, Human arm-like robot control based on human multi-joint arm viscoelastic properties and a modified forward gaze model, *JSME: Journal of System Design and Dynamics*, vol. 6, no. 2, pp. 170-185, 2012. (Chapter 3)
2. **A. Wang** and M. Deng, Operator-based robust nonlinear control for a manipulator with human multi-joint arm-like viscoelastic properties, *SICE Journal of Control, Measurement, and System Integration*, vol. 5, 2012 (Accepted for publication). (Chapter 4)
3. **A. Wang** and M. Deng, Operator-based robust nonlinear tracking control for a human multi-joint arm-like manipulator with unknown time-varying delays, *Applied Mathematics & Information Sciences*, vol. 6, no. 3, pp. 459-468, 2012. (Chapter 4)

Proceedings papers

1. **A. Wang** and M. Deng, Design of a human arm-like robot based on viscoelasticity of human multi-joint arm, *Proc. of 18th World Congress of IFAC*, pp. 5974-5979, 2011. (Chapter 3)
2. **A. Wang** and M. Deng, Human arm-like robot control using the viscoelasticity of human multi-joint arm, *Proc. of the 5th International Conference on Computer Sciences and Convergence Information Technology*, pp. 738-743, 2010. (Chapter 3)

Other papers

1. **A. Wang** and M. Deng, Robust nonlinear control design to a manipulator based on operator based approach, *ICIC Express Letters*, vol. 6, no. 3, pp. 617-623, 2012.
2. **A. Wang**, M. Deng, and D. Wang, Operator-based robust nonlinear control for ionic polymer metal composite with uncertainties and hysteresis, *Lecture Notes in Computer Science: Intelligent Robotics and Applications*, pp. 135-146, Springer, 2010.
3. **A. Wang** and M. Deng, Research on human multi-joint arm viscoelasticity estimation experiment with friction compensation, *The Papers of Technical Meeting on Control, IEE Japan*, CT-12-019, 2012.
4. M. Deng and **A. Wang**, Controller design of a manipulator with human multi-joint arm-like viscoelastic properties, *Proc. of SICE Annual Conference*, pp. 2919-2924, 2011.

5. M. Deng, Y. Teramura, **A. Wang**, and A. Yanou, Particle filter-based viscoelasticity estimation of human multi-joint arm, *Proc. of 18th World Congress of IFAC*, pp. 14312-14317, 2011.
6. M. Deng, **A. Wang**, M. Minami, and A. Yanou, Operator-based modeling for nonlinear ionic polymer metal composite with uncertainties, *Proc. of the 5th International Conference on Soft Computing and Intelligent Systems and 11th International Symposium on Advanced Intelligent Systems*, pp. 1110-1115, 2010.
7. M. Deng, **A. Wang**, S. Wakimoto, and T. Kawashima, Characteristic analysis and modeling of a miniature pneumatic curling rubber actuator, *Proc. of 2011 International Conference on Advanced Mechatronic Systems*, pp. 534-539, 2011.
8. T. Kawashima, **A. Wang**, S. Wakimoto, and M. Deng, SVR based estimation modeling and robust nonlinear control for a miniature pneumatic curling rubber actuator, *Proc. of 2012 International Conference on Advanced Mechatronic Systems*, pp. 304-309, 2012.
9. T. Hanawa, **A. Wang**, and M. Deng, Operator-based robust nonlinear control for an ionic-polymer metal composite with hysteretic properties compensation, *Proc. of 2012 International Conference on Advanced Mechatronic Systems*, pp. 12-17, 2012.
10. M. Deng, A. Yanou, Y. Tokuda, and **A. Wang**, Robust fault tolerant thermal control system design of an aluminum plate with peltier de-

- vice, *Proc. of 2012 International Conference on Advanced Mechatronic Systems*, pp. 223-228, 2012.
11. T. Kawashima, **A. Wang**, S. Wakimoto, and M. Deng, Robust nonlinear control for a miniature pneumatic curling rubber actuator by using, *The Papers of Technical Meeting on Control, IEE Japan*, CT-12-002, 2012. (in Japanese)
 12. T. Hanawa, **A. Wang**, and M. Deng, Robust nonlinear control of IPMC with nonsymmetric hysteresis, *The Papers of Technical Meeting on Control, IEE Japan*, CT-12-006, 2012. (in Japanese)